ENERGY-BASED SOLUTION FOR THE BUCKLING OF CFRP STIFFENED STAINLESS STEEL CYLINDRICAL SHELLS

BY

OSAMAH HAMOUD AHMAD DEHWAH

A Thesis Presented to the
DEANSHIP OF GRADUATE STUDIES

KING FAHD UNIVERSITY OF PETROLEUM & MINERALS

DHAHRAN, SAUDI ARABIA

In Partial Fulfillment of the
Requirements for the Degree of

MASTER OF SCIENCE

In

CIVIL ENGINEERING

NOVEMBER 2018

KING FAHD UNIVERSITY OF PETROLEUM & MINERALS

DHAHRAN- 31261, SAUDI ARABIA

DEANSHIP OF GRADUATE STUDIES

This thesis, written by **OSAMAH HAMOUD AHMAD DEHWAH** under the direction of his thesis advisor and approved by his thesis committee, has been presented and accepted by the Dean of Graduate Studies, in partial fulfillment of the requirements for the degree of **MASTER OF SCIENCE IN CIVIL ENGINEERING.**

Prof. Husain Jubran Al-Gahtani
(Advisor)

Dr. Salah U. Al-Dulaijan
Department Chairman

Prof. Alfarabi Mohammed Sharif
(Member)

Prof. Salam A. Zummo
Dean of Graduate Studies

Dr. Mohammed Ali Al-Osta
(Member)

13/11/18

Date

عمادة الدراسات العليا
DEANSHIP OF GRADUATE STUDIES

DEDICATED TO

MY BELOVED PARENTS, BROTHERS, SISTERS

AND ALL FAMILY MEMBERS

ACKNOWLEDGMENTS

I would like to begin with appreciation and gratitude to Almighty Allah, the most beneficent, and the most merciful, who bestowed health impetus, power and patience to accomplish this work and complete my degree.

First and foremost, I would like to express my deepest gratitude and thanks for my advisor Prof. Husain Jubran Al-Gahtani, who was a father before being an advisor. I highly appreciate his exceptional and endless support, valuable guidance and motivation. Thanks and appreciation are also due to the committee members Prof. Alfarabi Sharif and Dr. Mohammed Al-Osta for their recommendations and comments that contributed in improving the quality of this work.

I also would like to thank King Fahd University of Petroleum and Minerals, the Civil and Environmental Engineering Department and all the faculty members for their support and guidance during both my Bachelor and Master degrees.

Last but not least, I am grateful to my family and I would like to express my great love and sincere appreciation to my family members my parents, brothers and sisters. Thank you for your love, encouragement, empowerment, and truthful support without which I would not have gotten to this point in my journey.

TABLE OF CONTENTS

LIST OF TABLES

LIST OF FIGURES

LIST OF ABBREVIATIONS

CFRP	:	Carbon Fiber Reinforced Polymer
$\boldsymbol{D}$	:	Flexural rigidity of the shell
$\boldsymbol{E}$	:	Young's modulus of the shell material
$\boldsymbol{E_S}$	:	The secant modulus
$\boldsymbol{E_t}$	:	The tangent modulus
FEA	:	Finite Element Analysis
FEM	:	Finite Element Method
$\boldsymbol{L}$	:	Length of cylindrical shell
LPA	:	Linear Perturbation Analysis
$\boldsymbol{R}$	:	Radius of cylindrical shell
SS	:	Stainless steel
SSCS	:	Stainless Steel Cylindrical Shells
SST	:	Stainless Steel Tubes
$\boldsymbol{t}$	:	Thickness of cylindrical shell
$\boldsymbol{v}$	:	Poisson's ratio of the shell material

ABSTRACT

Full Name : OSAMAH HAMOUD AHMAD DEHWAH

Thesis Title : ENERGY-BASED SOLUTION FOR THE BUCKLING OF CFRP STIFFENED STAINLESS STEEL CYLINDRICAL SHELLS

Major Field : CIVIL ENGINEERING

Date of Degree : NOVEMBER 2018

Shell structures are widely used in numerous disciplines such as civil, mechanical and aerospace engineering. In particular, structural engineers are concerned with steel cylindrical shells when dealing with the analysis and design of tanks, silos and pipelines to mention a few. Cylindrical shells under axial compression are considered as one of the most common structural applications. The capacity of a cylindrical shell subjected to compressive loads is usually dominated by its buckling behavior which is the most common mode of failure in cylindrical shell structures. Tremendous investigations have been conducted to determine the buckling load for both stiffened and unstiffened cylindrical shells. However, most of these investigations are either based on experimental or numerical studies. The availability of analytical solutions is limited to simple cases. Analytical solutions have the advantage of dealing with closed-form or series type solutions that are more convenient for the design and optimization purposes.

Stainless steel tubes are recently used in structures due to their excellent resistance to corrosion and aesthetic appearance. Also, their properties can be improved by using stiffeners such as CFRP. Generally, CFRP jacketing is utilized to enhance the strength of the tubes by increasing the confinement effect, and consequently delay or prevent local buckling.

This research emphasizes on the utilization of CFRP jacketing on thin cylindrical shells against local buckling. The objective is to study and derive analytically the buckling load of unstiffened and CFRP stiffened cylindrical shells based on energy methods. The obtained results are verified using finite element method. It was found that the proposed Ritz method offers an excellent alternative analytical solution to the buckling of unstiffened and stiffened shells. The accuracy of all derived analytical formulas was verified with the ones in the literature (whenever available) as well as by FEM. The use of Mathematica greatly reduced the effort of formulating and performing the detailed computations and achieving analytical formulas that are more suitable for design purposes.

ملخص الرسالة

الاسم الكامل: أسامة حمود أحمد دحوة

عنوان الرسالة: حل انبعاج الاسطوانات القشرية المصنوعة من الفولاذ المقاوم للصدأ والمدعمة باللدائن المقواة بالألياف الكربونية باستخدام الطرق القائمة على مبدء الطاقة.

التخصص: الهندسة المدنية

تاريخ الدرجة العلمية: نوفمبر 2018

تستخدم المنشآت القشرية على نطاق واسع في العديد من التخصصات مثل الهندسة المدنية والميكانيكية والهندسة الفضائية. وعلى سبيل المثال يهتم المهندسون الانشائيون بالمنشأت الاسطوانية القشرية والمصنوعة من الحديد عند تحليل وتصميم الخزانات والصوامع وخطوط الأنابيب. وتعتبر المنشآت الاسطوانية القشرية تحت الضغط المحوري من أكثر التطبيقات الانشائية شيوعًا. حيث تعتمد قدرة تحمل المنشآت الاسطوانية القشرية والمعرضة للضغط على قدرة التحمل للانبعاج والذي يعتبر السبب الرئيسي في فشل المنشآت الاسطوانية القشرية. نفذت العديد من الدراسات لتحديد مقدار حمل الانبعاج لكلا من المنشآت الاسطوانية القشرية المقواة وغير المقواة. ومع ذلك ، فإن معظم هذه الدراسات إما أن تستند إلى دراسات تجريبية أو عددية. حيث يقتصر توفر الحلول التحليلية على الحالات البسيطة. وتتميز الحلول التحليلية بكونها أكثر ملاءمة لاستخدامات التصميم والتحسين الامثل في المنشآت.

يستخدم الفولاذ المقاوم للصدأ (Stainless Steel) مؤخرا في المنشآت بسبب مقاومتها الممتازة للتآكل ومظهرها الجمالي، حيث يمكن تحسين خصائص المنشأت القشرية باستخدام اللدائن المقواة بألياف كربونية (CFRP). وعموما فأن استخدام اللدائن المقواة بألياف كربونية يكون بغرض تحسين قوة وخصائص المنشآت القشرية وذلك من خلال زيادة التدعيم والحصر وبالتالي تأخير او منع الانبعاج.

يؤكد هذا البحث على استخدام اللدائن المقواة بألياف كربونية (CFRP) على المنشآت الاسطوانية القشرية لتلافي الانبعاج المحلي. حيث أن الهدف هو الدراسة والاشتقاق التحليلي لحمل الانبعاج للمنشآت الاسطوانية القشرية غير المقواة والمقواة ب CFRP وذلك باستخدام الطرق القائمة على مبدء الطاقة. تم التحقق من النتائج الذي تم الحصول

عليها باستخدام طريقة العناصر المتناهية (FEM). وقد وجد أن طريقة ريتز المقترحة تقدم حلاً بديلاً تحليليًا ممتازًا لانبعاج المنشآت القشرية غير المقواة والمقواة. تم التحقق من دقة جميع الصيغ التحليلية المشتقة مع تلك الموجودة في الابحاث السابقة (عند توفرها) وكذلك بواسطة طريقة العناصر المتناهية (FEM). أدى استخدام برنامج ماثيماتكا (Wolfram Mathematica) إلى تقليل الجهد المبذول في صياغة الحسابات التفصيلية وتنفيذها وتحقيق الصيغ التحليلية الأكثر ملاءمة لأغراض التصميم.

CHAPTER 1

INTRODUCTION

1.1 General

Cylindrical shell structures have many applications in various fields of engineering such as civil, mechanical and aeronautical engineering. Examples are tanks, pressure vessels, pipes cooling towers and silos, airplanes and space shuttles to mentions a few (Figure 1.1). The loading conditions vary depending on the function of shells. Here are some common forms of loading conditions: axial compression, internal or external pressure, global bending and wind loading. However, a cylindrical shell subjected to a uniformly axial compression load is considered as one of the most common structural application worldwide [1]. Furthermore, the buckling load for this type of load leads to those for other loads.

Figure 0.1: Examples of shell structures from left to right tank, pressure vessel and silos

Failure of shells is catastrophic which affects health, economy and environment. Generally shell structures fail often by either global or local buckling. Therefore, it is extremely

essential to understand comprehensively the behavior of shell structures under buckling. The common modes of failure in shell structures are either ring buckle (axisymmetric) or chessboard pattern (non-symmetric), but both are categorized under local buckling.

Unlike plates and columns, very thin shell structures under axial compression do not exhibit a clear correlation between the theoretical and the experimental critical load. As an example, for thin cylindrical shell, a wide persistent discrepancy is observed between the theoretical elastic buckling load and the corresponding experimental values in which the latter results in a much lower critical load. This is due to several factors such as imperfection of geometry and imprecision of loading which will develop an eccentricity, and consequently bending and increasing load magnitude [2]. The deviations between the two results diminish as the radius/thickness ratio approaches the value corresponding to plastic buckling.

Stainless steel (SS) is commonly used in water tanks and aerospace structural alloys. Stainless Steel Cylindrical Shells (SSCS) is widely used in structures due to its aesthetic appearance as well as its excellent resistance against corrosion. SSCS structures are more durable and provide more confinement especially when they are filled with concrete, there are many applications of SSCS filled with concrete such as bridge piers and high-rise buildings [3].

Carbon Fiber Reinforced Polymer (CFRP) stiffeners are lately used to enhance some of the properties of structures. They can be utilized to be jacketed on Stainless Steel Tubes (SST) columns to provide more strength and ductility, which significantly improve the ability of

steel to resist local buckling. Basically, they delay or prevent local buckling by increasing the confinement effect against lateral pressure that is coming from axial compression.

This research emphasizes on the utilization of CFRP jacketing on thin cylindrical shells against local buckling. The objective is to study and derive analytically the buckling load of CFRP stiffened cylindrical shell based on energy methods. In addition, to verify the obtained results by using finite element method.

1.2 Fundamentals of Shells

A shell is defined as a body that is bounded by two curved, inner and outer, surfaces. Its thickness (t) is confined between the two surfaces and considered to be small when compared to other dimensions of the body. Shells are mainly divided into two main types: thick shells and thin shells. Type of shells are classified based on thickness-to-radius ratio. A shell is called thin if the following expression is satisfied, otherwise the shell is considered to be thick [4]:

$$\frac{R}{t} \geq 20 \tag{1.1}$$

where R is the radius of the shell, from the center to the middle surface. Where the middle surface is the locus at which the inner and outer surfaces are equally spaced, at distance $t/2$ from the inner surface as illustrated in Figure 1.2. The thickness of a shell can vary, however in this research shells of constant thickness were considered.

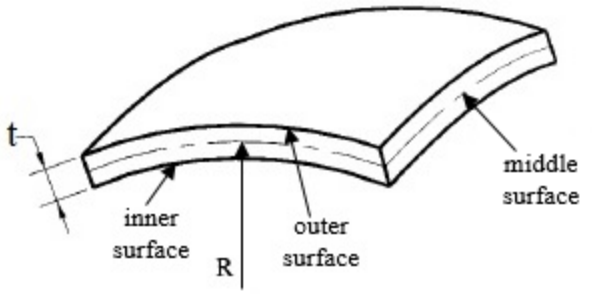

Figure 0.2: Middle, inner and outer surfaces of a shell element

Curvature is the special characteristic that distinguishes between plates and shells. Contingent on the curvature, shells are classified into different kinds e.g. circular and noncircular cylindrical, ellipsoidal, spherical and conical shells. Moreover, circular shells usually follow cylindrical coordinate system consisting of three main axes, as shown in Figure 1.3. where x-axis is in the longitudinal direction, θ is in the circumferential direction and z is the transverse axis. For cylindrical shells the curvature is equal to zero in the longitudinal direction.

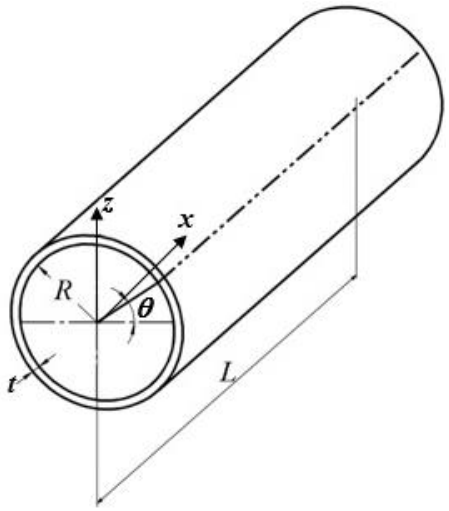

Figure 0.3: Cylindrical shell's coordinates system

1.3 Problem Statement

In the design of thin shell structures, the buckling failure is the main concern. A cylindrical shell subjected to uniformly axial compression load is considered as one of the most common structural applications. Buckling in shell structures is either global or local. Moreover, the common modes of failure in shell structures are elastic as well as plastic buckling, both are categorized under local buckling. Hence, understanding the behavior of shell structures under buckling by knowing its type, obtaining the buckling stresses and modes are the main goals of this research.

1.3.1 Local Buckling

Let us consider a thin circular cylindrical shell of radius R, thickness t and length L subjected to a uniform axial compression load N, as show in Figure 1.4; Then the expected failure is due to local buckling, which could be either elastic or plastic depending on the ratio R/t. Furthermore, the expected mode is either symmetric (ring buckle) or non-symmetric (chessboard pattern). Figure 1.5 illustrates the buckling modes of a compressed circular cylindrical shell [5].

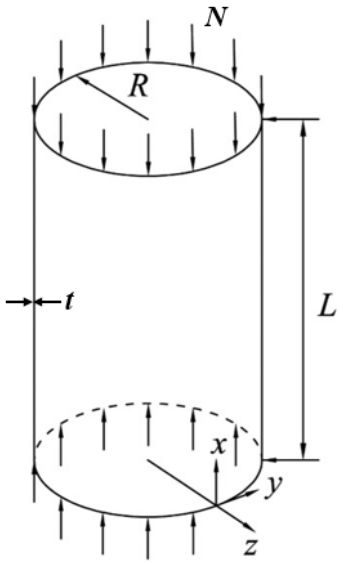

Figure 0.4: Cylindrical shell under axial compression

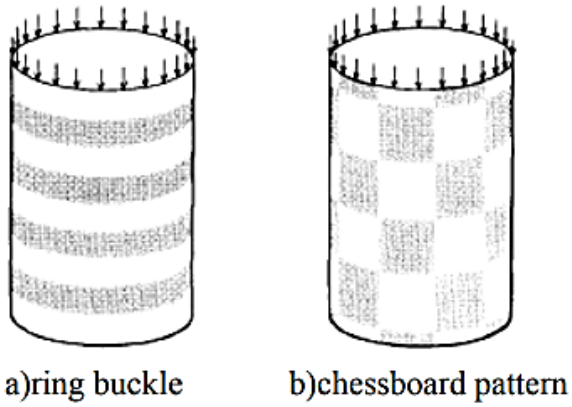

Figure 0.5: Cylindrical shell buckling modes [5]

1.3.2 Elastic Buckling

Elastic deformation in a circular cylindrical shell due to axial compression may take the form of axisymmetric or non-symmetric shapes depending on the shell geometric parameters. Axisymmetric buckling is also known as ring buckle and its graphical shape is like a sine wave as shown in Figure 1.6; The deformation is involved only in the radial direction.

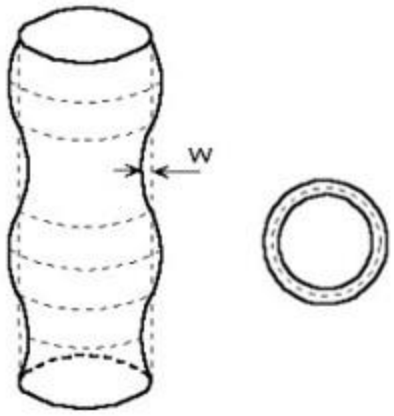

Figure 0.6: Axisymmetric deformation of cylindrical shell, where dashed lines show the original shape.

Unlike the formulations of axisymmetric buckling which involves only the deformation in the axial and radial direction, the governing equations of non-symmetric buckling (Figure 1.7) are more general as they should allow the deformation of the shell in the axial and tangential directions in addition to the deformation in the radial direction. The non-symmetric buckling formulations can be solved as an eigenvalue problem, to obtain the solution that determines the buckling loads and their corresponding buckling modes.

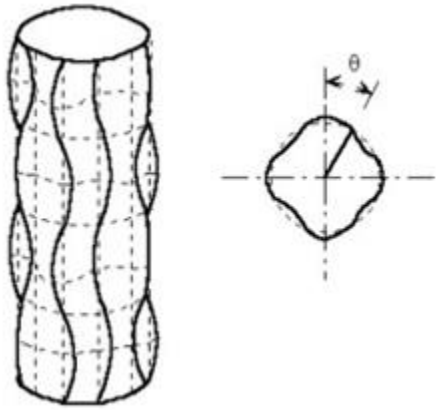

Figure 0.7: Non-symmetric deformation of cylindrical shells, where dashed lines show the original shape.

1.3.3 Plastic Buckling

Buckling of steel material is quite different from other materials such as concrete and aluminum. For relatively thicker SSCS, the critical stress exceeds the yielding stress (inelastic region) and plastic local buckling occurs. Researchers have shown through excremental work that local buckling is initiated at the beginning of yielding stage, therefore ductility behavior is prevented. When a steel tube is loaded, both ends starts to yield before plastic buckling takes place, resulting in enhancement of loading carrying capacity in steel tubes. Figure 1.8 shows how the strength decreases exponentially with the increase in loading. Nevertheless, from theoretical point of view local buckling takes place at both ends of the steel tube simultaneously. However, the situation is different experimentally in which local buckling occurs at one end of the steel tube. This is because of small imperfections in geometry, boundary conditions and material behavior [6-9].

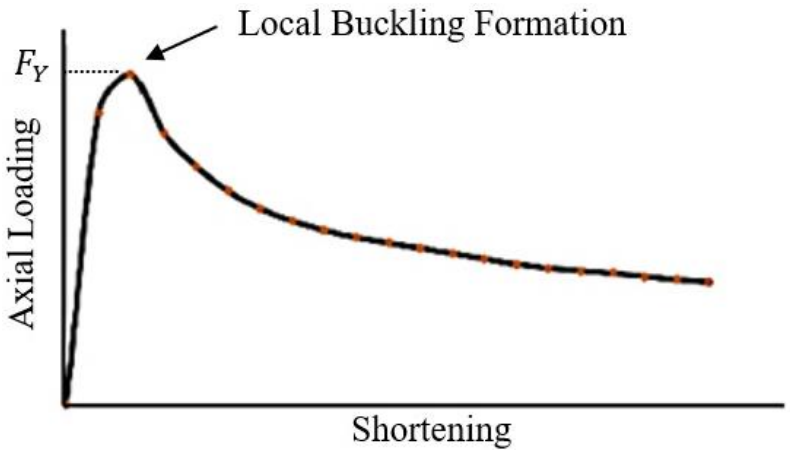

Figure 0.8: Plastic Buckling

Local buckling can be formed anywhere in cylindrical shell structures, but more likely to initiate at the supports or ends of the structure taking a shape of sine wave. Then, other

waves are initiated within the structure. Local buckling takes place when the critical load (N_{cr}) is achieved.

Shell geometry and material property play the main role in defining the buckling type and mode. The three shell geometric parameters: the length (L), radius (R) and thickness (t) and material properties: modules of elasticity and yield stress, are the main characteristics that categorize the buckling type and mode. For plastic buckling, the shape of the stress-strain curve after yielding has a major effect on the buckling capacity. It is the purpose of this study to investigate the effects of the above geometric and material parameters on identifying the buckling type (elastic or plastic) and the buckling mode (global or local, symmetric or non-symmetric).

1.3.4 Stainless Steel

The design of carbon steel structures is well established because of its clear behavior, mechanically. In contrast, the structural performance of stainless steel is dissimilar and complex due to its nonlinearity stress-strain relationship with an undefined yield plateau [6], as shown in Figure 1.9. The former difficulty, defining stress-strain relation, is tackled by introducing the Ramberg-Osgood model [10]. This model is widely used for non-linear metallic materials and it was proposed in 1943, then enhanced by Hill [11] and is given by the following expression:

$$\varepsilon = \frac{\sigma}{E_0} + 0.002\left(\frac{\sigma}{\sigma_{0.2}}\right)^n \tag{1.2}$$

where ε and σ are the engineering strain and stress, respectively, E_0 is the young's modulus, $\sigma_{0.02}$ is the proof stress that corresponds to 0.2% of plastic strain, and n is a

constant. However, this expression gives an excellent prediction of stress-strain behavior of stainless steel up to 0.2% proof stress [6].

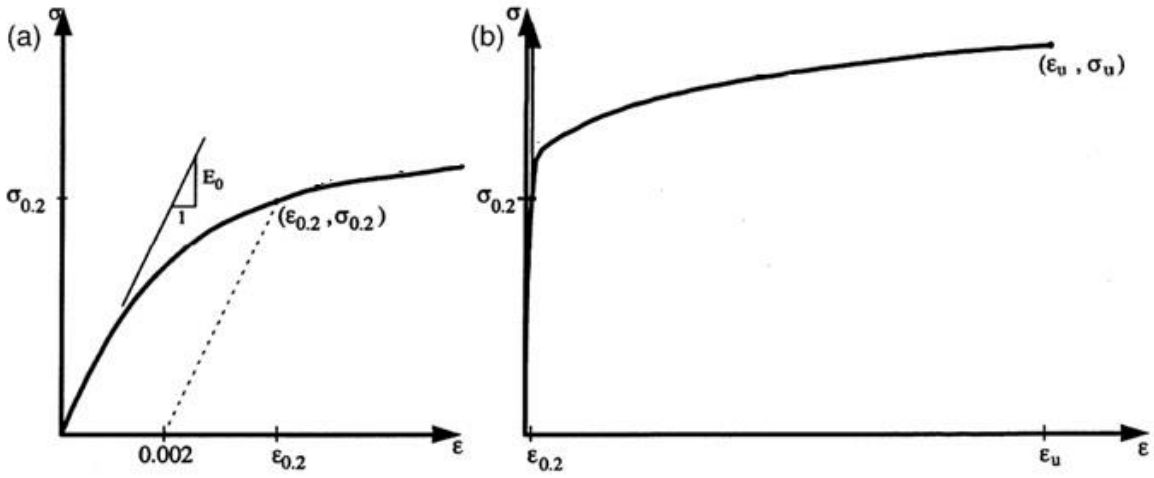

Figure 0.9: Stainless steel stress-strain curve; (a) Initial σ-ε curve, (b) Full range of σ-ε curve [12]

The second difficulty is the roundness of the stress-strain curve in which the yield stress cannot be identified easily, compared to ordinary carbon steel, as shown in Figure 1.10. This problem is solved by taking the yield stress at 0.2% plastic strain $(\sigma_{0.02})$.

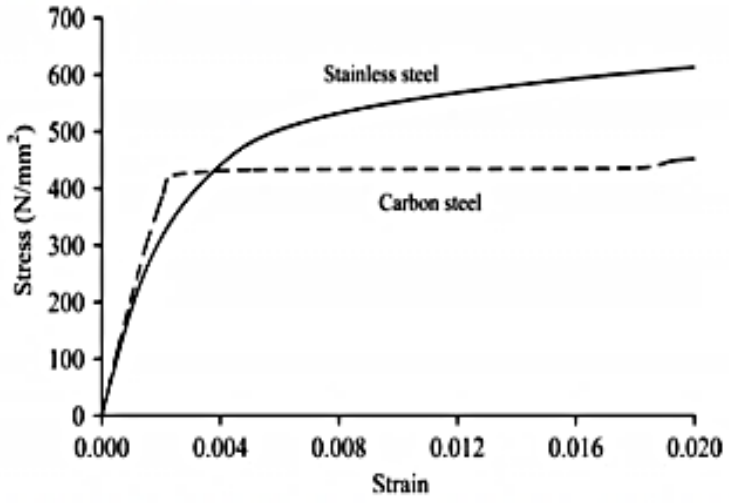

Figure 0.10: Stress-strain behavior of stainless steel and carbon steel [6]

1.3.5 CFRP

Carbon Fiber Reinforced Polymer, AKA Carbon Fiber Reinforced Plastic, CFRP-stiffeners are used for the purpose of strengthening stainless steel cylindrical shells. CFRP has the following material properties: linear elastic behavior (very high modulus of elasticity exceeding that of steel) , high ultimate strength, no yielding point , lower strain at failure. Figure 1.11 shows a typical stress- strain behavior of CFRP.

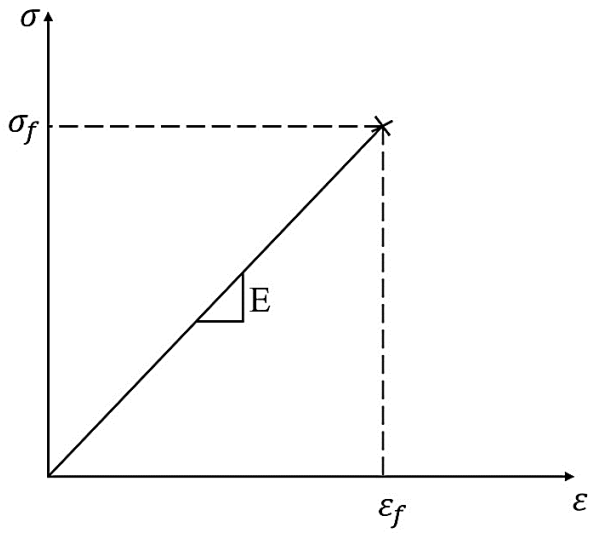

Figure 0.11: Stress-strain behavior of CFRP

1.3.6 Buckling of CFRP Stiffened Circular Cylindrical Shells

The analytical solution of CFRP stiffened cylindrical shell is complicated. The problem is usually tackled by the use of numerical techniques mainly by FEM. It is the purpose of this research to extend the analytical solutions obtained earlier for unstiffened shells to the case of stiffened shell. The energy method such as the Ritz-method is utilized to generate the eigenvalue problem leading to the buckling loads and modes.

1.4 Objectives

The main purpose of this research is to study and derive analytically the buckling load of CFRP stiffened SSCS based on energy methods. Moreover, the specific objectives are to:

- Formulate the problem of CFRP-unstiffened and stiffened SSCS subjected to axial compression.
- Formulate the eigenvalue problem based on Ritz method.
- Implement the above two formulations in a Mathematica computer code to obtain the analytical solution for the elastic buckling of stiffened/unstiffened SSCS.
- Repeat the above tasks for the plastic buckling of shells with small R/t ratios.
- Carryout FEM analysis for some selected cases and verify the accuracy of the developed analytical solutions by comparison with the obtained FEM results.
- Study the effect of various geometric and material parameters on the buckling behavior of both stiffened and unstiffened SSCS.
- Develop simplified formulas that can be utilized for design purposes.

1.5 Outline of Thesis

The organization of this thesis is in the following sequence. Chapter 1 gives an introduction about shells including a brief description about local elastic and plastic buckling, stainless steel, and CFRP-stiffeners. It also provides a description of the problem undertaken and its objectives. A brief literature review related to previous work on buckling of structures, with more emphasis on buckling of cylindrical shells and CFRP stiffened cylindrical shells is presented in Chapter 2.

Chapter 3 contains the formulations of thin shells (unstiffened and CFRP-stiffened) and the derivation of the general differential equations (governing equations) for elastic and plastic buckling of cylindrical shells. Also, it gives a brief description on the analytical, numerical and computational tools used throughout the thesis.

Chapter 4 involves the buckling load derivation by equilibrium and energy approaches for symmetrical elastic buckling of unstiffened and CFRP-stiffened cylindrical shells. This chapter ends with simplified buckling formulas for non-symmetric elastic buckling that could be utilized for design purposes.

The buckling load derivation of plastic buckling of unstiffened and CFRP-stiffened SSCS is given in Chapter 5. In addition, a description on the use of Ramberg-Osgood model along with a worked example is provided.

In Chapter 6, the validation of the analytical solutions for the elastic and plastic buckling load is carried out by FEM, using ABAQUS software. The Numerical analysis method, element type, mesh and size and boundary conditions are explained. Also, a sensitivity analysis on mesh size and mesh element is implemented in order to achieve accurate results in a reasonable time. Finally, a summary of the key findings of this research, conclusions and recommendations for future research are stated in Chapter 7.

CHAPTER 2

LITERATURE REVIEW

2.1 Buckling of Structures

Analysis of structure instability was introduced by Leonhard Euler, [1707-1783], who is mathematician and physicist scientist. Euler conducted the first mathematical analysis of bifurcation buckling in 1757. He began by studying the behavior of a simply supported column subjected to axial loading in order to understand the post-buckling behavior. Basically, he used calculus of variations theory to obtain the critical load (P_{cr}), see equation (2.1) below, by using equilibrium equations of the deformed column. Furthermore, Euler established governing equations in the form of eigenvalue problem. Figure 2.1 illustrates the first eigenmode of Euler buckling (Timoshenko, [13]).

$$P_{cr} = \frac{\pi^2 E\, I}{L^2} \tag{2.1}$$

This solution is considered to be the first theoretical solution for stability problems as well as the first solution and formulation of eigenvalue problems [14]. Further studies conducted on buckling include. Furthermore, Warner Koiter, 1945 worked on his dissertation in classical nonlinear bifurcation theory and he was the one who initiated it [15]. Hutchinson (1970s) played a main role in nonlinear branching theory of structures that are loaded within the plastic range[16]. Both Koiter and Hutchinson (1970) worked on post buckling theory[17].

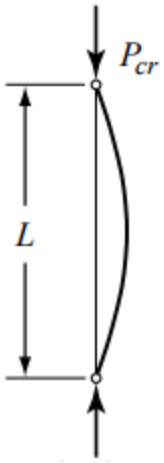

Figure 0.1: The first eigen mode, half sine wave (Euler buckling)

2.2 Buckling of Cylindrical Shells

The twentieth century had the biggest share in shell research and development. The first shell buckling problem was solved theoretically by (Lorenz, 1908 [18]; Timoshenko, 1910 [19]; Southwell, 1914 [20]). They all concluded that for a perfect cylinder subjected to a uniform axial compression load the critical stress is given by the following expression:

$$\sigma_{cl} = \frac{E}{\sqrt{3\,(1-\mu^2)}}\frac{t}{R} \tag{2.2}$$

This buckling stress (σ_{cl}) was obtained based on several assumptions, the cylinder is elastic of a moderate length, simply supported at both ends, and with pre-buckling stress state that is not influenced by boundary conditions. However, this classical elastic buckling stress formula has been used till the current era, also it is used as a reference stress for complex shell buckling problems.

In the 1930s, different load cases on cylindrical shells were studied and investigated analytically by many pioneers such as Flügge (1932 and 1934) Donell (1934) and Timoshenko (1936). Their main analysis focused on load cases such as torsion, external pressure and bending [13], [21–23].

Tremendous research work has been conducted to investigate the behavior of cylindrical shells under compression load. The main focus of these studies was on the buckling load (critical load). It was observed that there is a large discrepancy in calculating the critical load between theoretical and experimental analysis.

Bijlaard [24] derived the differential equations of plastic buckling of plates and shells for different types of loading and boundary conditions, using the total deformation theory. The results showed a good agreement with the experimental work conducted by N.A.C.A and Kollbrunner. The derivation of the plastic buckling constitutive equations has been done for several cases of loading and boundary conditions (Table 2.1). The author also presented a comparison of his theory with other theories including Stowell, Ilyushin and Handelman and Prager.

Batista and Gonçalves [2] investigated theoretically the buckling load of different types of shells, namely cylindrical shells under axial load and spherical shells under external pressure. The obtained results were compared with existing experimental data. Figure 2.2 shows a comparison of buckling load of cylindrical shells subjected to axial compression obtained theoretically with the experimental results.

Table 0.1:Different cases of loading and their corresponding boundary condition factor (β).

Case	Boundary conditions, and loading	$\beta = \varrho_2/\varrho_1$	Ratio σ_B/σ_E or τ_B/τ_E with buckling just below the yield stress
1		0	0.878
2		0	0.830
3		0	0.804
4		0	0.778
5		−1	0.775
6	σ	−1	0.747
7	σ	1	0.612
8		1	0.612
9		0	0.536
10	σ	1	0.488
11	σ/2	1/2	0.446
12		0	0.417

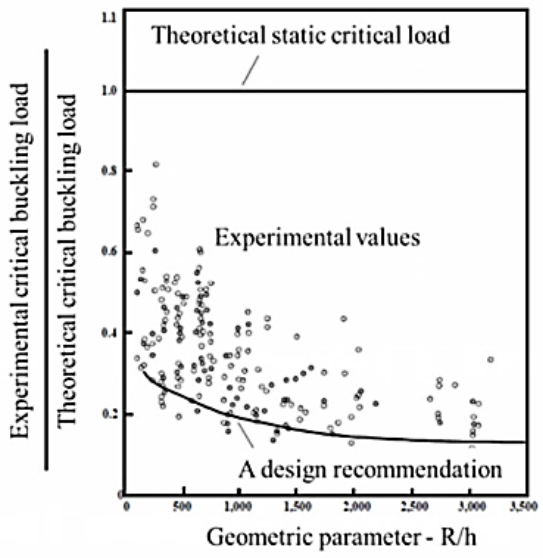

Figure 0.2: Comparison of the experimental and theoretical static critical load [25]

Referring to Figure 2.2, (R/h) is the radius to thickness ratio, it can be clearly seen that the critical load obtained experimentally is much lower than theoretical buckling load.

Bisagni [26] studied experimentally and numerically composite cylindrical shells subjected to dynamic and static axial loading. Initially, the static buckling test was performed after which the dynamic test carried out. Also, in the same experiment one shell was tested statically until complete failure. Also, one shell was tested statically in the same experiment until complete failure. The results obtained experimentally was compared with finite element model performed using ABAQUS. It was found that the dynamic buckling load in composite shells are higher than the static by 5%.

Sun, Xu, Lim and Tan [1] conducted a theoretical analysis to propose a new energy method, namely symplecticticity approach. Basically, they integrated Legendre transformation with the Hamiltonian's canonical equations to come up with new governing equilibrium equations, to find symplectic eigenvalues and eigen-solutions. They obtained similar modes of buckling; axisymmetric and asymmetric, also they extended their study to find special buckling modes.

Som and Deb [27] formulated a generalized Ritz approach to find buckling mode and load of cylindrical shells. The approach accounts for pre-buckling deformation and non-linearity of geometry of cylindrical shells under uniform axial compression. The method was validated using numerical solutions and analytical results.

Seung and Chang [28] studied buckling strength of both geometrically perfect and imperfect thin cylindrical shells (e.g. tanks) analytically and numerically. The study focused mainly on thin cylindrical shells of diameter-to-thickness ranging from 800 to

2000 and height-to-diameter ratio of 0.5 to 3. The analytical solution was developed for simply supported shells that are subjected to a uniform compressive load. The solution is used as a benchmark for the numerical model. Regarding numerical analysis, FEM software (Abaqus) was used to verify the proposed design equation.

In addition, they proposed a design equation for geometrically perfect shells that can estimate the buckling strength. The practical design equations were developed by regression analysis of the FEM results. They concluded that, in FEA (Finite element analysis), element type and size play a significant and critical role in predicting the buckling strength and mode. Also, the buckling strength decreases slightly as height-to-diameter ratio increases, while it increases remarkably as diameter-to-thickness ratio increases.

Himayat Ullah [29] studied analytically, numerically and semi-empirically the buckling of an axially loaded lightweight thin-walled shells. The analytical solution was obtained using classical shell small deflection theory, based on Kirchoff-Love hypothesis, also the analysis was carried by equilibrium methods. A numerical model was built to verify the obtained results, using ANSYS software. A semi-empirical model was obtained by employing buckling coefficients (correction factors) based on existing test results. Both linear and non-linear buckling analysis including imperfections were carried out in this investigation. In addition, a parametric study has been conducted to investigate the effect of thickness, radius and length of shells. It was concluded that the buckling strength of analytical and numerical linear models were matching. Also, it was found that the main reason of discrepancy between theoretical and experimental results is the non-linearity and geometric imperfections.

Giljith, Divya and Preetha [30] investigated experimentally the buckling behavior of thin cylindrical shells with and without cutout. The study considered different cutout locations as well as different size (diameter) of cutout. It was concluded that the buckling load decreased significantly when cutout is created in the shell. Also, the increase in the diameter of the cutout plays a major rule in reducing the buckling strength.

2.3 CFRP Stiffened Cylindrical Shells

Fiber reinforced polymer (FRP) composites are widely used in reinforced concrete (RC) rehabilitation and repair. Although tremendous investigations have been performed in this area, FRP composites are still in an elementary level when considering steel structures. FRP is recommended to be used for external retrofitting because of its characteristics e.g. high strength to weight ratio and excellent resistance against corrosion [31]. Unlike FRP, CFRP are not commonly used in strengthening SST against local buckling, and this area was not duly addressed in the literature.

Teng and Hu [8] investigated experimentally the behavior of CFRP jacketing on carbon steel that is under axial compression. After which a finite element model is conducted to verify the experimental outputs. Both results indicated that the use of FRP jackets is promising and provide more strength to resist local buckling of carbon steel tubes.

Haedir and Zhao [7] evaluated experimentally the influence of bonded CFRP sheets for strengthening circular carbon tube short columns under axial loading. The CFRP sheets were externally bonded and were orthogonal on each other (hoop and longitudinal). This study revealed that enhancing the axial strength against compression load is possible using CFRP.

Sundarraja and Prabhu [32] studied the structural enhancement of concrete filled steel tubes (CFST) with normal strength concrete that is externally bonded with CFRP strips. CFRP was used horizontally as a lateral tie, with some variable parameters e.g. number of layer, width of CFRP sheet and spacing between strips. This investigation was conducted experimentally and analytically. Tests were conducted until the complete failure of columns, to comprehensively understand the influence of CFRP strips on the compressive resistance ability of a square CFST. On the other hand, the analytical model was used to predict the axial compression load capacity of stiffened CFS tubes. They concluded that, the CFRP sheets develop external confinement pressure that can prevent or delay local buckling hence further improvement of load carrying capacity was achieved.

Alam and Fawzia [33] conducted a numerical study on CFRP strengthened steel hollow square column (SHSC) subjected to transverse impact load in order to predict the performance as well as the failure mode. Using finite element (FE) tool (ABAQUS), it was found that the impact resistance of SHSC-strengthened with CFRP has been enhanced up to 58%.

Punitha Kumar and Senthil [34] investigated the performance of CFRP-strengthened steel circular tube (SCT) subjected to axial static and cyclic loading. They also studied the axial strength alteration in SCT in case of one or two layers (in two different directions hoop and longitudinal) of CFRP. It was concluded that the axial capacity of SCT increased significantly, up to 39% for static loading and 41% for cyclic loading, as a result of using CFRP.

Arani, Loghman, Barazoki and Kolahchi [35] used Ritz method to study the elastic stability of stiffened cylindrical shells subjected to axial compression as well as internal and external pressure. The stiffeners were ring and stringer (longitudinal) and located at inner and outer surfaces of the shell at different arrangements. Moreover, the critical buckling loads were obtained analytically by energy method (Ritz). They concluded that, outside rings can enhance the stability of cylindrical shells more practically than the inside rings. Also, shells with inside stringers are more stable compared to those with outside stringers. Furthermore, when stringers (inside and outside) were used, the stability of cylindrical shells was found to be almost the same in case an internal or external pressure is applied.

CHAPTER 3

FORMULATIONS AND TOOLS OF ANALYSIS

3.1 Introduction

The first part of this thesis deals with the elastic analysis of cylindrical shells which is based on the following assumptions:

- The deflection is small when compared to the thickness of shell.
- The ratio of shell thickness to radius of curvature (t/R) is very small when compared to unity.
- The plane section through a shell before deformation remains plane and normal to the deformed mid-surface after shell is subjected to bending ($\varepsilon_z = \gamma_{xz} = \gamma_{yz} = 0$).
- The normal stress in the z-direction is negligible ($\sigma_z = 0$).

The above type of analysis applies to very thin shell with high R/t ratios. For shells with low R/t ratios, the shell starts to yield before failing plasticly. The second part of the thesis deals with shells having low R/t ratios and therefore requires dealing with plastic buckling. In this chapter the formulations of unstiffened and stiffened cylindrical shells are illustrated for both elastic and plastic buckling. In addition, the tools to be utilized in this thesis is explained.

3.2 Elastic Buckling of Unstiffened Cylindrical Shells

The term elasticity is referred to the tendency of a body to return to its original shape when a force or stress is applied and then released. Elastic materials have the ability of being deformed when a force is applied, and when it is released they return back to their original shape (reversible).

Assumptions of linear elasticity theory:

- Linear behavior of the material.
- Deformation is small and dynamic effects are neglected.
- The material is homogenous and has same mechanical properties at all points and in all directions.

3.2.1 Equilibrium Equations for Non-Symmetric Buckling

The equilibrium equations of cylindrical shells under general loads are illustrated in this section. Let us consider a differential element of a cylindrical shell as shown in Figure 3.1. The shell has a radius R, the stress resultants are $(N_x\ , Q_x\ , N_\theta , Q_\theta , N_{x\theta}\ and\ N_{\theta x})$ and surface loading components are $P_x\ , P_y\ and\ P_r$. For diagram simplification purposes, the notation N_x^+ is used to denote $N_x + (\partial N_x/\partial x)\ dx$ and so on with the other notations.

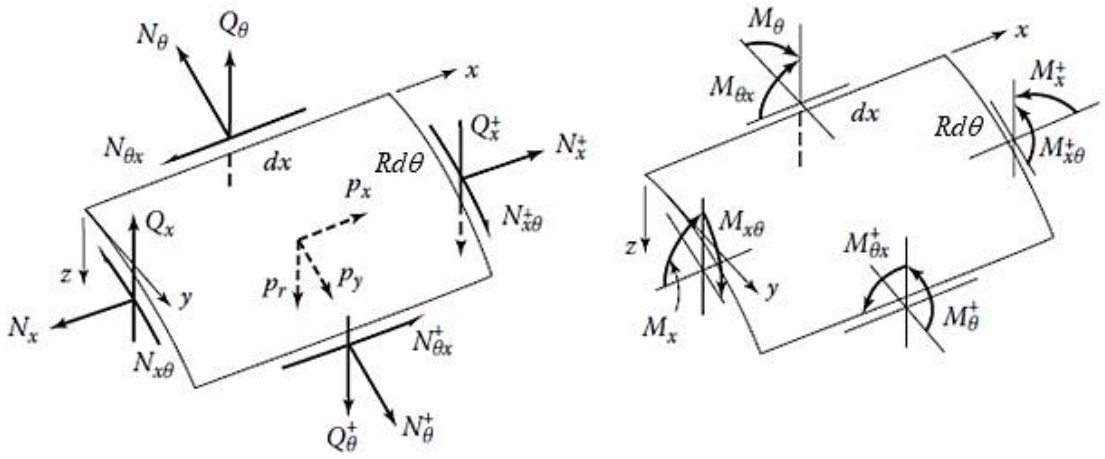

Figure 0.1: Typical differential element of a loaded cylindrical shell

Referring to Figure 3.1

The force equilibrium in the x, y and z directions are:

$$R\frac{\partial N_x}{\partial x}+\frac{\partial N_{\theta x}}{\partial \theta}+P_x\,R=0 \tag{3.1}$$

$$\frac{\partial N_\theta}{\partial \theta}+R\frac{\partial N_{x\theta}}{\partial x}-\ Q_\theta+P_y\,R=0 \tag{3.2}$$

$$\frac{\partial Q_\theta}{\partial \theta}+R\frac{\partial Q_x}{\partial x}+\ N_\theta+P_r\,R=0 \tag{3.3}$$

Note that: the equilibrium equations are already divided by $d_x\ d_\theta$.

The equilibrium of moments about x and y coordinate directions are expressed as follow:

$$\frac{\partial M_\theta}{\partial \theta}+R\frac{\partial M_{x\theta}}{\partial x}-R\,Q_\theta=0 \tag{3.4}$$

$$R\frac{\partial M_x}{\partial x}+\frac{\partial M_{\theta x}}{\partial \theta}-R\,Q_x=0 \tag{3.5}$$

The sixth equilibrium equation, summation of moment about z axis, $\sum \mathrm{M_z} = 0$, leads to an identity which does not add any new information. A special case of a general loaded shell is the uniformly axial loaded shell, where the shell is loaded in compression only. All surface forces are assumed to be very small except N_x. Also, shear forces e.g. Q_x and Q_y might be eliminated. Therefore, equations of equilibrium (3.1-3.5) in cylindrical shells become:

$$R\frac{\partial N_x}{\partial x} + \frac{\partial N_{\theta x}}{\partial \theta} = 0 \tag{3.6}$$

$$\frac{\partial N_\theta}{\partial \theta} + R\frac{\partial N_{x\theta}}{\partial x} + R\,N_x\frac{\partial^2 v}{\partial x^2} - \frac{1}{R}\,\frac{\partial M_\theta}{\partial \theta} - \frac{\partial M_{x\theta}}{\partial x} = 0 \tag{3.7}$$

$$\frac{1}{R}\,\frac{\partial^2 M_\theta}{\partial \theta^2} + 2\,\frac{\partial^2 M_{x\theta}}{\partial x\,\partial \theta} + R\,N_x\,\frac{\partial^2 w}{\partial x^2} + N_\theta = 0 \tag{3.8}$$

Strain-Displacement Relations

Shell mid-surface strains are related to the displacement components by the following kinematic expressions:

$$\varepsilon_x = \frac{\partial u}{\partial x} \tag{3.9}$$

$$\varepsilon_\theta = \frac{1}{R}\frac{\partial v}{\partial \theta} - \frac{w}{R} \tag{3.10}$$

$$\gamma_{x\theta} = \frac{1}{R}\frac{\partial u}{\partial \theta} + \frac{\partial v}{\partial x} \tag{3.11}$$

whereas changes in curvatures and twist are expressed in terms of displacements as:

$$\chi_x = \frac{\partial^2 w}{\partial x^2} \tag{3.12}$$

$$\chi_\theta = \frac{1}{R^2}\left(\frac{\partial v}{\partial \theta} + \frac{\partial^2 w}{\partial \theta^2}\right) \tag{3.13}$$

$$\chi_{x\theta} = \frac{1}{R}\left(\frac{\partial v}{\partial x} + \frac{\partial^2 w}{\partial x\, \partial \theta}\right) \tag{3.14}$$

Middle surface force-strain relations

Stress resultants are explained in terms of middle surface strains:

$$N_x = \frac{E\ t}{1-v^2}[\varepsilon_x + v\ \varepsilon_\theta] \tag{3.15}$$

$$N_\theta = \frac{E\ t}{1-v^2}[\varepsilon_\theta + v\ \varepsilon_x] \tag{3.16}$$

$$N_{x\theta} = \frac{E\ t}{2(1+v)}\ [\gamma_{x\theta}] \tag{3.17}$$

Middle surface moment-curvature relations

By using the plate bending theory, the relationship between bending moments and curvature are derived as:

$$M_x = -D[\chi_x + v\ \chi_\theta] \tag{3.18}$$

$$M_\theta = -D[\chi_\theta + v\ \chi_x] \tag{3.19}$$

$$M_{x\theta} = -\frac{D}{R}(1-v)[\chi_{x\theta}] \tag{3.20}$$

Where D is the stiffness of the shell given by:

$$D = \frac{E\ t^3}{12\ (1 - v^2)} \tag{3.21}$$

Stress resultants

The formulation governing the deflection of cylindrical shells is accomplished by substituting equations (3.9-3.14) into equations (3.15-3.20) resulting in the following stress-resultants and displacements expressions:

$$N_x = \frac{E\ t}{1-v^2}\left[\frac{\partial u}{\partial x} + v\ \left(\frac{1}{R}\ \frac{\partial v}{\partial \theta} - \frac{w}{R}\right)\right] \tag{3.22}$$

$$N_\theta = \frac{E\ t}{1-v^2}\left[\frac{1}{R}\ \frac{\partial v}{\partial \theta} - \frac{w}{R} + v\ \frac{\partial u}{\partial x}\right] \tag{3.23}$$

$$N_{x\theta} = \frac{E\ t}{2(1+v)}\left[\frac{\partial v}{\partial x} + \frac{1}{R}\frac{\partial u}{\partial \theta}\right] \tag{3.24}$$

$$M_x = -D\left[\frac{\partial^2 w}{\partial x^2} + \frac{v}{R^2}\left(\frac{\partial v}{\partial \theta} + \frac{\partial^2 w}{\partial \theta^2}\right)\right] \tag{3.25}$$

$$M_\theta = -D\left[\frac{1}{R^2}\left(\frac{\partial v}{\partial \theta} + \frac{\partial^2 w}{\partial \theta^2}\right) + v\ \frac{\partial^2 w}{\partial x^2}\right] \tag{3.26}$$

$$M_{x\theta} = -\frac{D}{R}(1 - v)\left[\frac{\partial v}{\partial x} + \frac{\partial^2 w}{\partial x\ \partial \theta}\right] \tag{3.27}$$

Differential equations

Now by introducing the elastic law (3.22-3.27) into equilibrium equations (3.6-3.8), in order to express the stress resultants in terms of displacements ($u, v\ and\ w$) and their derivatives. Moreover, the axial compressive force ($N_x = N$) is considered to be positive in compression. Hence, the differential equations of buckling of cylindrical shells are:

$$\frac{\partial^2 u}{\partial x^2} + \frac{1+v}{2R}\frac{\partial^2 v}{\partial x \partial \theta} - \frac{v}{R}\frac{\partial w}{\partial x} + \frac{1-v}{2R^2}\frac{\partial^2 u}{\partial \theta^2} = 0 \tag{3.28}$$

$$\frac{1+v}{2R}\frac{\partial^2 u}{\partial x \partial \theta} + \frac{1-v}{2}\frac{\partial^2 v}{\partial x^2} + \frac{1}{R^2}\frac{\partial^2 v}{\partial \theta^2} - \frac{1}{R^2}\frac{\partial w}{\partial \theta} - \frac{N(1-v^2)}{Et}\frac{\partial^2 v}{\partial x^2} + \frac{t^2}{12R^2}\left[\frac{1}{R^2}\frac{\partial^2 v}{\partial \theta^2} + \frac{1}{R^2}\frac{\partial^3 w}{\partial \theta^3} + \frac{\partial^3 w}{\partial x^2 \partial \theta} + (1-v)\frac{\partial^2 v}{\partial x^2}\right] = 0 \tag{3.29}$$

$$v\frac{\partial u}{\partial x} + \frac{1}{R}\frac{\partial v}{\partial \theta} - \frac{w}{R} - \frac{t^2}{12R^2}\left[\frac{1}{R}\frac{\partial^3 v}{\partial \theta^3} + (2-v)R\frac{\partial^3 v}{\partial x^2 \partial \theta} + R^3\frac{\partial^4 w}{\partial x^4} + \frac{1}{R}\frac{\partial^4 w}{\partial \theta^4} + 2R\frac{\partial^4 w}{\partial x^2 \partial \theta^2}\right] - \frac{N\,R\,(1-v^2)}{E\,t}\frac{\partial^2 w}{\partial x^2} = 0 \tag{3.30}$$

3.2.2 Equilibrium Equation for Axi-Symmetric Buckling

In case of axi-symmetrically loaded circular cylindrical shells, the general differential equations are reduced to a single ordinary differential equation because of symmetry. The circumferential force (N_θ) and moment (M_θ) do not vary with θ. Thus, the circumferential displacement (v) vanishes and only the axial and radial (u and w) displacements are considered and they are function of x only. The derivation of the governing equation is illustrated below.

Let us assume that the shell is axi-symmetrically loaded, and displacements functions are given by:

$$u = \mathrm{u(x)}, \quad v = 0 \text{ and } w = \mathrm{w(x)}$$

where u is the axial displacement, v is the circumferential displacement and w is the radial displacement. By substitution of the above displacement fields into equilibrium equations (3.4 and 3.6), the following expressions are obtained:

$$\frac{du}{dx} = \frac{\nu}{R}\,\mathrm{w\,(x)} \tag{3.31}$$

$$-\frac{w}{R} + \nu\,\mathrm{U'(x)} - \frac{R\,N\,(1-\nu^2)}{E\,t}\frac{d^2w}{dx^2} - \frac{1}{12}R\,t^2\frac{d^4w}{dx^4} = 0 \tag{3.32}$$

Now introducing Eq. 3.31 into Eq. 3.32, the governing equation becomes:

$$D\frac{d^4w}{dx^4} + N\frac{d^2w}{dx^2} + \frac{E\,t}{R^2}w = 0 \tag{3.33}$$

3.3 Elastic Buckling of CFRP-Stiffened Cylindrical Shells

The CFRP fibers are assumed to run in the circumferential direction and snice it circumferential elastic modulus is much larger than its modulus in the axial direction, we can neglect the contribution of CFRP sheet in resisting the axial buckling and therefore only the term $E_f\ t_f$ will be added to the last term of equation (3.33).The governing equation of elastic buckling of stiffened cylindrical shells becomes:

$$D_s \frac{d^4w}{dx^4} + N \frac{d^2w}{dx^2} + \frac{E_s\ t_s}{R^2}\ (1 + n\ \alpha)\ w = 0 \tag{3.34}$$

where

$$\alpha = \frac{E_f\ t_f}{E_s\ t_s} \tag{3.35}$$

The subscripts s and f are used here to denote the stainless steel tube and CFRP, respectively and n is the number of CFRP layers.

3.4 Plastic Buckling of Unstiffened Cylindrical Shells

3.4.1 Constitutive Equations

The shell membrane strains are related to the displacement components by the following kinematic expressions:

$$\varepsilon_{x0} = \frac{du}{dx} \tag{3.36}$$

$$\varepsilon_{\theta 0} = \frac{w}{R} \tag{3.37}$$

whereas changes in curvature occur only in x and expressed in terms of displacements as:

$$\kappa_x = \frac{\partial^2 w}{\partial x^2} \tag{3.38}$$

Hence the total strains in terms of displacement are:

$$\varepsilon_x = \varepsilon_{x0} - z\,\kappa_x \tag{3.39}$$

$$\varepsilon_\theta = \varepsilon_{\theta 0} = \frac{w}{R} \tag{3.40}$$

According to the theory of deformation plasticity [24], the stress-strain relations can be written as

$$\sigma_x = C_{11}\,\varepsilon_x + C_{12}\,\varepsilon_\theta \tag{3.41}$$

$$\sigma_\theta = C_{12}\,\varepsilon_x + C_{13}\,\varepsilon_\theta \tag{3.42}$$

Where C_{11}, C_{12} and C_{13} are functions of the elastic modulus, the tangential modulus, the secant modulus and Poisson's ratio, the derivation of which is explained in Appendix A. The obtained expressions of these functions are;

$$C_{11} = \frac{E\,(\lambda + 3e + 3)}{\lambda(5 + 3e - 4v) - (1 - 2v)^2} \tag{3.43}$$

$$C_{12} = \frac{2E\,(\lambda - 1 + 2\mathcal{V})}{\lambda(5 + 3e - 4v) - (1 - 2v)^2} \tag{3.44}$$

$$C_{13} = \frac{4E\,\lambda}{\lambda(5 + +3e - 4v) - (1 - 2v)^2} \tag{3.45}$$

where the parameters e and λ are:

$$e = \frac{E}{E_s} - 1 \tag{3.46}$$

$$\lambda = \frac{E}{E_t} \tag{3.47}$$

In which E_s is the secant modulus and given by the following relation:

$$E_s = \frac{\sigma}{\varepsilon} \tag{3.48}$$

And E_t is the tangent modulus and expressed as:

$$E_t = \frac{d\sigma}{d\varepsilon} \tag{3.49}$$

The secant and tangent modulus's can be obtained from the uniaxial stress-strain relation of the material represented by Ramberg-Osgood model. The Membrane forces become:

$$N_x = \int_{-t/2}^{t/2} \sigma_x \, dz = \frac{C_{12}\, t\, w}{R} + C_{11}\, t \frac{du}{dx} \tag{3.50}$$

$$N_\theta = \int_{-t/2}^{t/2} \sigma_\theta \, dz = \frac{C_{13}\, t\, w}{R} + C_{12}\, t \frac{du}{dx} \tag{3.51}$$

The bending moments become:

$$M_x = \int_{-t/2}^{t/2} \sigma_x \, z \, dz = -\frac{1}{12}\, C_{11}\, t^3\, \frac{d^2w}{dx^2} \tag{3.52}$$

$$M_\theta = \int_{-t/2}^{t/2} \sigma_\theta \, z \, dz = -\frac{1}{12}\, C_{12}\, t^3 \frac{d^2w}{dx^2} \tag{3.53}$$

For axially loaded circular cylindrical shells, plastic buckling is expected to be in the form of rings (axi-symmetric), The equilibrium equations are:

Equilibrium of forces along x :

$$\frac{\partial N_x}{\partial x} = 0 \tag{3.54}$$

Equilibrium of forces along z :

$$R\frac{\partial Q_x}{\partial x} + R\,N_x\frac{\partial^2 w}{\partial x^2} + N_\theta \tag{3.55}$$

Equilibrium of moments about y :

$$R\frac{\partial M_x}{\partial x} + \frac{\partial M_{\theta x}}{\partial \theta} - R\,Q_x = 0 \tag{3.56}$$

However, the rest of equilibrium equation are already satisfied because of symmetry.

By substitution of Eq. (3.50) into Eq. (3.54):

$$\frac{C_{12}\,t}{R}\,\frac{dw}{dx} + C_{11}\,t\,\frac{d^2u}{dx^2} = 0 \tag{3.57}$$

and substituting Eq. 3.51 into Eq. 3.55:

$$\frac{C_{13}\,t}{R}\,w + R\,Qx'(x) + C_{12}\,t\,\frac{du}{dx} + N\,R\frac{d^2w}{dx^2} = 0 \tag{3.58}$$

Also, substituting Eq. (3.52) into Eq. (3.56):

$$R\,\mathrm{Qx}(x) - \frac{1}{12}C_{11}\,R\,t^3\,\frac{d^3w}{dx^3} = 0 \tag{3.59}$$

Integrating Eq. (3.57) yields to:

$$\frac{du}{dx} = -\frac{C_{12}\, t}{C_{11}\, t\, R}\, w \tag{3.60}$$

Now differentiate Eq. (3.59) w.r.t. x and then substitute it back into Eq. (3.58), leading to the following expression:

$$\frac{C_{13}\, t}{R} w + C_{12}\, t\, \frac{du}{dx} + N\, R\, \frac{d^2w}{dx^2} = \frac{1}{12}\, C_{11}\, R\, t^3 \frac{d^4w}{dx^4} \tag{3.61}$$

By Substitution of Eq. (3.60) into Eq. (3.61) results in the following general governing equation:

$$\frac{C_{11}\, t^3}{12}\frac{d^4w}{dx^4} + \mathrm{N}\ \frac{d^2w}{dx^2} + \left(C_{13} - \frac{{C_{12}}^2}{C_{11}}\right)\frac{t}{R^2}\ \ w = 0 \tag{3.62}$$

3.5 Plastic Buckling of CFRP-Stiffened Cylindrical Shells

Similar to stiffened cylindrical shells in elastic buckling, the parameter α refers to the relative $(E\ t)$ of steel to that in CFRP. However, herein the modulus elasticity is $C_{13} - \frac{{C_{12}}^2}{C_{11}}$. Hence, the governing equation of plastic buckling of CFRP-stiffened cylindrical shells is given by:

$$\frac{C_{11}\, t^3}{12}\frac{d^4w}{dx^4} + \mathrm{N}\ \frac{d^2w}{dx^2} + \left(C_{13} - \frac{{C_{12}}^2}{C_{11}}\right)\frac{t_s}{R^2}\ \ (1 + n\,\alpha)\ \ w = 0 \tag{3.63}$$

3.6 Analytical, Numerical & Computational Tools

Exact solutions for buckling problems are either too difficult or impossible, especially for nonlinear cases such as those involving plastic buckling. In this study, the following tools

will be utilized to perform various tasks of symbolic and numerical computation throughout all stages of the study starting from the formulation to the analysis up to the verification of the obtained results.

3.6.1 Ritz Method

This energy-based method is an alternative and efficient way of obtaining the analytical solutions for various boundary value problems in structural mechanics. In this research, all the analytical solutions are derived using Ritz method. This method was given the name after the Swiss mathematician scientist Walther Ritz. The application of the method leads to approximate but fairly accurate solution by using the principal of minimum potential energy (Π). The potential energy is given by the following expression:

$$\Pi = \mathrm{U} - \mathrm{W} \tag{3.64}$$

where

U: strain energy stored in an elastic body

W: work done by external forces

The steps of finding the analytical solution are as follow: firstly, a deflection function is assumed in which the geometric boundary conditions of the shell should be satisfied. This deflection function (w) is in the form of a series:

$$w = c_i \, f(x, y, \theta, \dots) \tag{3.65}$$

Secondly, the principal of minimum potential energy is used to obtain the values of c_i . Since Π is minimum at equilibrium, the following condition should be obtained:

$$\frac{\partial \Pi}{\partial c_i} = 0 \;\Rightarrow\; \frac{\partial}{\partial c_i}(\mathrm{U} - \mathrm{W}) = 0 \qquad i = 1,2,3,\ldots,\mathrm{n} \tag{3.66}$$

The coefficient variable c_i is obtained by solving equation (3.66), hence the function w can be fully expressed. However, Ritz method has an advantage over other methods in which the solution can be obtained by satisfying the essential geometrical boundary conditions e.g. deflection and slope only. Equation (3.66) requires the computation of the strain energy which is discussed below.

For a general state of stress, the strain energy stored in an elastic body is given as:

$$\mathrm{U} = \iiint_V \left[\left(\sigma_x \varepsilon_x + \sigma_y \varepsilon_y + \sigma_z \varepsilon_z + \tau_{xy}\gamma_{xy} + \tau_{xz}\gamma_{xz} + \tau_{yz}\gamma_{yz}\right)\right] dx\, dy\, dz \tag{3.67}$$

As discussed earlier for the assumption of thin shells, the following terms $\sigma_z, \gamma_{xz}\ and\ \gamma_{yz}$ may be omitted. Now introducing Hook's law, the above form Eq. (3.67) reduces to include only stresses and Elastic constants as follow:

$$\mathrm{U} = \iiint_V \left[\frac{1}{2\,E}\left(\sigma_x^2 + \sigma_y^2 - 2\,\sigma_x\sigma_y\right) + \frac{1}{2\,G}\tau_{xy}^2\right] dx\ \ dy\, dz \tag{3.68}$$

Note that the $x, y\ and\ z$ coordinates are preferred in plates analysis; while for shells, the cylindrical system is preferred.

There are two main components of strain energy of deformed shells namely membrane-strain energy due to stretching (U_m) and bending-strain energy due to bending (U_b)

$$\mathrm{U} = U_m + U_b \tag{3.69}$$

The membrane-strain energy is accompanied with stretching of the mid-surface that is initiated by the in-plane forces:

$$U_m = \frac{1}{2}\iint_A [[(N_x\ \varepsilon_x) + (N_y\ \varepsilon_y) + (N_{xy}\ \varepsilon_{xy})]\ dx\ dy \tag{3.70}$$

where A is the shell surface area.

The bending strain energy is dependent on the change of curvature and given by:

$$U_b = \frac{1}{2} D \iint_A \left[(\chi_x + \chi_y)^2 - 2(1-v)(\chi_x \chi_y - \chi_{xy}^2)\right] dx\ dy \tag{3.71}$$

3.6.2 Wolfram Mathematica

Wolfram Mathematica, also termed as Mathematica, is a symbolic mathematical computation software which was produced by Wolfram company. It allows users to carry out algebraic calculations and derive solutions for eigenvalue problems, such as buckling of shells, symbolically. It is a very powerful program that has an extensive range of applications in many engineering fields with the advantage of saving time and engine while computing symbolic mathematical functions. It can plot and visualize 2 and 3-dimentional problems and graphs. Also, it can be utilized as a very sophisticated calculator while the language of this program is considered to be easy and understandable. It is also easy to use in terms of coding and programing. The aforementioned points are the prime reasons of selecting this program as a core tool in this research. In this study, Mathematica will be used extensively to develop various buckling formulations and the implementation of Ritz method for computing the buckling load for various cases (elastic/plastic and stiffened/unstiffened, etc.).

3.6.3 FEM ABAQUS

Finite element method (FEM) is a numerical approach utilized to approximately solve engineering and mathematical physical problems, e.g. partial differential equations (PDEs) describe physical phenomena. The concept of FEM is basically dividing the body into finite elements, the finer the elements the more accurate the results. There are several tools used for finite element analysis (FEA), however, herein ABAQUS commercial software was employed.

ABAQUS is a finite element-based commercial software package. It is a general-purpose solver and simulation software which consists of three core products: Abaqus/Standard, Abaqus/Explicit and Abaqus/CAE. The first type is a general-purpose solver that solves finite element analysis (FEA) using a traditional implicit integration while the second one solves nonlinear transient dynamic by using traditional explicit integration scheme. However, the last type provides an integrated model and visualization for the analysis product (Preprocessing and Postprocessing). Moreover, it is used for solving unlimited number of engineering and physics applications either academic, research or industrial application. One of these applications is the buckling analysis of shells, which is mainly used in this research to verify the analytical solution obtained by Ritz method.

CHAPTER 4

ELASTIC BUCKLING OF CYLINDRICAL SHELLS

4.1 Symmetrical Elastic Buckling of Unstiffened SSCS

The governing equation of elastic axi-symmetric buckling of unstiffened cylindrical shells has been derived in Chapter 3 which is given by:

$$D\frac{d^4w}{dx^4} + N\frac{d^2w}{dx^2} + \frac{E\,t}{R^2}w = 0 \tag{4.1}$$

Where D is the bending rigidity, w is the deformation of local buckling, x is the axial coordinates, N is the uniform axial loading (Positive in compression), E is the elastic modulus, t is the thickness of cylindrical shell and R is the radius. In a case of simply supported cylindrical shell, the radial deflection function that is satisfying boundary conditions is given by [36]:

$$w = c\,sin\frac{m\,\pi\,x}{L} \tag{4.2}$$

In this formula, c is a constant, m is an integer and refers to the number of half sine waves and L is the shell length. To clarify the buckling phenomena, a graphical solution is shown in Figure 4.1 (where L_w is half sine wave length and N_{cr} is the critical uniform axial load).

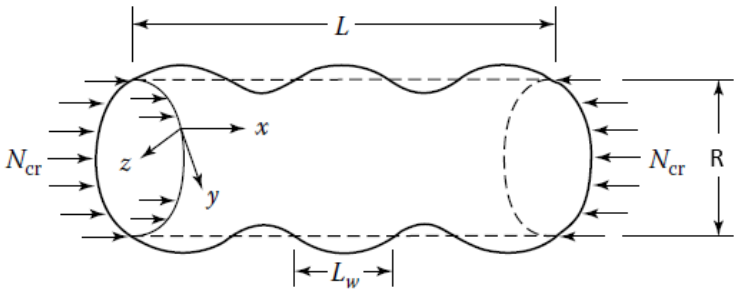

Figure 0.1: Deformed cylindrical shell under axial compression, where dashed lines show the original shape [37]

4.1.1 Critical Buckling Load Based on Equilibrium

By substituting the radial deflection function (Eq. 4.2) into the governing equation (4.1) and by solving the equation with respect to N; the buckling load can be found as:

$$N = \frac{R^2 \, \mathrm{D} \, m^4\pi^4 + \mathrm{E} \, L^4 \, t}{R^2 L^2 m^2 \pi^2} \tag{4.3}$$

Taking the stationary condition of Eq. (4.3), by equating the derivative of the equation to zero with respect to number of waves (m):

$$m = \frac{\mathrm{E}^{1/4} \, L \, t^{1/4}}{\sqrt{R} \, \mathrm{D}^{1/4} \, \pi} \tag{4.4}$$

By substituting Eq. (4.4) into Eq. (4.3), and noting that $D = \frac{\mathrm{E} \, t^3}{12(1-\nu^2)}$; the critical buckling load is found to be:

$$N_{cr} = \frac{\mathrm{E} \, t^2}{R \sqrt{3(1-\nu^2)}} \tag{4.5}$$

4.1.2 Critical Buckling Load Based on Energy Method

The membrane strains after buckling are given by:

$$\varepsilon_x = -\nu \frac{w}{R} \tag{4.6}$$

$$\varepsilon_\theta = \frac{w}{R} \tag{4.7}$$

The membrane stresses after buckling are:

$$\sigma_x = -\frac{N}{t} \tag{4.8}$$

$$\sigma_\theta = E\ \epsilon_\theta \tag{4.9}$$

Membrane strain energy per unit volume is given by:

$$u_m = \sigma_x\ \epsilon_x + \frac{1}{2}\ \sigma_\theta\ \epsilon_\theta \tag{4.10}$$

The membrane strain energy can be obtained by integrating over the volume to get:

$$\mathrm{U}_m = 2\pi\ R\ t\ \int_0^L u_m\ dx = \frac{L\ c\ (E\ m\ t\ c\ \pi + 4(-1 + (-1)^m) R\ N\ \nu)}{2\ R\ m} \tag{4.11}$$

The bending strain energy per unit volume is given by:

$$u_b = \frac{D}{2}\ {w_{xx}}^2 \tag{4.12}$$

where $w_{xx} = \frac{d^2 w}{dx^2}$

The bending strain energy can be obtained by integrating over the volume to get:

$$\mathrm{U}_b = 2\pi\ R\ t\ \int_0^L u_b\ dx = \frac{R\ D\ \ t\ c^2\ m^4\ \pi^5}{2\ L^3} \tag{4.13}$$

Work due to membrane strain is given by:

$$\mathrm{W1} = 2\pi\, R\, N \int_0^L \frac{{w_x}^2}{2}\, dx = \frac{R\ \mathrm{Nc}^2 m^2\, \pi^3}{2\, L} \tag{4.14}$$

where $w_x = \frac{dw}{dx}$

Work due to bending strain is given by:

$$\mathrm{W2} = 2\pi\, R\, N \int_0^L \nu \frac{w}{R}\, dx = \frac{2\, L\, (-1 + (-1)^m)\, N\, c\, \nu}{m} \tag{4.15}$$

Applying conservation of energy principle and solving it for buckling load (N).

$$\mathrm{U} - \mathrm{W} = 0 \Rightarrow \mathrm{U}_m + \mathrm{U}_b = \mathrm{W1} + \mathrm{W2}$$

$$N = \frac{(E\, L^4 + D\, m^4 \pi^4 R^2) t}{R^2\, L^2 m^2 \pi^2} \tag{4.16}$$

By setting the derivative of the obtained buckling load (N) with respect to number of waves (buckling mode, m) to be equal to zero.

$$m = \frac{\mathrm{E}^{1/4}\, L\, t^{1/4}}{\sqrt{R}\, \mathrm{D}^{1/4}\, \pi} \tag{4.17}$$

By substituting Eq. (4.17) back into Eq. (4.16), the critical buckling load is found to be:

$$N_{cr} = \frac{E\, t^2}{R\, \sqrt{3(1 - \nu^2)}} \tag{4.18}$$

It can be noted that the critical buckling load obtained by the energy method is identical to the load obtained by equilibrium; Also, it is similar to the critical buckling load obtained

by Timoshenko [13]. The theoretical elastic buckling stress is simply the critical buckling load divided by the thickness of the shell, which is given as:

$$\sigma_{cr} = \frac{E}{(R/t)\sqrt{3(1-v^2)}} \tag{4.19}$$

For $v = 0.3$, the theoretical buckling stress is approximately equal:

$$\sigma_{cr} \approx 0.6\frac{E}{(R/t)} \tag{4.20}$$

The axisymmetric critical buckling stress formula is controlled by radius-to-thickness $(\mathrm{R/t})$ ratio regardless of the length of the shell. It is used when $\mathrm{R/t}$ ratio is greater than $\frac{E}{\sqrt{3}\sqrt{1-\nu^2}\sigma y}$, and for perfect shells that do not have imperfections. However, it has been proven through experiments that the buckling stress obtained experimentally is far away below the theoretical stress [2], [38].Because of that a correction factors, also known as knockdown factor, is utilized for practical uses in the design of shells. Figure 4.2 displays experimental data (scattered) obtained from several tests and an empirical equation that defines the lower bound of the results obtained. Knockdown factor (C) is a correction of the theoretical buckling solution and given by equation 4.21 [38]. Figure 4.3 shows the variance between the theoretical buckling stress and buckling stress that is used in design of shells.

$$C = 1 - 0.9\left(1 - e^{\left(-\frac{1}{16}\right)\sqrt{\frac{R}{t}}}\right) \tag{4.21}$$

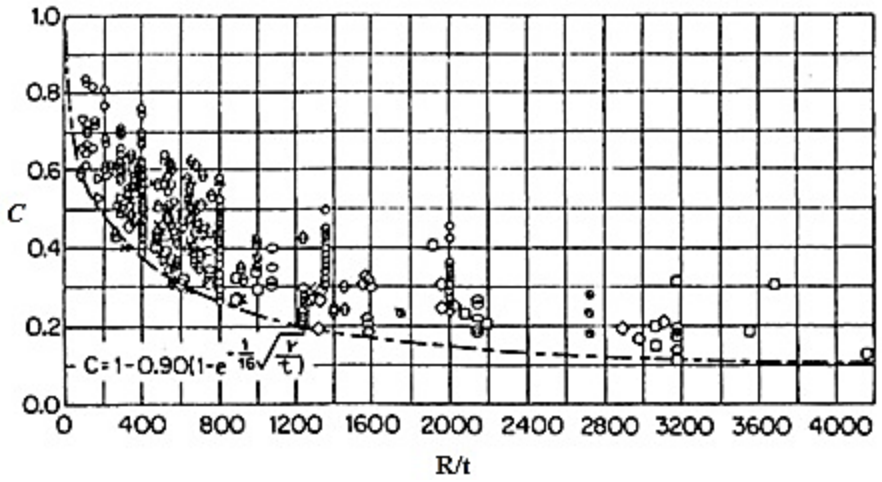

Figure 0.2: Buckling stresses obtained experimentally (scattered) and empirical equation of lower bound (dashed) [38].

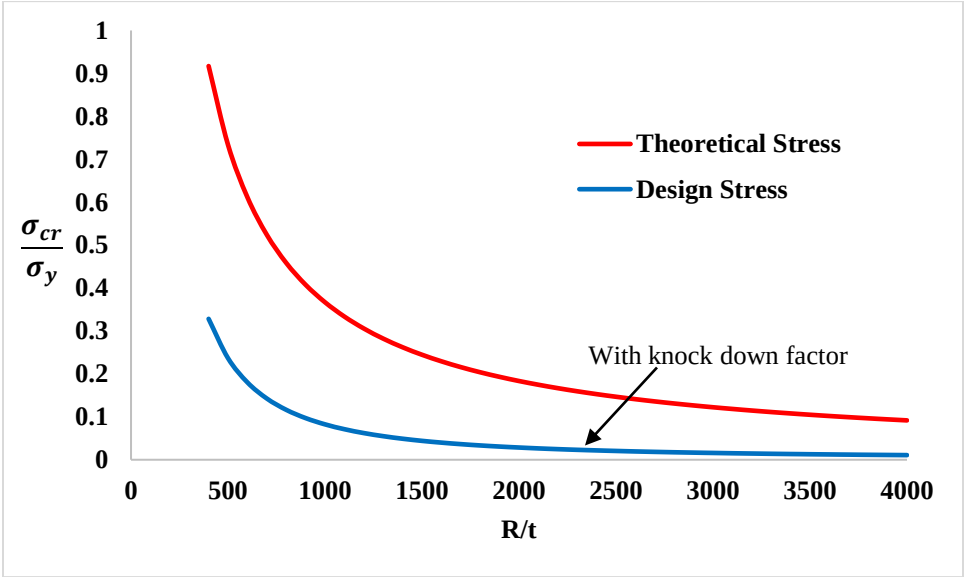

Figure 0.3: The variance between theoretical stress and design stress

From the figures above, it can be concluded that the theoretical axisymmetric buckling stress is dangerously an overestimation of the actual/experimental critical stress. The wide gap between the two values is attributed to three main reasons: 1) Any slight imperfection in the shell can lead to a large reduction in the buckling; 2) the above obtained classical buckling load is based on small deflection theory while the shell could be subjected to finite

deformation prior to buckling; 3) The above formula assumes axi-symmetric buckling, while non-symmetric buckling is likely to take place at a lower buckling load as will be discussed in the next section.

4.2 Non-Symmetrical Elastic Buckling of Unstiffened SSCS

4.2.1 Differential Equations

Thin cylindrical shells often fail by buckling and most probably in a non-symmetrical mode. Let us consider a cylindrical shell that is subjected to axial compression load and initial imperfections are considered to be small, in other words neglected. Hence, all surface forces are assumed to be very small except N_x.

For simplification purposes of the differential equations obtained in chapter 3 equations (3.28- 3.30), the following dimensionless parameters are introduced:

$$\alpha = \frac{t^2}{12\,R^2} \qquad q = \frac{N\,(1-v^2)}{E\,t}$$

Finally, the differential equations of buckling of cylindrical shells become:

$$\frac{\partial^2 u}{\partial x^2} + \frac{1+v}{2R}\frac{\partial^2 v}{\partial x \partial \theta} - \frac{v}{R}\frac{\partial w}{\partial x} + \frac{1-v}{2R^2}\frac{\partial^2 u}{\partial \theta^2} = 0 \tag{4.22}$$

$$\begin{aligned}\frac{1+v}{2R}\frac{\partial^2 u}{\partial x \partial \theta} + \frac{1-v}{2}\frac{\partial^2 v}{\partial x^2} + \frac{1}{R^2}\frac{\partial^2 v}{\partial \theta^2} - \frac{1}{R^2}\frac{\partial w}{\partial \theta} - q\,\frac{\partial^2 v}{\partial x^2} \\ + \alpha\left[\frac{1}{R^2}\frac{\partial^2 v}{\partial \theta^2} + \frac{1}{R^3}\frac{\partial^3 w}{\partial \theta^3} + \frac{\partial^3 w}{\partial x^2 \partial \theta} + (1-v)\frac{\partial^2 v}{\partial x^2}\right] = 0\end{aligned} \tag{4.23}$$

$$v\frac{\partial u}{\partial x}+\frac{1}{R}\frac{\partial v}{\partial \theta}-\frac{w}{R}-\alpha\left[\frac{1}{R}\frac{\partial^3 v}{\partial \theta^3}+(2-v)R\frac{\partial^3 v}{\partial x^2\partial\theta}+R^3\frac{\partial^4 w}{\partial x^4}+\frac{1}{R}\frac{\partial^4 w}{\partial \theta^4}+2R\frac{\partial^4 w}{\partial x^2\partial\theta^2}\right] - R\,q\frac{\partial^2 w}{\partial x^2}=0 \tag{4.24}$$

It can be shown, easily, that the above equations reduce to those for axi-symmetric case if the circumferential displacement (v) is set to zero and all derivatives with respect to θ are set to zero.

4.2.2 Analytical Solution for Nonsymmetrical Elastic Buckling of SSCS

Consider the differential equations of buckling of uniformly compressed cylindrical shells (4.22-4.24). To find their solution, let the coordinates' origin placed at one end of the shell, then the general solution of the differential equations is expressed by the following displacement fields:

$$u=c_1\frac{x}{v\,R}+c_2+\sum_m^\infty\sum_n^\infty A_{mn}\sin(n\theta)\cos\left(\frac{m\pi x}{L}\right) \tag{4.25}$$

$$v=\sum_m^\infty\sum_n^\infty B_{mn}\cos(n\theta)\sin\left(\frac{m\,\pi\,x}{L}\right) \tag{4.26}$$

$$w=c_1+\sum_m^\infty\sum_n^\infty C_{mn}\sin(n\theta)\sin\left(\frac{m\pi x}{L}\right) \tag{4.27}$$

where m is the number of half sine waves along the length of the shell, n is the number of full waves in the transverse (hoop direction), both m and n are integers; A_{mn}, B_{mn} and C_{mn} are unknown buckling amplitudes. Note that the constants $c_1$and c_2 do not play a role in the final solution for buckling because they will disappear after carrying out the differential operators in equations (4.22-4.24) By substituting

equations (4.25-4.27) into (4.22-4.24) and denoting that β notation is termed for $m\pi R/L$; The following linear (algebraic) equations are obtained:

$$A_{mn}\left(\beta^2+\frac{1-v}{2}n^2\right)+B_{mn}\frac{n(1+v)\beta}{2}+C_{mn}v\beta=0 \tag{4.28}$$

$$\begin{aligned}A_{mn}&\frac{n(1+v)\beta}{2}\\&+B_{mn}\left[(1-v)\left(\frac{1}{2}+\frac{t^2}{12R^2}\right)\beta^2+\left(1+\frac{t^2}{12R^2}\right)n^2\right.\\&\left.-\frac{N(1-v^2)}{Et}\beta^2\right]+C_{mn}n\left[1+\frac{t^2}{12R^2}(n^2+\beta^2)\right]=0\end{aligned} \tag{4.29}$$

$$\begin{aligned}&A_{mn}v\beta+B_{mn}n\left\{1+\frac{t^2}{12R^2}[n^2+(2-v)\beta^2]\right\}\\&+C_{mn}\left[1-\frac{N(1-v^2)}{Et}\beta^2+\frac{t^2}{12R^2}(n^2+\beta^2)^2\right]=0\end{aligned} \tag{4.30}$$

The buckling condition of the shell is solved as an eigenvalue problem. In other words, the buckling loads and their corresponding buckling modes are determined by setting the determinant of coefficients of equations (4.28-4.30) equal to zero.

The coefficient matrix is obtained to be:

$$\begin{pmatrix}\beta^2+\frac{1}{2}n^2\,(1-\nu) & \frac{1}{2}n\,\beta\,(1+\nu) & \beta\,\nu\\ \frac{1}{2}n\,\beta\,(1+\nu) & n^2\left(1+\frac{t^2}{12R^2}\right)+\left(\frac{1}{2}+\frac{t^2}{12R^2}\right)\beta^2(1-\nu)-\frac{\beta^2(1-\nu^2)\sigma_{cr}}{\mathrm{E}} & n\left(1+\frac{t^2(n^2+\beta^2)}{12R^2}\right)\\ \beta\,\nu & n\left(1+\frac{t^2\left(n^2+\beta^2(2-\nu)\right)}{12\,R^2}\right) & 1+\frac{t^2(n^2+\beta^2)^2}{12\,R^2}-\frac{\beta^2(1-\nu^2)\,\sigma_{cr}}{\mathrm{E}}\end{pmatrix}$$

where $\frac{N}{t}$ has been replaced by σ_{cr}. The equation resulted from setting the determinate of the above matrix to zero is complicated and highly non-linear. Furthermore, it involves a

constraint on the numbers of half modes m and n to be positive integers. Mathematica offer an efficient built-in function called “Minimize” which searches for the minimum buckling load while satisfying the above constraint. The obtained analytical solution was checked with the exact solution obtained by Wang [37] and it was exactly matching. Since the analytical solution is too lengthy, it has been placed in Appendix B along with the corresponding Mathematica code. The solution is simplified by Timoshenko [13], neglecting higher order terms containing $\propto^2$ and q^2 because they are small when compared to unity and therefore, the solution may be expressed as:

$$\sigma = \frac{E}{1-v^2}\frac{\Phi}{\psi} \tag{4.31}$$

where:

$$\Phi = (1-v^2)\beta^4 + \frac{1}{12\left(\frac{R}{t}\right)^2}((n^2+\beta^2)^4 - (3-v)(2+v)n^2\beta^4 + 2(1-v^2)\beta^4 - (7 + v)n^4\beta^2 + n^4 - 2n^6)$$

$$\psi = \beta^2((n^2+\beta^2)^2 + (n^2+\frac{2}{1-v}\beta^2)(1+\frac{1}{12\left(\frac{R}{t}\right)^2}(n^2+\beta^2)^2) - \frac{2v^2\beta^2}{1-v} + \frac{1}{12\left(\frac{R}{t}\right)^2}(n^2+\frac{2}{1-v}\beta^2)(n^2+(1-v)\beta^2))$$

The solution is further simplified by taking the minimum value of the stress (σ) when both β^2 and n^2 are large numbers, equation (4.31) is further simplified to become:

$$\sigma = \frac{E}{1-v^2}\left(\frac{1}{12\left(\frac{R}{t}\right)^2}\frac{(n^2+\beta^2)^2}{\beta^2}+\frac{(1-v^2)\beta^2}{(n^2+\beta^2)^2}\right) \tag{4.32}$$

Both simplified solutions given by Eqs. 4.31 and 4.32 are conservative and they are functions of the geometric parameters L/R and R/t, the mode numbers m and n and the material properties. The remaining step is to minimize the obtained expressions for σ with respect to the mode numbers m and n. This task along with further simplification to get more suitable and simple design formulas are discussed in the next section.

4.2.3 Simplified Buckling Formulas for Non-Symmetric Elastic Buckling

As mentioned earlier, the non-symmetric solution for the buckling stress is lengthy and not suitable for design. Furthermore, it needs to be minimized with respect to the mode numbers m and n. The procedure involves lengthy computations and therefore have been placed in Appendix B which contains two Mathematica codes for that purpose. The first code utilizes the built-in function "Minimize" and includes the statements that explain the procedure and the final symbolic, numerical and graphical solution for buckling. The second code uses the built-in function "FindFit" to fit the variation of σ_{cr} which is a complicated and lengthy function of L/R and R/t with simple polynomials. A typical 3-D plot which has been generated to study the variation of the buckling stress with L/R and R/t is shown in Figure 4.4.

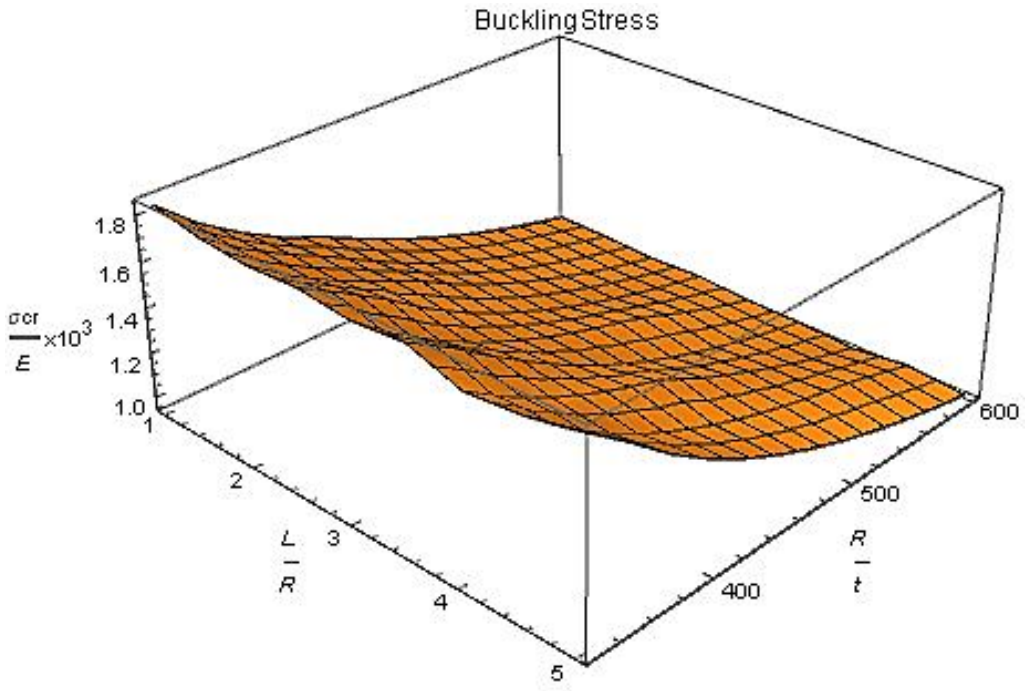

Figure 0.4: Buckling stress of different geometric ratios

After several trials, the following two simple have been found to fit the complicated analytical solutions with minimum errors:

$$\sigma_{cr} = \frac{c_1}{(\mathrm{R/t})}\left(\frac{\mathrm{L}}{\mathrm{R}}\right)^{c_2} \tag{4.33}$$

$$\sigma_{cr} = c_1\left(\frac{\mathrm{R}}{\mathrm{t}}\right)^{c_2}\left(\frac{\mathrm{L}}{\mathrm{R}}\right)^{c_3} \tag{4.34}$$

A typical plot that shows the fitting of the analytical solution (solid surface) with one of the above simple models (the dots) is sown in Figure 4.5.

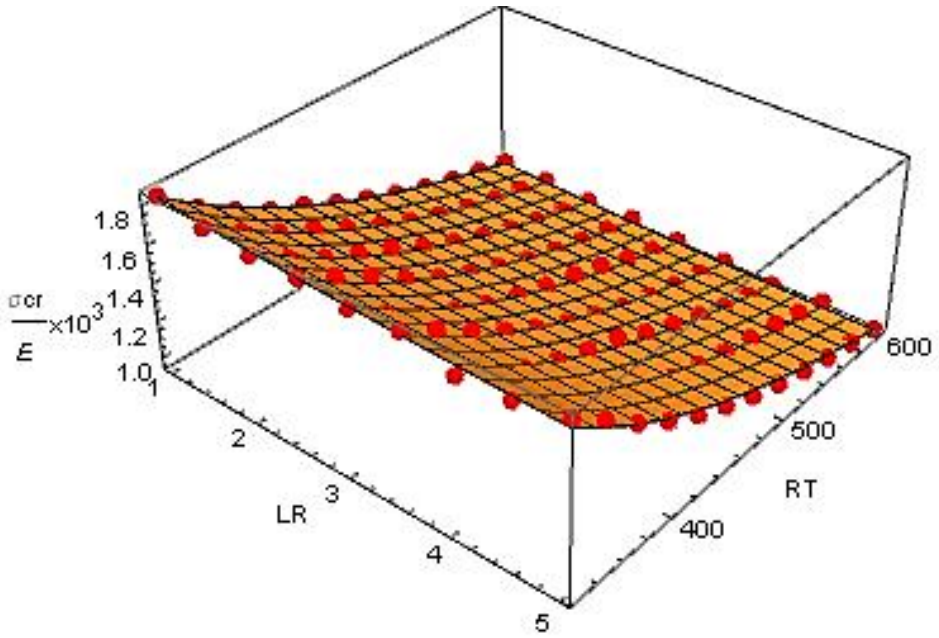

Figure 0.5: An example of fitted buckling stresses with the compact model, dotted points indicate the fitted data

The results of the minimization and fitting computations (see Appendix B) produced the following design models:

For $1 < L/R < 5$ *and* $325 < R/t < 600$:

$$\sigma_{cr} = \frac{600.42}{(R/t)} \left(\frac{L}{R}\right)^{-0.0297} \tag{4.35}$$

For $6 < L/R < 10$ *and* $325 < R/t < 600$:

$$\sigma_{cr} = 534.79 \left(\frac{L}{R}\right)^{-.033} \left(\frac{R}{t}\right)^{-0.983} \tag{4.36}$$

Models for R/t> 600 do not have civil engineering applications and therefore, were not included. To summarize, Figure 4.6 shows the theoretical (symmetrical buckling) in red and design model (with knock down factor) in green and the dotted points indicate the non-symmetrical buckling of different L/R ratios at same R/t ratio. As can be seen that the nonsymmetrical buckling is more critical than the symmetrical buckling and it can reduce the buckling stress up to approximately 50%. This brings the buckling stress much closer to the experimental buckling.

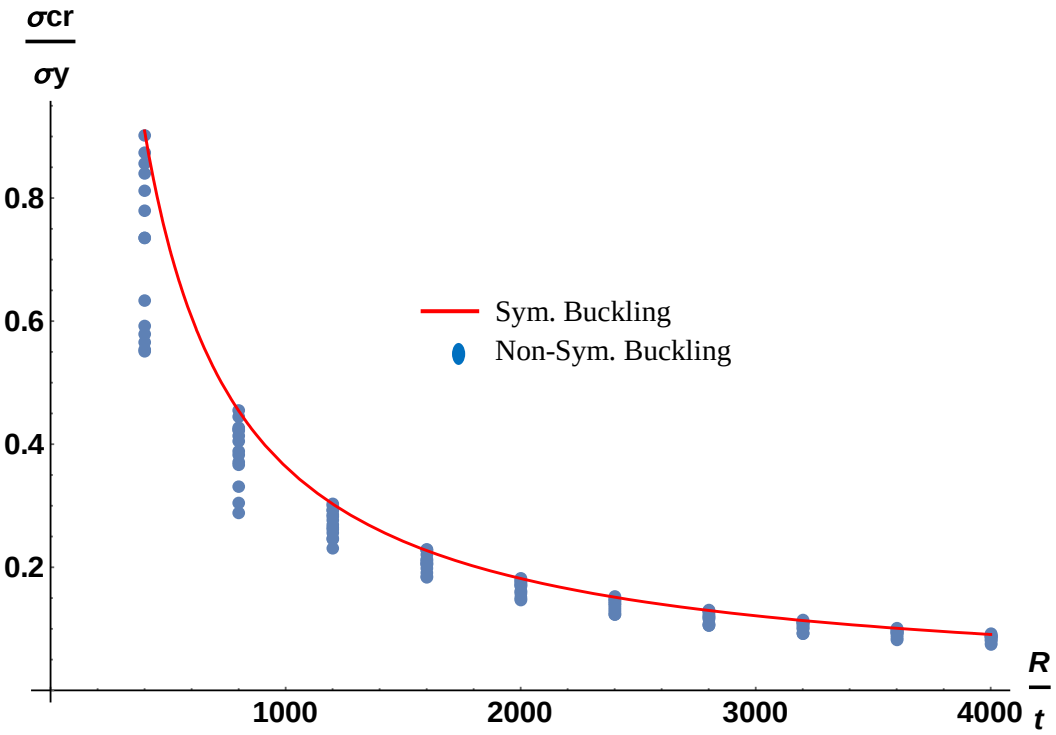

Figure 0.6: The non-symmetrical buckling (dots), symmetrical buckling (solid line)

4.3 Elastic Buckling of CFRP-Stiffened SSCS

For simplicity, we will assume the axi-symmetry of the formulation. A more convincing reason is the fact that a knockdown factor is going to be used which will make the design buckling load much less than both theoretical symmetric and non-symmetric solutions. The governing equation of elastic buckling of CFRP-stiffened cylindrical shells is derived in Chapter 3 and given by:

$$D_s \frac{d^4w}{dx^4} + N\frac{d^2w}{dx^2} + \frac{E_s\, t_s}{R^2}\,(1+\alpha)\, w = 0 \tag{4.37}$$

where α is given by:

$$\alpha = \frac{E_f\, t_f}{E_s\, t_s} \tag{4.38}$$

where the subscript s is used for stainless steel tube while f is for CFRP stiffeners.

4.3.1 Critical Buckling Load Based on Equilibrium

The radial deflection function is defined as:

$$\mathrm{w(x)} = C_m\, Sin\left(\frac{m\,\pi\,x}{L}\right) \tag{4.39}$$

Substituting the radial deflection function (Eq. 4.39) into the governing equation (4.33) and by solving the equation with respect to N; the buckling load can be found as:

$$N = \frac{R^2\, D_s\, m^4\, \pi^4 + E_s\, L^4\, t_s(1+\alpha)}{R^2\, L^2\, m^2\, \pi^2} \tag{4.40}$$

Taking the stationary condition of Eq. (4.40), by equating the derivative of the equation to zero with respect to number of waves (m):

$$m = \frac{{E_s}^{1/4}\, L\, {t_s}^{1/4}\, (1+\alpha)^{1/4}}{\sqrt{R}\, {D_s}^{1/4}\, \pi} \tag{4.41}$$

By substituting Eq. (4.41) into Eq. (4.40), the critical buckling load is found to be:

$$N_{cr} = \frac{\sqrt{(1+\alpha)}\, E_s\, {t_s}^2}{R\, \sqrt{3(1-\nu^2)}} \tag{4.42}$$

4.3.2 Critical Buckling Load Based on Energy Method

The membrane strains after buckling are given by:

$$\varepsilon_x = -\nu \frac{w}{R} \tag{4.43}$$

$$\varepsilon_\theta = \frac{w}{R} \tag{4.44}$$

The membrane stresses after buckling are:

$$\sigma_x = -\frac{N}{t_s} \tag{4.45}$$

$$\sigma_{\theta s} = E_s\, \epsilon_\theta \tag{4.46}$$

$$\sigma_{\theta f} = E_f\, \epsilon_\theta$$

Membrane strain energy per unit volume is given by:

$$u_{ms} = \sigma_x\, \epsilon_x + \frac{1}{2}\, \sigma_{\theta s}\, \epsilon_\theta \tag{4.47}$$

$$u_{mf} = \frac{1}{2}\, \sigma_{\theta f}\, \epsilon_\theta \tag{4.48}$$

The membrane strain energy can be obtained by integrating over the volume to get:

$$\mathrm{U}_m = 2\pi\, R \int_0^L (u_{ms} + u_{mf})\, dx$$
$$= \frac{C_m\, L\, (C_m\, E_s\, m\, \pi\, t_s\, (1+\alpha) - 4(-1+(-1)^m) N\, \nu\, R)}{2\, m\, R} \tag{4.49}$$

The bending strain energy per unit volume is given by:

$$u_b = \frac{D_s}{2}\, {w_{xx}}^2 \tag{4.50}$$

where $w_{xx} = \frac{\partial^2 w}{\partial x^2}$

The bending strain energy can be obtained by integrating over the volume to get:

$$\mathrm{U}_b = 2\pi\, R \int_0^L u_b\, dx = \frac{{C_m}^2\, D_s\, m^4\, \pi^5\, R}{2\, L^3} \tag{4.51}$$

Work due to membrane strain is given by:

$$\mathrm{W1} = 2\pi\, R\, N \int_0^L \frac{{w_x}^2}{2}\, dx = \frac{{C_m}^2\, m^2\, \mathrm{N}\, \pi^3\, R}{2\, L} \tag{4.52}$$

where $w_x = \frac{\partial w}{\partial x}$

Work due to bending strain is given by:

$$\mathrm{W2} = 2\pi\, R\, N \int_0^L \nu \frac{w}{R}\, dx = \frac{2\,(1+(-1)^{1+m})\, C_m\, L\, \mathrm{N}\, \nu}{m} \tag{4.53}$$

Applying conservation of energy principle and solving it for buckling load (N).

$$\mathrm{U} - \mathrm{W} = 0 \Rightarrow \mathrm{U}_m + \mathrm{U}_b = \mathrm{W1} + \mathrm{W2}$$

$$N = \frac{R^2\, D_s\, m^4\, \pi^4 + E_s\, L^4\, t_s\, (1+\alpha)}{R^2\, L^2\, m^2\, \pi^2} \tag{4.54}$$

By setting the derivative of the obtained buckling load (N) with respect to number of waves (m)to be equal to zero

$$m = \frac{{E_s}^{1/4}\, L\, {t_s}^{1/4}\, (1+\alpha)^{1/4}}{\sqrt{R}\, {D_s}^{1/4}\, \pi} \tag{4.55}$$

By substituting Eq. (4.55) back into (4.54), the critical buckling load is:

$$N_{cr} = \frac{\sqrt{(1+\alpha)}\, E_s\, {t_s}^2}{R\, \sqrt{3(1-v^2)}} \tag{4.56}$$

In case several layers of CFRP have been used then only the thickness of CFRP increases so a constant n can be added to the critical buckling load and it represents number of layer, then the critical buckling load become:

$$N_{cr} = \frac{\sqrt{(1+n\,\alpha)}\, E_s\, {t_s}^2}{R\, \sqrt{3(1-v^2)}} \tag{4.57}$$

As explained earlier, this obtained theoretical value needs to be multiplied by the knockdown factor given by Eq. (4.21).

CHAPTER 5

PLASTIC BUCKLING OF CYLINDRICAL SHELLS

5.1 Introduction

Plastic buckling takes the form of rings, in other words axisymmetric buckling and it occurs in thin shells of low R/t ratios. For plasticity buckling, Ramberg-Osgood model [10] along with the total deformation theory [24] are utilized to develop the constitutive equations required for the plastic buckling computations. The constitutive relations of deformation theory are valid for proportional loading only [39]. The total strain is the summation of both parts elastic (ε_{ij}^{e}) and plastic strains ε_{ij}^{p}, and given by $\varepsilon_{ij} = \varepsilon_{ij}^{e} + \varepsilon_{ij}^{p}$. In this chapter, the plastic buckling solution of cylindrical shells is derived analytically by both equilibrium and energy methods.

5.2 Plastic Buckling of Unstiffened SSCS

The governing equation has been derived in Chapter 3 which is given by:

$$\frac{C_{11}\, t^3}{12}\frac{d^4w}{dx^4} + N\ \frac{d^2w}{dx^2} + \left(C_{13} - \frac{{C_{12}}^2}{C_{11}}\right)\frac{t}{R^2}\ \ w = 0 \qquad (5.1)$$

Where the parameters C_{11}, $C_{12}$and C_{13} are dependent on the secant and tangent modulus and they are defined in Chapter 3, w is the deformation of local buckling, x is the axial coordinates, N is the uniform axial loading (positive in compression), t is the thickness of cylindrical shell and R is the radius. However, in the case of simply supported cylindrical shell, the radial deflection function that satisfies the boundary conditions is given by:

$$w = c\ sin\frac{\pi\ x}{L} \tag{5.2}$$

where c is a constant, and L is the unknown wave length of the ring buckles.

5.2.1 Critical Buckling Load Based on Equilibrium

By substituting the radial deflection function (Eq. 5.2) into the governing equation (5.1) and by solving the equation with respect to N, the buckling load can be found as:

$$N = \frac{\left(-{C_{12}}^2 + C_{11}\ C_{13}\right) L^2\ t}{R^2\ C_{11}\ \pi^2} + \frac{C_{11}\ \pi^2\ t^3}{12\ L^2} \tag{5.3}$$

Taking the stationary condition of Eq. (5.3), by equating the derivative of the equation to zero with respect to the length (L):

$$L = \frac{\sqrt{R\ C_{11}\ t}\ \pi}{\sqrt{2}\ (3)^{1/4}(-{C_{12}}^2 + C_{11}\ C_{13})^{1/4}} \tag{5.4}$$

Now, substitute Eq. (5.4) into Eq. (5.3), the critical buckling load (N_{cr})is found to be:

$$N_{cr} = \frac{\sqrt{-{C_{12}}^2 + C_{11}\ C_{13}\ t^2}}{\sqrt{3}\ R} \tag{5.5}$$

5.2.2 Critical Buckling Load Based on Energy Method

The membrane strains after buckling are given by:

$$\varepsilon_x = -\frac{C_{12}}{C_{11}}\ \frac{w}{R} \tag{5.6}$$

$$\varepsilon_\theta = \frac{w}{R} \tag{5.7}$$

The membrane stresses after buckling are:

$$\sigma_x = -\frac{N}{t} \tag{5.8}$$

$$\sigma_\theta = C_{13}\,\varepsilon_\theta + C_{12}\,\varepsilon_x \tag{5.9}$$

Membrane strain energy per unit volume is given by:

$$u_m = \sigma_x\,\epsilon_x + \frac{1}{2}\,\sigma_\theta\,\epsilon_\theta \tag{5.10}$$

The membrane strain energy can be obtained by integrating over the volume to get:

$$\begin{aligned} U_m &= 2\pi\,R \int_0^L \int_{-t/2}^{t/2} u_m\,dz\,dx \\ &= \frac{c\,L\,(8\,C_{12}\,N\,R - {C_{12}}^2\,c\,\pi t + C_{11}C_{13}\,c\,\pi t)}{2\,C_{11}\,R} \end{aligned} \tag{5.11}$$

The bending strain energy per unit volume is given by:

$$u_b = \frac{\kappa_x}{2}\,M_x \tag{5.12}$$

where

$$M_x = \frac{C_{11}\,t^3}{12}\,w_{xx} \tag{5.13}$$

where $w_{xx} = \frac{\partial^2 w}{\partial x^2}$

The bending strain energy can be obtained by integrating over the volume to get:

$$\mathrm{U}_b = 2\pi\, R\, t \int_0^L u_b\, dx = \frac{C_{11}\, c^2\, \pi^5\, R\, t^3}{24\, L^3} \tag{5.14}$$

Work due to membrane strain is given by:

$$\mathrm{W1} = 2\pi\, R\, N \int_0^L \frac{{w_x}^2}{2}\, dx = \frac{c^2\, N\, \pi^3\, R}{2\, L} \tag{5.15}$$

where $w_x = \frac{\partial w}{\partial x}$

Work due to bending strain is given by:

$$\mathrm{W2} = 2\pi\, R\, N \int_0^L \frac{C_{12}}{C_{11}}\, \frac{w}{R}\, dx = \frac{4\, C_{12}\, c\, L\, N}{C_{11}} \tag{5.16}$$

Applying conservation of energy principle and solving it for buckling load (N).

$$\mathrm{U} - \mathrm{W} = 0 \Rightarrow \mathrm{U}_m + \mathrm{U}_b = \mathrm{W1} + \mathrm{W2}$$

$$N = \frac{\left(-{C_{12}}^2 + C_{11}\, C_{13}\right) L^2\, t}{R^2\, C_{11}\, \pi^2} + \frac{C_{11}\, \pi^2\, t^3}{12\, L^2} \tag{5.17}$$

By setting the derivative of the obtained buckling load (N) with respect to the length to be equal to zero.

$$L = \frac{\sqrt{R\, C_{11}\, t}\ \pi}{\sqrt{2}\, (3)^{1/4} (-{C_{12}}^2 + C_{11}\, C_{13})^{1/4}} \tag{5.18}$$

By substituting Eq. (5.18) back into (5.17), the critical buckling load is found to be:

$$N_{cr} = \frac{\sqrt{-{C_{12}}^2 + C_{11}\, C_{13}}\, t^2}{\sqrt{3}\, R} \tag{5.19}$$

Now substituting the values of C_{11}, C_{12} and C_{13} [24], equations (3.43-3.45) in Chapter 3, into equation 5.19 , and dividing by the tube thickness, the final form of the buckling stress becomes:

$$\sigma_{cr} = \left(\frac{2}{\sqrt{3}\sqrt{\lambda(5+3e-4\nu)-(1-2\nu)^2}}\right)\frac{E\ t}{R} \tag{5.20}$$

5.3 Plastic Buckling of CFRP-Stiffened SSCS

The governing equation of plastic buckling of CFRP-stiffened cylindrical shells is derived in Chapter 3 and given by:

$$\frac{C_{11}\ t^3}{12}\frac{d^4w}{dx^4} + \mathrm{N}\ \frac{d^2w}{dx^2} + \left(C_{13} - \frac{{C_{12}}^2}{C_{11}}\right)\frac{t_s}{R^2}\ (1+n\,\alpha)\ w = 0 \tag{5.21}$$

where α is given by:

$$\alpha = \frac{E_f\ t_f}{E_s\ t_s} \tag{5.22}$$

In this section the subscript s is used for stainless steel tube while f for CFRP stiffeners.

The membrane strains after buckling are given by:

$$\varepsilon_x = -\frac{C_{12}}{C_{11}}\ \frac{w}{R} \tag{5.23}$$

$$\varepsilon_\theta = \frac{w}{R} \tag{5.24}$$

The membrane stresses after buckling are:

$$\sigma_x = -\frac{N}{t_s} \tag{5.25}$$

$$\sigma_{\theta s} = C_{13}\,\varepsilon_\theta + C_{12}\,\varepsilon_x \tag{5.26}$$

$$\sigma_{\theta f} = E_f\,\varepsilon_\theta \tag{5.27}$$

Membrane strain energy per unit volume is given by:

$$u_m = \sigma_x\,\epsilon_x + \frac{1}{2}\,\sigma_\theta\,\epsilon_\theta \tag{5.28}$$

The membrane strain energy can be obtained by integrating over the volume to get:

$$\begin{aligned} U_m &= 2\pi\,R\left[t_s\int_0^L u_m\,dx + t_f\int_0^L \frac{1}{2}\,\sigma_{\theta f}\,\varepsilon_\theta\,dx\right] \\ &= \frac{c\,L(8\,C_{12}\,N\,R - {C_{12}}^2\,c\,\pi t + C_{11}C_{13}\,c\,\pi t_s)}{2\,C_{11}\,R} \\ &+ \frac{c^2 E_s\,L\,\pi t_s\,\alpha}{2\,R} \end{aligned} \tag{5.29}$$

The bending strain energy per unit volume is given by:

$$u_b = \frac{\kappa_x}{2}\,M_x \tag{5.30}$$

where:

$$M_x = \frac{C_{11}\,{t_s}^3}{12}\,w_{xx} \tag{5.31}$$

where $w_{xx} = \frac{\partial^2 w}{\partial x^2}$

The bending strain energy can be obtained by integrating over the volume to get:

$$\mathrm{U}_b = 2\pi\, R\, t \int_0^L u_b\, dx = \frac{C_{11}\, c^2\, \pi^5\, R\, {t_s}^3}{24\, L^3} \tag{5.32}$$

Work due to membrane strain is given by:

$$\mathrm{W1} = 2\pi\, R\, N \int_0^L \frac{{w_x}^2}{2}\, dx = \frac{c^2\, N\, \pi^3\, R}{2\, L} \tag{5.33}$$

Work due to bending strain is given by:

$$\mathrm{W2} = 2\pi\, R\, N \int_0^L \frac{C_{12}}{C_{11}}\, \frac{w}{R}\, dx = \frac{4\, C_{12}\, c\, L\, N}{C_{11}} \tag{5.34}$$

Applying conservation of energy principle and solving it for buckling load (N).

$$\mathrm{U} - \mathrm{W} = 0 \Rightarrow \mathrm{U}_m + \mathrm{U}_b = \mathrm{W1} + \mathrm{W2}$$

$$N = \frac{t_s \left(-12\, {C_{12}}^2 L^4 + C_{11}\, (12\, C_{13}\, L^4 + C_{11}\, \pi^4\, R^2\, {t_s}^2 + 12\, E_s\, L^4\, \alpha)\right)}{12\, C_{11}\, L^2\, \pi^2\, R^2} \tag{5.35}$$

By setting the derivative of the obtained buckling load (N) with respect to the length to be equal to zero.

$$L = \frac{\sqrt{R\, C_{11}\ t_s}\ \pi}{\sqrt{2}\, (3)^{1/4} \left(-{C_{12}}^2 + C_{11}\, C_{13} + C_{11}\, E_s\, \alpha\right)^{1/4}} \tag{5.36}$$

By substituting Eq. (5.36) back into (5.35), the critical buckling load is found to be:

$$N_{cr} = \frac{{t_s}^2 \sqrt{-{C_{12}}^2 + C_{11}(\, C_{13} + E_s\, \alpha)}}{\sqrt{3}\, R} \tag{5.37}$$

Now substituting the values of C_{11}, C_{12} and C_{13} [24], equations (3.43-3.45) in Chapter 3, into equation 5.37, the final form of the buckling stress becomes:

$$\sigma_{cr} = \frac{2}{\sqrt{3}}\left(\frac{\sqrt{1+\alpha(3/4+3/4\,e+\lambda/4)}}{\sqrt{\lambda(5+3e-4\nu)-(1-2\nu)^2}}\right)\frac{E\,t}{R} \tag{5.38}$$

As mentioned earlier in chapter 3, the parameters e and λ are found from the stress-strain curve of the stainless steel, hence Ramberg-Osgood model is utilized to obtain the $\sigma - \varepsilon$ curve for both unstiffened and CFRP- stiffened cylindrical shells.

5.4 Ramberg-Osgood Model

The Ramberg-Osgood model [10] is commonly used for non-linear stress-strain behavior and it was proposed in 1943, then enhanced by Hill [11]. Ramberg-Osgood (R-O) model is expressed as follow:

$$\varepsilon = \frac{\sigma}{E_0} + 0.002\left(\frac{\sigma}{\sigma_{0.2}}\right)^n \quad (\sigma \leq \sigma_{0.2}) \tag{5.39}$$

where ε and σ are the engineering strain and stress, respectively, E_0 is the young's modulus of the material, $\sigma_{0.02}$ is the proof stress that corresponds to 0.2% of plastic strain, and n is a strain hardening exponent. However, this expression gives an excellent prediction of stress-strain behavior of stainless steel in the initial part of the stress strain curve up to 0.2% proof stress, but markedly over-estimates the stress, at higher strains, beyond that level. Figure 5.1 shows a comparison between a measured Stress-Strain curve and the proposed Ramberg-Osgood expression given by equation (5.39) [40].

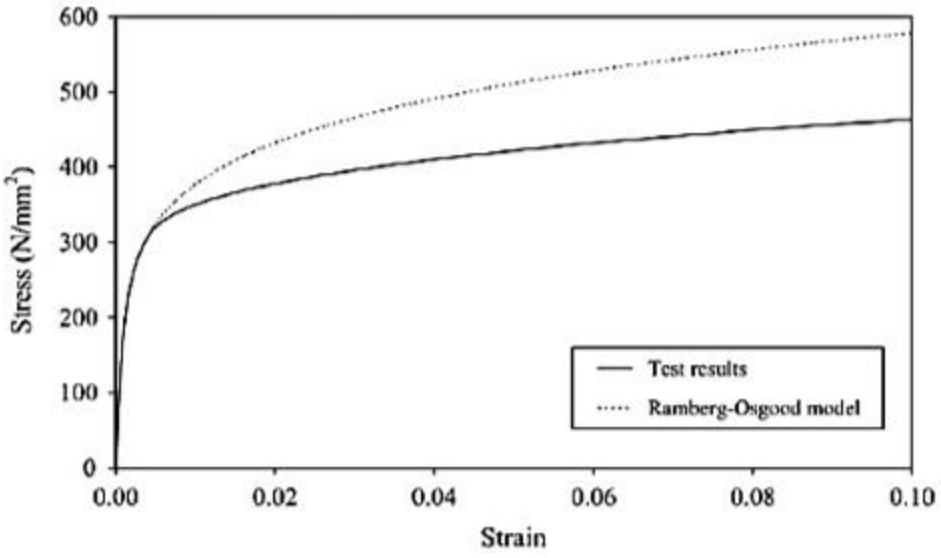

Figure 0.1: A comparison between measured Stress-Strain curve and the proposed R-O expression (Eq. 5.39) [6]

For stresses greater than 0.2% proof stress, the proposed Ramberg-Osgood model is given by the following expression [40]:

$$\varepsilon = \frac{(\sigma-\sigma_{0.2})}{E_{0.2}} + \left(0.008 - \frac{\sigma_{0.2}-\sigma_{0.2}}{E_{0.2}}\right)\left(\frac{\sigma-\sigma_{0.2}}{\sigma_{1.0}-\sigma_{0.2}}\right)^{n'_{0.2,1.0}} + \varepsilon_{t0.2} \qquad (\sigma \geq \sigma_{0.2}) \qquad (5.40)$$

where $E_{0.2}$ is the stiffness at 0.2% proof stress (initial modulus to the σ-ε curve), also known as the tangent modulus of $\sigma - \varepsilon$ at 0.2% proof stress and given by equation (5.41). Moreover, $\sigma_{1.0}$ is the proof stress at 1%, $n'_{0.2,1.0}$ is the strain hardening coefficient that passes through both stresses $\sigma_{0.2}$ and $\sigma_{1.0}$ and $\varepsilon_{t0.2}$ is the total strain at the 0.2% proof stress and given by equation (5.42) [12]. Figure 5.2 shows more illustration regarding the above parameters.

$$E_{0.2} = \frac{(E_0)\,(\sigma_{0.2})}{\sigma_{0.2} + 0.002\,n\,E_0} \qquad (5.41)$$

$$\varepsilon_{t0.2} = \frac{\sigma_{0.2}}{E_0} + 0.002 \tag{5.41}$$

Therefore, it is preferred to use the two-stage model for stress-strain curve of stainless steel in order to obtain more accurate results [40]. Hence, the full-range stress-strain curve can be expressed as follows [12]:

$$\varepsilon = \begin{cases} \frac{\sigma}{E_0} + 0.002\left(\frac{\sigma}{\sigma_{0.2}}\right)^n & (\sigma \le \sigma_{0.2}) \\ \frac{(\sigma-\sigma_{0.2})}{E_{0.2}} + \left(0.008 - \frac{\sigma_{0.2}-\sigma_{0.2}}{E_{0.2}}\right)\left(\frac{\sigma-\sigma_{0.2}}{\sigma_{1.0}-\sigma_{0.2}}\right)^{n'_{0.2,1.0}} + \varepsilon_{t0.2} & (\sigma > \sigma_{0.2}) \end{cases} \tag{5.42}$$

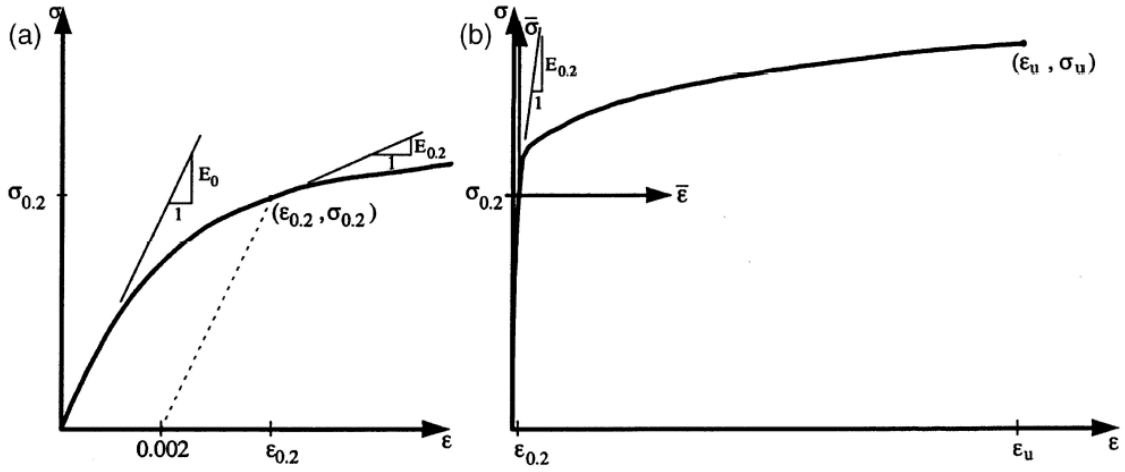

Figure 0.2: Stainless steel stress-strain curve; (a)Initial σ-ε curve, (b)Full range of σ-ε curve [12].

The key material parameters of stainless steel properties needed for this research are the Young's modulus (E), the 0.2% proof strength $\sigma_{0.2}$, the 1.0% proof stress $\sigma_{1.0}$, the ultimate tensile strength σ_u and the strain hardening exponents both n and $n'_{0.2,1.0}$ which described in [9].

In this research, the two-stage Ramberg-Osgood model is utilized to generate the engineering stress-strain curve of stainless steel material. However, the analysis requires the true stress-strain curve, hence, the engineering stresses and strains are converted into

true stresses and log-plastic strains. To convert engineering stresses into true stresses and engineering strains into true log-plastic strains, equations (5.43 and 5.44) are used respectively [41].

$$\sigma_{true} = \sigma_{Eng}(1 + \varepsilon_{Eng}) \tag{5.43}$$

$$\varepsilon_{true} = ln(1 + \varepsilon_{Eng}) \tag{5.44}$$

5.5 Worked Example

In order to explain the procedure for solving the nonlinear equations 5.20 and 5.38 and hence obtaining the plastic buckling load, the following example is presented. Consider a stainless steel of the characteristics and dimensions described in Table 5.1.

Table 0.1: Stainless Steel Properties

E_0 (MPa)	$\sigma_{0.2}$ (MPa)	$\sigma_{1.0}$ (MPa)	σ_u (MPa)	n	$n'_{0.2,1.0}$	L (mm)	D (mm)	t (mm)
200,000	330	370	650	9.5	1.95	330	110	1.1

Herein, the two-stage Ramberg-Osgood model is used to generate the engineering stress-strain curve of this stainless steel material as shown in Figure 5.3. Also, the true stress-strain curve is generated by using equations (5.43 and 5.44) for analysis purposes. The true stress-strain curve of this material is shown in Figure 5.4.

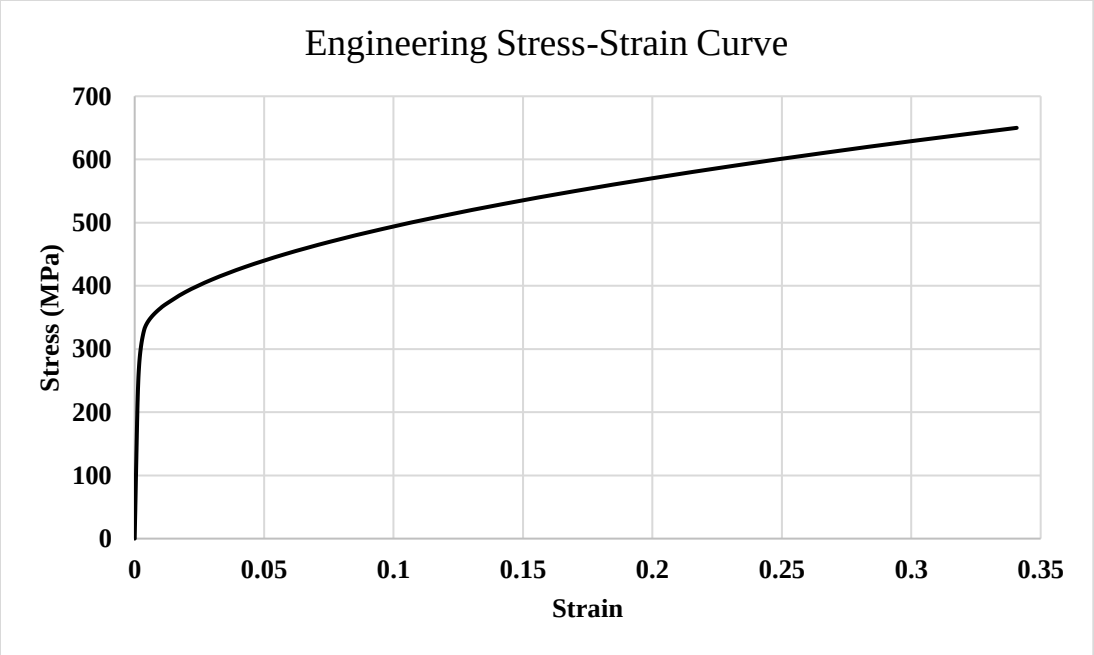

Figure 0.3: Engineering stress-strain curve

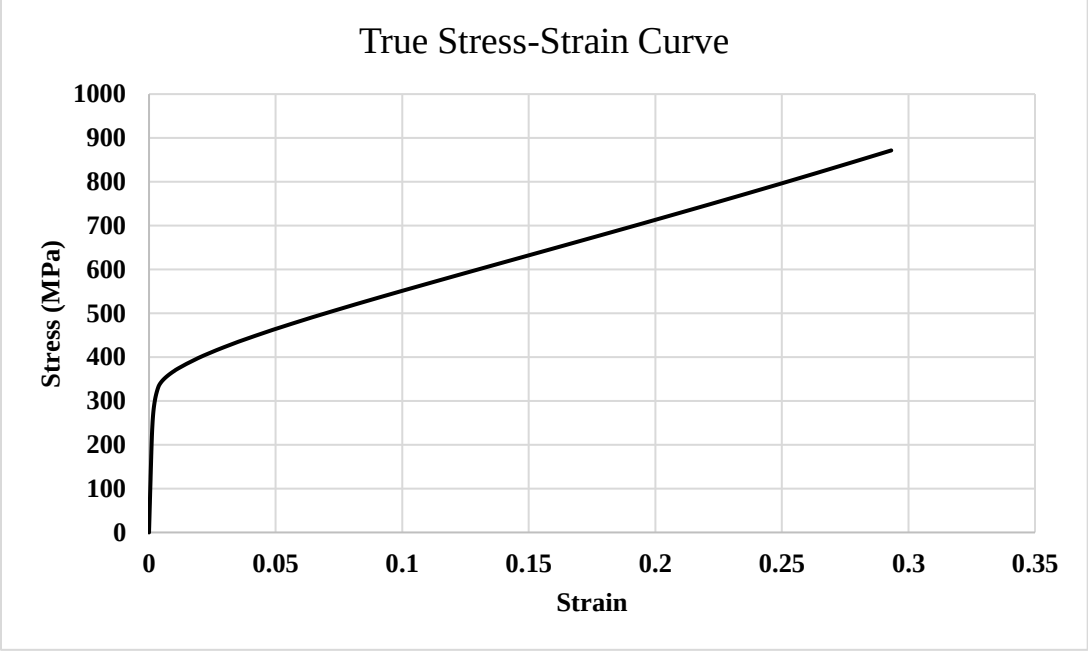

Figure 0.4: True stress-strain curve

Computation of plastic buckling load:

$$\frac{R}{t} = \frac{D/2}{t} = \frac{110/2}{1.1} = 50$$

$$E_{0.2} = \frac{(E_0)\,(\sigma_{0.2})}{\sigma_{0.2} + 0.002\,n\,E_0} = \frac{(200{,}000)(330)}{330 + (0.002)(9.5)(200{,}000)}$$

$$= 15{,}980.63 \text{ MPa}$$

$$\varepsilon_{t0.2} = \frac{\sigma_{0.2}}{E_0} + 0.002 = \frac{330}{200{,}000} + 0.002 = 0.00365$$

The buckling load is given by (Eq. 5.20):

$$N_{cr} = \left(\frac{2}{\sqrt{3}\sqrt{\lambda(5 + 3e - 4\nu) - (1 - 2\nu)^2}}\right)\frac{E}{R/t}$$

$$e = \frac{E}{E_s} - 1, \lambda = \frac{E}{E_t}$$

where the secant modulus and tangent modulus are given by

$$E_s = \frac{\sigma}{\varepsilon}, E_t = \frac{d\sigma}{d\varepsilon}$$

Now, Ramberg-Osgood model should be utilized to solve those parameters. The R-O parameters used in the calculation of buckling load is obtained by fitting the stress-strain curve of stainless steel using Mathematica, Appendix C provides the code used in Mathematica. the buckling load for this example was found to be 130.192 kN.

CHAPTER 6

VALIDATION OF ANALYTICAL SOLUTION

6.1 Introduction

Finite element method (FEM) is used in this research to verify the obtained analytical solution. Verification of results is concentrated mainly on eigenvalues (buckling loads) and eigenmodes (buckling modes). There are several tools for finite element analysis (FEA), however, herein the general-purpose finite element analysis package ABAQUS was employed [42]. Both geometric and material non-linearities have been involved in this study. In this chapter, the analysis of elastic and plastic buckling of unstiffened and CFRP-stiffened cylindrical shells is carried out.

6.2 Analysis Method

In general, buckling analysis is mainly divided into Bifurcation analysis and Load-deflection analysis (Figure 6.1) [28]. The former type occurs when a maximum axial compressive stress reaches the buckling stress while the latter yields first reaching its stability limit load (buckling load). Bifurcation and Load-deflection analyses were carried out in this research for elastic and plastic buckling of SSCS respectively.

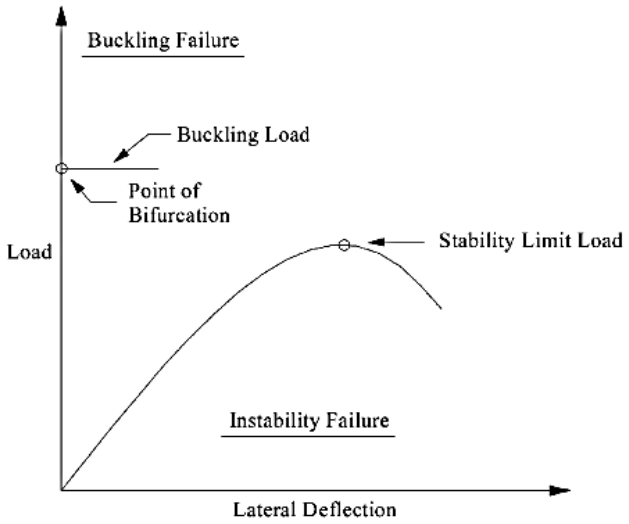

Figure 0.1: Buckling Analysis [28]

6.3 Elastic Buckling

6.3.1 Finite Element Analysis

Bifurcation analysis deals with the model as an eigenvalue problem, and its equation is expressed as:

$$([K] + \lambda[\sigma])\{m\} = 0 \qquad (6.1)$$

where $[K]$ is the system stiffness matrix, $[\sigma]$ is stress stiffness matrix, λ is an eigenvalue or load factor that determines the buckling load, $\{m\}$ is a vector that determines the buckling mode. If a structure is loaded by N force, the critical buckling load is denoted by λN. Both buckling stress and failure mode can be captured by the bifurcation analysis.

The buckling stresses were obtained by ABAQUS using Linear Perturbation Analysis (LPA), in this analysis, the linear stress-strain behavior is considered. There are two main types of analysis under the LPA which are static\displacement stress analysis and

dynamic/displacement stress analysis. In this thesis, the Eigenvalue buckling load prediction analysis has been utilized which is under the static stress/displacement analysis. In this analysis, the applied compressive load is kept until the cylindrical shell is buckled. In ABAQUS, in STEP command, the needed number of eigenvalues should be selected before running the analysis, and the critical buckling stress is the minimum stress which is the first eigenvalue.

6.3.2 Sensitivity Analysis

Mesh Size

The accuracy of FEA is dependent on the number of finite elements within the model. The finer the elements the more accurate the results; considering that the time will be longer as the number of elements increases. Hence, a sensitivity analysis was conducted in order to find the optimum mesh size at which the results are accurate and the time is short. In other words, the change in the value of buckling stress from mesh size to the next smaller mesh size should be very small or no difference.

Buckling strength was obtained for different mesh sizes and compared with the analytical solution. Five different mesh elements were used in the axial direction ($5, 10, 20, 30$ and 40) and nine mesh sizes were selected in the circumferential direction ($8, 12, 16, 20, 24, 28, 32, 36$ and 64). Furthermore, it was observed that the maximum error reduced dramatically when the number of elements in circumferential direction increased. It was decreased from 17% to 0.3% when the number of elements in circumferential direction increased from 8 to 36, as shown in Figure 6.2. Also, it can be clearly observed that the results are accurate after 32 elements; Nevertheless, the time was also short when 64 elements were used.

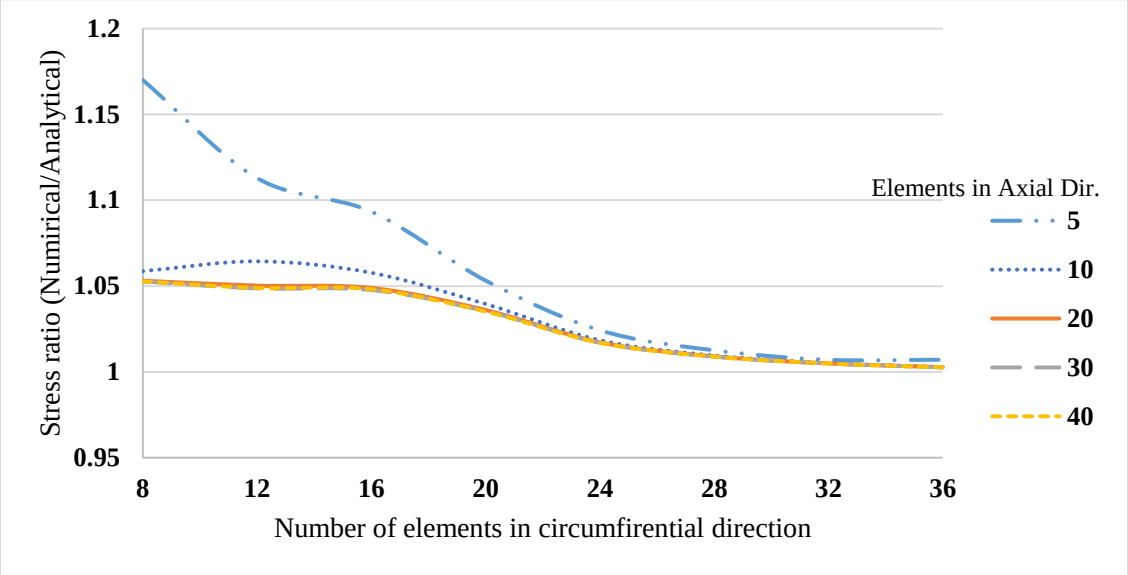

Figure 0.2: Buckling stresses associated with different numbers of elements in both axial and circumferential directions

Regarding the number of elements in axial direction, the buckling strength was merely sensitive not like what it was noticed with the number of elements in circumferential direction. For 32 elements in the circumferential direction, the maximum error was slightly reduced from 0.7% to 0.5% when the number of elements in the axial direction increased from 5 elements to 40. When 64 elements in the circumferential direction and 40 elements in axial direction were selected, the estimated buckling stress was very accurate (error within 0.1%). Figure 6.3 shows the percentage error in buckling stress for different mesh sizes.

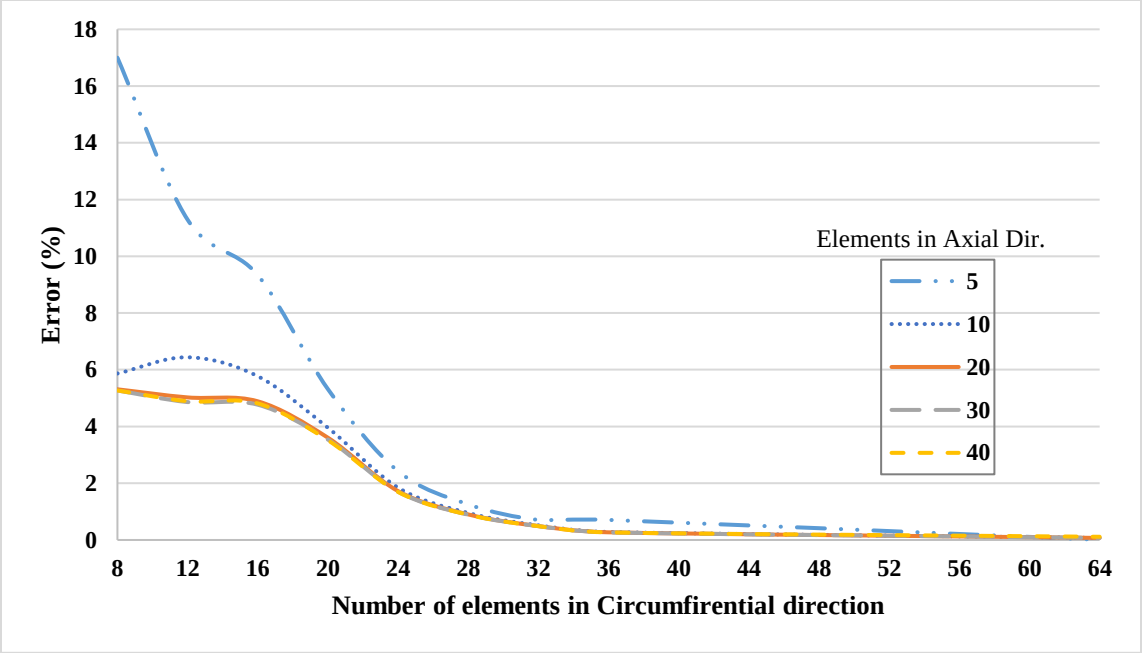

Figure 0.3: Percentage error in buckling stress for different mesh sizes

One more important point to be taken into consideration is the sensitivity of the buckling mode with mesh size. It was found that the buckling mode is extremely sensitive to mesh size; the correct buckling mode was obtained accurately when the number of circumferential elements was more than 32 elements regardless of the number of axial elements. To illustrate the phenomena, Figure 6.5 shows a buckled shell that has a geometric ratio of L/R of 4 and R/t of 800 for a fixed number of axial elements (40) and different number of elements in the circumferential elements (16, 24, 32 and 64). The expected buckling mode occurs at $(m = 1)$ and $(n = 6)$. It can be clearly seen from Figure 6.4 that the buckling mode was obtained correctly when the number of circumferential elements is 32 or more.

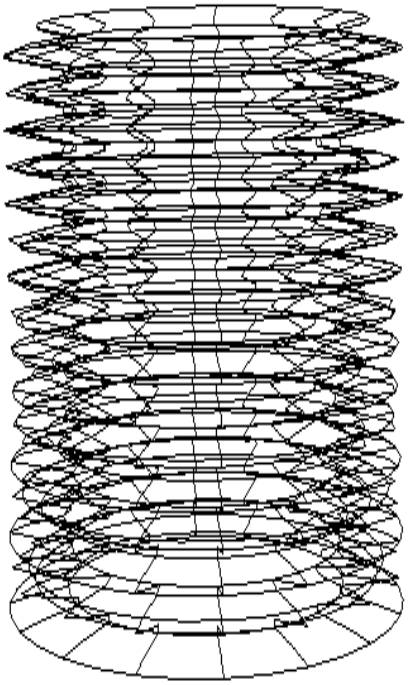

a) 16 Circumferential elements

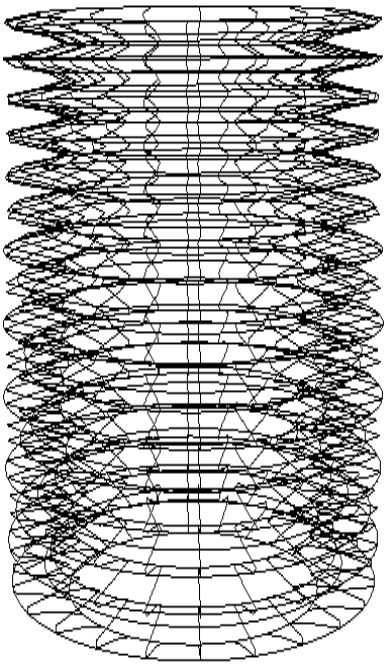

b) 24 Circumferential elements

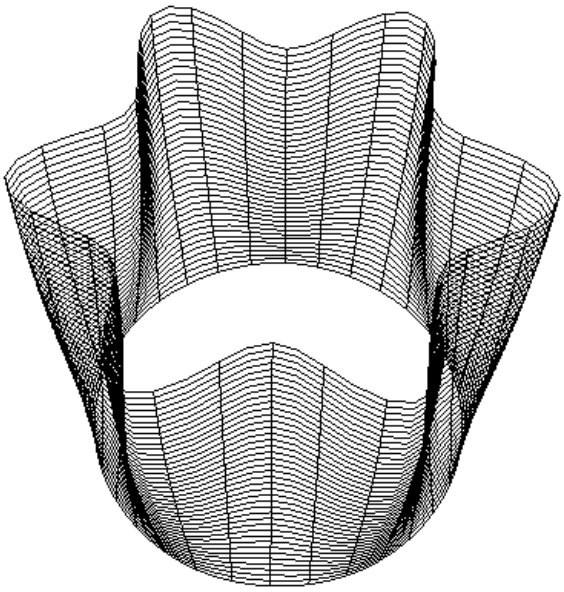

c) 32 Circumferential elements

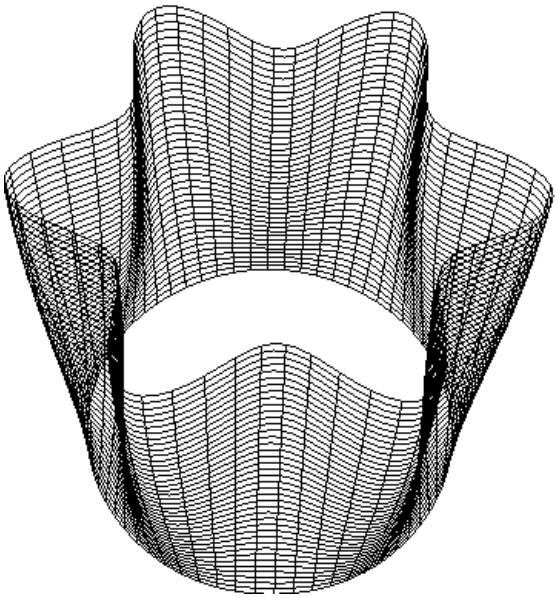

d) 64 Circumferential elements

Figure 0.4: Buckling mode of a shell with L/R=4 and R/t=800 obtained by FEM, for 40 longitudinal elements and different Nu. of circumferential elements a) 16, b) 24, c) 32 and d) 64

Element Type

The elemental type used in this model is shell element. This type of element is usually used when the thickness is significantly small compared to other dimensions. ABAQUS offers several types of elements that can be classified into three main types. Firstly, four node element (S4R, S4R5) which divide the element into four-nodes. Secondly, eight node elements (S8R, S8R5) in which the shell element is divided into eight-nodes. Thirdly, based on the *degree of freedom* (dof) of each element, there are five and six degrees of freedom namely five-dof (S4R5, S8R5) and six-dof (S4R, S8R) respectively. Five-dof means that the element has 3-displacements and 2-rotational components, while six-dof has three translations and three rotations.

An investigation has been conducted to decide about the best type of mesh to be selected, Figure 6.5 shows the critical stresses associated with each element type. In this analysis all mesh sizes were equal (40 and 64 elements in axial and circumferential directions respectively). The buckling stresses were a bit high and the modes were not obtained correctly when S4R and S4R5 were selected, while S8R5 shell element was more accurate in finding the buckling stresses but some of the modes were not obtained correctly. However, when S8R shell element was used, the accuracy of buckling stresses was very close from the analytical solution (less than 0.5%, see Figure 6.6) and the modes were obtained correctly. Thus, the eight-node shell element (S8R) with six degrees of freedom was selected for this thesis.

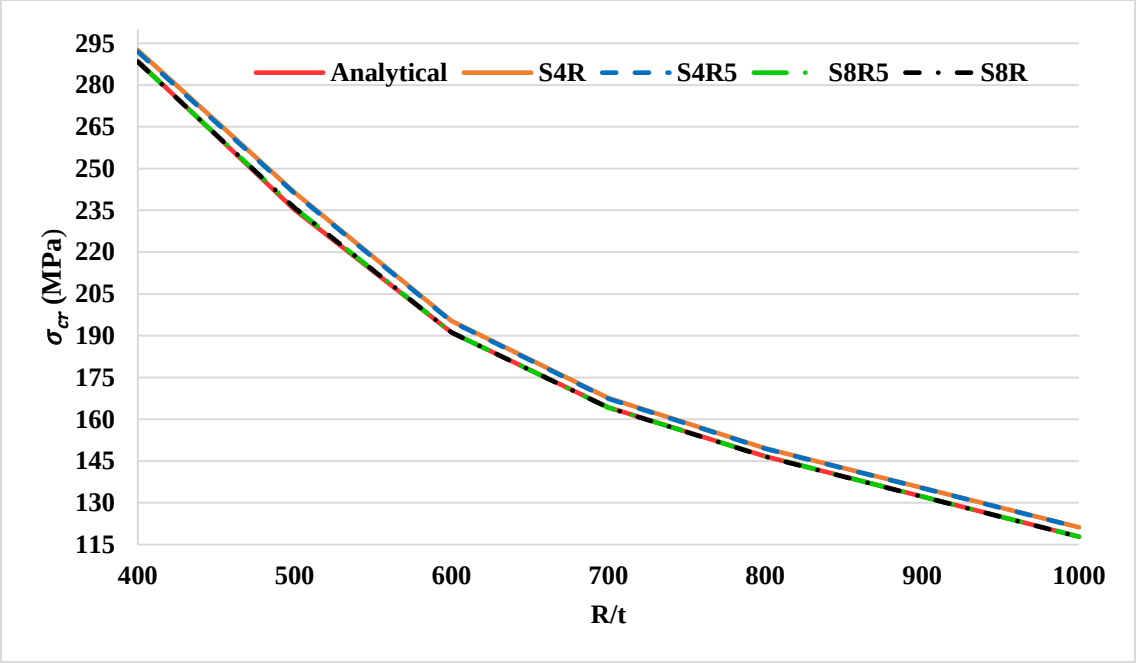

Figure 0.5: Critical stresses associated with element type

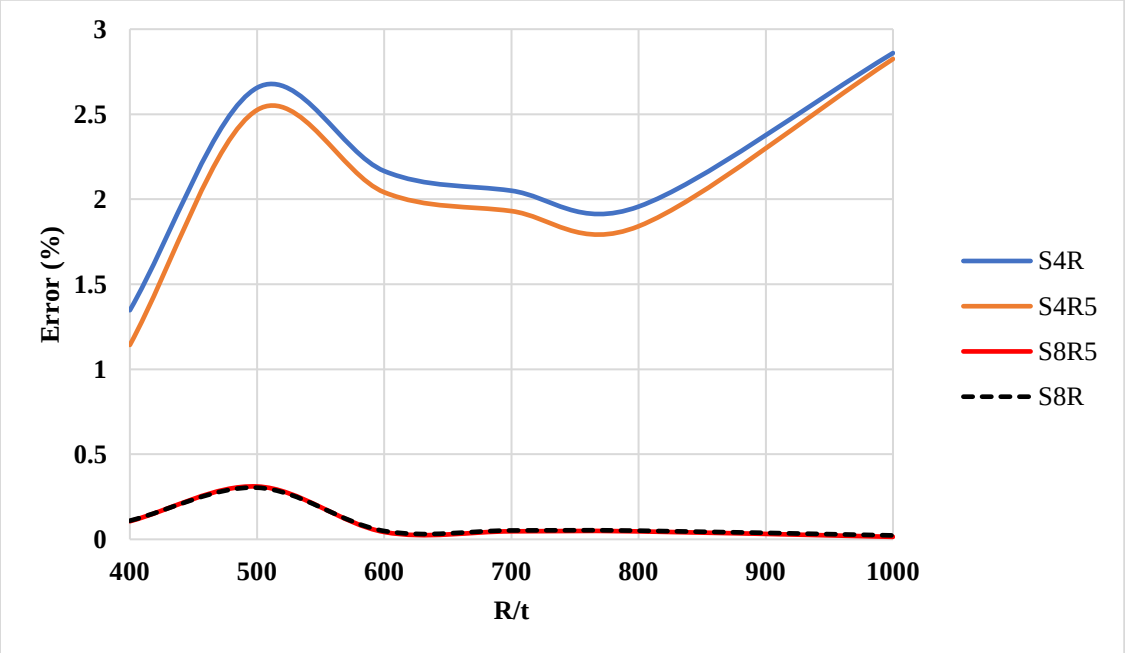

Figure 0.6: Percentage error in buckling stresses for each element type

6.3.3 Boundary Conditions

The cylindrical shell is clamped (simply supported) at both ends and it is free to move axially in the longitudinal direction at the top where the load is applied; also, it is free to move in the radial direction at top and bottom. These boundary conditions were applicable for most of the models but when long models were analyzed the buckling stresses were not predicted accurately, so half-model in height was used [28]. Figure 6.7 shows samples of a full and half shell models. In a half-model the boundary conditions are clamped at the top (displacement in the x-axis (U1) and displacement in the y-axis equal zero) and symmetric boundary conditions at the bottom. Symmetric boundary conditions are about z-axis (*z-symmetry* command in ABAQUS), which means that displacement in the z-axis (U3) and rotations in both x (UR1) and y-axis (UR2) are zero ($U3 = UR1 = UR2 = 0$). A cylindrical shell model with the applied boundary conditions and load is shown in Figure 6.8.

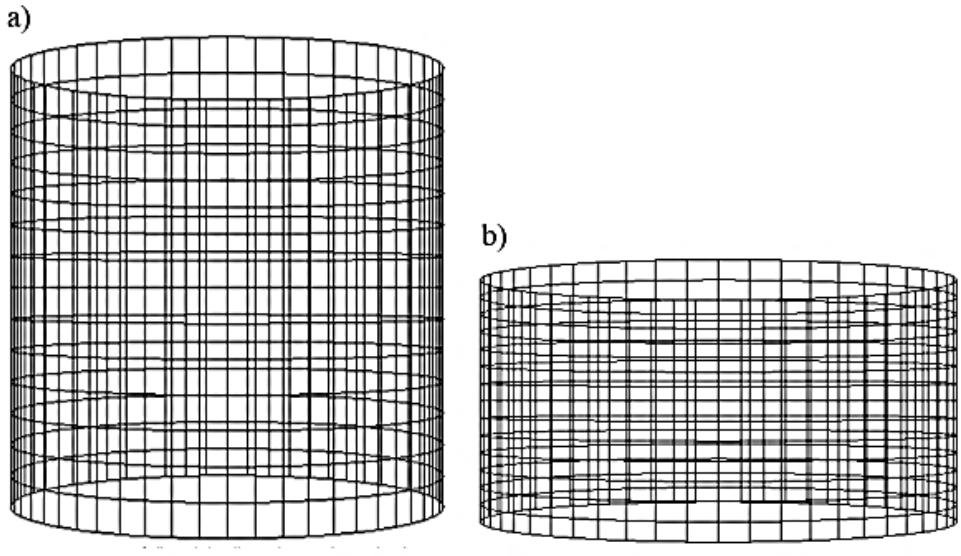

Figure 0.7: Cylindrical shell Model: a) Full Model; B) Half-Model

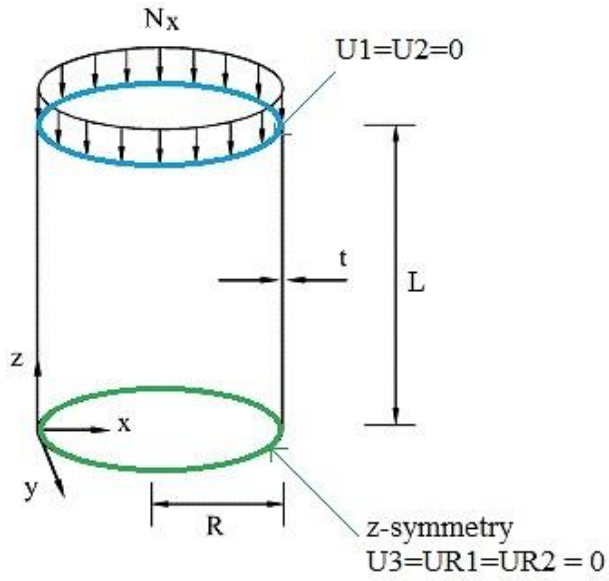

Figure 0.8: A cylindrical shell model with the applied boundary conditions and load

6.3.4 Results and Discussion of Unstiffened SSCS

Buckling Stress

The eigenvalues obtained by FEA was very close from the analytical solution. Here is a sample comparison between the analytical and the numerical results for two different cylindrical shells. The first one has a geometrical property of $L/R = 4$ and $R/t = 400$ while the second $L/R = 4$ and $R/t = 800$. The stainless steel modulus of elasticity (E) was 200 GPa and Poisson's ratio (v) was 0.3. The obtained eigenvalues are summarized in Table 6.1 below, it is obvious that the eigenvalues obtained numerically show an excellent agreement with the analytical eigenvalues.

Table 0.1: The First three eigenvalues (in MPa) for two different cylindrical shells, for L/R = 4

Eigenvalue stress	R/t =400			R/t =800		
	FEM	Analytical	Error %	FEM	Analytical	Error %
First	57.661	57.720	0.102	29.327	29.320	0.023
Second	59.045	59.060	0.026	29.855	29.860	0.017
Third	59.866	59.840	0.043	30.048	30.040	0.027

For more comprehensive comparison, the normalized critical buckling stresses ($\frac{\sigma_{cr}}{E} \times 10^3$) obtained numerically are compared with the corresponding analytical solution for L/R ranging from 1 to 6 and R/t ranging from 400 to 1000 as shown in Table 6.2. A similar comparison is given in Table 6.3 for the simplified designed models generated in Chapter 4. Both tables confirm the good agreement among the theoretical, the design formula and the FEM solutions.

Table 0.2: Buckling stresses of a perfect cylindrical shell, $\left(\frac{\sigma_{cr}}{E} \times 10^3\right)$, compared to theoretical stresses

	L/R = 1			L/R = 2			L/R = 4			L/R = 6		
R/t	σ FEM	σ1*	σ2**	σ FEM	σ1*	σ2**	σ FEM	σ1*	σ2**	σ FEM	σ1*	σ2**
400	1.49	1.49	1.51	1.49	1.49	1.51	1.44	1.44	1.51	1.43	1.43	1.51
450	1.34	1.33	1.34	1.32	1.32	1.34	1.32	1.33	1.34	1.32	1.34	1.34
500	1.19	1.19	1.21	1.18	1.18	1.21	1.18	1.18	1.21	1.17	1.17	1.21
550	1.09	1.08	1.10	1.07	1.07	1.10	1.05	1.05	1.10	1.04	1.04	1.10
600	1.00	1.00	1.01	0.98	0.98	1.01	0.96	0.96	1.01	0.94	0.94	1.01
650	0.93	0.92	0.93	0.92	0.92	0.93	0.88	0.88	0.93	0.86	0.86	0.93
700	0.85	0.85	0.86	0.86	0.86	0.86	0.82	0.82	0.86	0.80	0.80	0.86
750	0.80	0.80	0.81	0.79	0.79	0.81	0.77	0.77	0.81	0.75	0.75	0.81
800	0.75	0.75	0.76	0.74	0.74	0.76	0.73	0.73	0.76	0.71	0.71	0.76
850	0.71	0.71	0.71	0.69	0.69	0.71	0.70	0.70	0.71	0.67	0.67	0.71
900	0.67	0.67	0.67	0.66	0.66	0.67	0.66	0.67	0.67	0.65	0.65	0.67
950	0.63	0.63	0.64	0.63	0.63	0.64	0.63	0.63	0.64	0.62	0.62	0.64
1000	0.60	0.60	0.61	0.60	0.60	0.61	0.59	0.59	0.61	0.60	0.59	0.61

*The theoretical (non-symmetric) critical buckling stress

**The theoretical (symmetric) buckling stress

Table 0.3: Buckling stresses of a perfect cylindrical shell, $\left(\frac{\sigma_{cr}}{E} \times 10^3\right)$, compared to design models

	L/R = 1		L/R = 2		L/R = 4		L/R = 6	
R/t	σ (FEM)	σ*	σ (FEM)	σ*	σ (FEM)	σ*	σ (FEM)	σ**
400	1.492	1.501	1.490	1.470	1.442	1.441	1.429	1.395
450	1.339	1.334	1.322	1.307	1.320	1.280	1.322	1.243
500	1.194	1.201	1.176	1.176	1.179	1.152	1.168	1.121
550	1.086	1.092	1.067	1.069	1.052	1.048	1.037	1.020
600	1.004	1.001	0.984	0.980	0.956	0.960	0.937	0.937
650	0.925	0.924	0.920	0.905	0.880	0.886	0.860	0.866
700	0.855	0.858	0.858	0.840	0.821	0.823	0.798	0.805
750	0.798	0.801	0.793	0.784	0.773	0.768	0.748	0.752
800	0.751	0.751	0.739	0.735	0.733	0.720	0.708	0.706
850	0.712	0.706	0.695	0.692	0.701	0.678	0.674	0.665
900	0.668	0.667	0.657	0.654	0.662	0.640	0.646	0.629
950	0.631	0.632	0.626	0.619	0.626	0.607	0.622	0.596
1000	0.599	0.600	0.599	0.588	0.589	0.576	0.597	0.567

*First Design model: $\sigma_{cr} = \frac{600.42}{(R/t)} \left(\frac{L}{R}\right)^{-0.0297}$

** Second Design model: $\sigma_{cr} = 534.79 \left(\frac{L}{R}\right)^{-.033} \left(\frac{R}{t}\right)^{-0.983}$

Buckling Mode

The buckling modes obtained using FEA were matching exactly the buckling modes found analytically. Here are examples that have been solved analytically and numerically, consider a cylindrical shell of L/R and R/t ratios of 4 and 400 respectively. the first, second and third eigenmode shapes obtained using FEM are shown in Figures (6.9 - 6.11) respectively. The first eigenmode occurs at $m = 1$ and $n = 5$, while the second mode at $m = 3$ and $n = 9$ and third mode when $m = 5$ and $n = 11$.

Another example: consider a cylindrical shell of L/R ratio of 4 and R/t ratio of 800; The first, second and third eigenmode shapes obtained numerically are shown in Figures (6.12-6.14) respectively. The first mode shape is found at $m = 1$ and $n = 6$, while the second mode shape at $m = 3$ and $n = 11$, and third mode shape occurs at $m = 7$ and $n = 16$.

On the other hand, the modes obtained analytically are found in Table 6.4. It can be clearly seen from the modes obtained numerically that the buckling modes exactly identical to the analytical modes.

Table 0.4: The First three analytical eigenmodes for two different cylindrical shells of L/R =4

Eigenmode	R/t = 400		R/t = 800	
	m	n	m	n
First	1	5	1	6
Second	3	9	3	11
Third	5	11	7	16

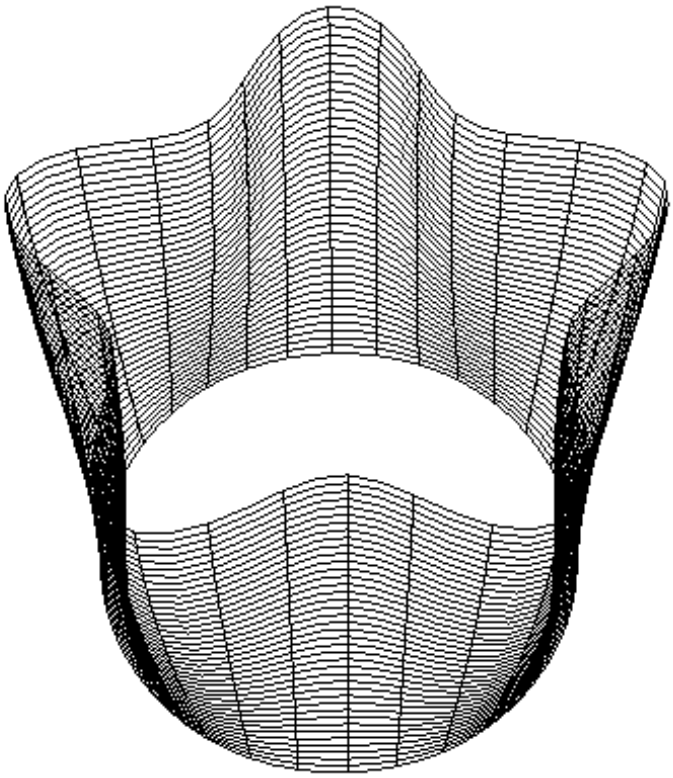

Figure 0.9: First eigenmode for cylindrical shell of L/R=4 and R/t=400 (m=1, n =5)

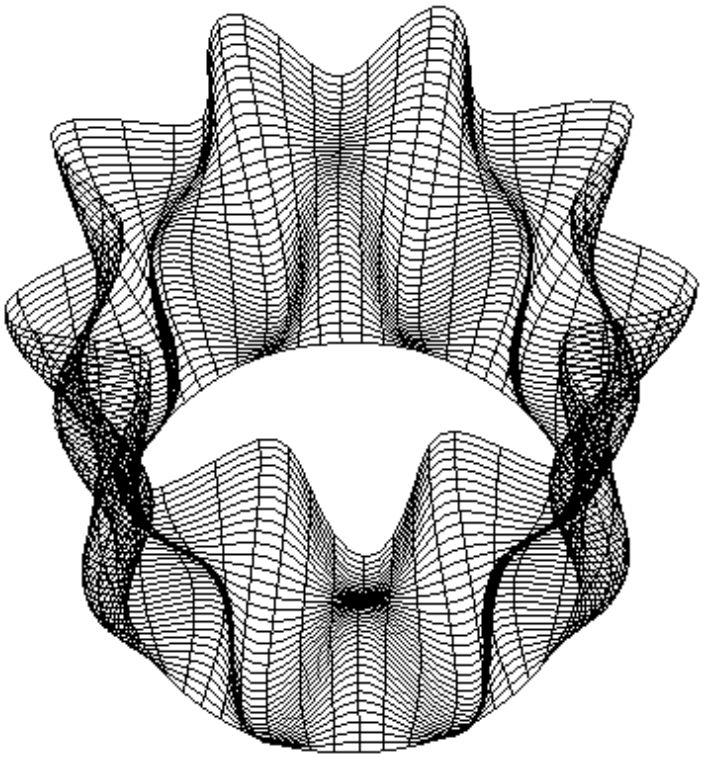

Figure 0.10: Second eigenmode for cylindrical shell of L/R=4 and R/t=400 (m =3, n = 9)

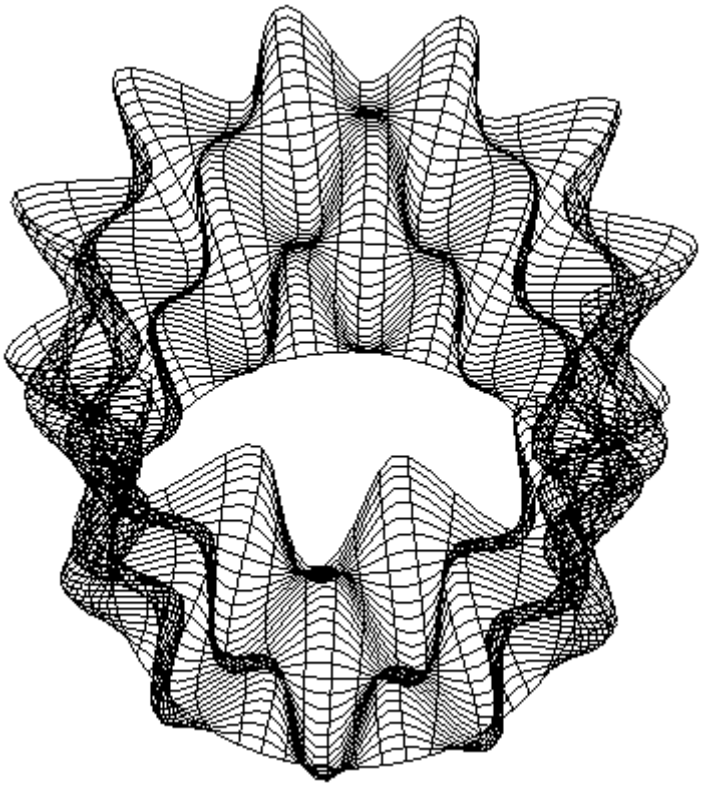

Figure 0.11: Third eigenmode for cylindrical shell of L/R = 4 and R/t = 400 (m =5, n = 11)

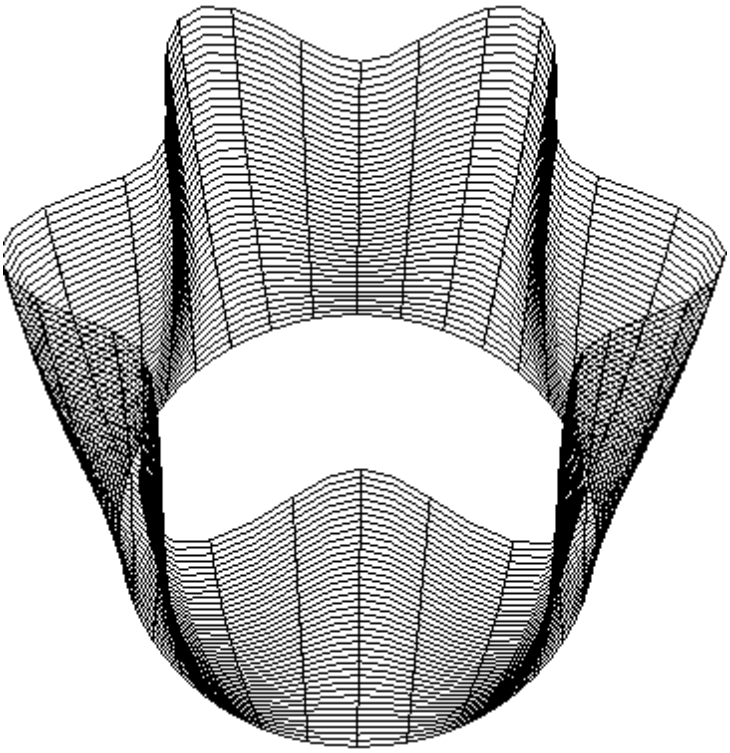

Figure 0.12: First eigenmode for cylindrical shell of L/R=4 and R/t=800 (m=1, n =6)

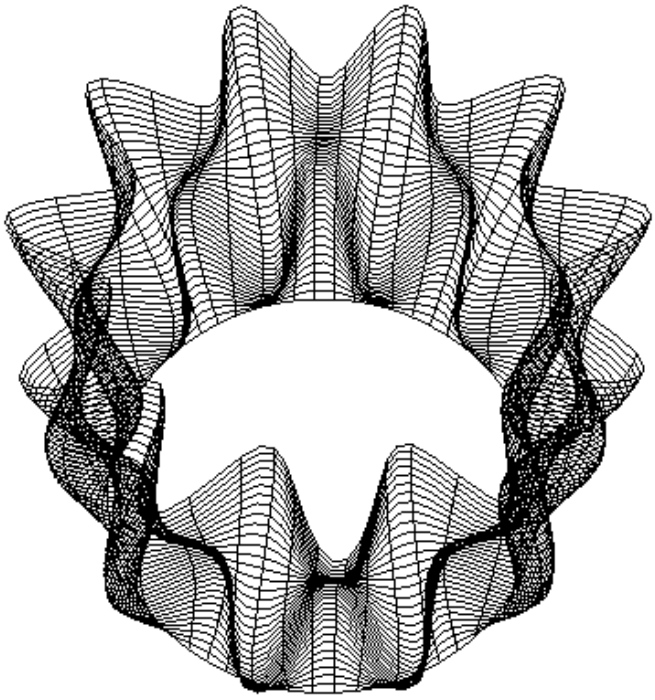

Figure 0.13: Second eigenmode for cylindrical shell of L/R=4 and R/t=800 (m =3, n = 11)

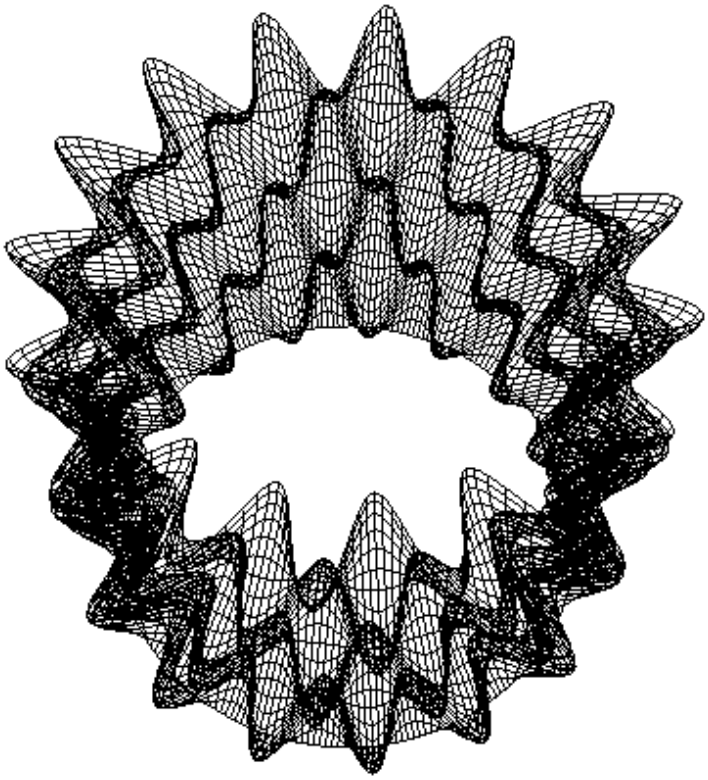

Figure 0.14: Third eigenmode for cylindrical shell of L/R=4 and R/t=800 (m =7, n = 16).

6.3.5 Results and Discussion of Stiffened SSCS

As discussed in Chapter 4, the analytical solution of stiffened cylindrical shells was given by (Eq. 4.57). Herein, different layers of CFRP sheets are used in order to increase the critical buckling stress and enhance the strength and stability of shells. Moreover, each layer has a thickness of 0.29 mm and is placed in the hoop direction only. The CFRP-sheets were fully wrapped in order to obtain maximum enhancement in other words the maximum buckling load. Moreover, the bond between CFRP and the stainless steel tube is considered to be tied (perfect bond) so no translation is allowed.

The analysis of stiffened cylindrical shells (LPA analysis), element type, mesh size and boundary conditions are similar to that of unstiffened cylindrical shells. The FEM buckling stresses were compared with the obtained analytical solution. Tables (6.5 - 6.8) compare the buckling stresses obtained analytically and numerically for different L/R and R/t ratios, noting that the critical stress indicated is $\frac{\sigma_{cr}}{E} \times 10^3$. .

Table 0.5: Buckling stresses of stiffened and unstiffened cylindrical shell of L/R ratio of 1

Analytical					**FEM**			
R/T	**Unstiffened**	**Stiffened**			**Unstiffened**	**Stiffened**		
		1-Layer	2-Layers	3-Layers		1-Layer	2-Layers	3-Layers
400	1.513	1.522	1.531	1.539	1.492	1.492	1.498	1.500
500	1.210	1.219	1.228	1.237	1.194	1.196	1.212	1.230
800	0.757	0.765	0.774	0.782	0.751	0.767	0.775	0.783
1000	0.605	0.614	0.623	0.631	0.599	0.623	0.633	0.644

Table 0.6: Buckling stresses of stiffened and unstiffened cylindrical shell of L/R ratio of 2

Analytical					FEM			
R/T	Unstiffened	Stiffened			Unstiffened	Stiffened		
		1-Layer	2-Layers	3-Layers		1-Layer	2-Layers	3-Layers
400	1.513	1.522	1.531	1.539	1.490	1.492	1.504	1.516
500	1.210	1.219	1.228	1.237	0.984	0.995	1.009	1.024
800	0.757	0.765	0.774	0.782	0.739	0.757	0.775	0.788
1000	0.605	0.614	0.623	0.631	0.599	0.612	0.623	0.632

Table 0.7: Buckling stresses of stiffened and unstiffened cylindrical shell of L/R ratio of 4

Analytical					FEM			
R/T	Unstiffened	Stiffened			Unstiffened	Stiffened		
		1-Layer	2-Layers	3-Layers		1-Layer	2-Layers	3-Layers
400	1.513	1.522	1.531	1.539	1.442	1.448	1.459	1.470
500	1.210	1.219	1.228	1.237	0.956	0.972	0.990	1.009
800	0.757	0.765	0.774	0.782	0.733	0.744	0.756	0.769
1000	0.605	0.614	0.623	0.631	0.589	0.610	0.624	0.632

Table 0.8: Buckling stresses of stiffened and unstiffened cylindrical shell of L/R ratio of 6

Analytical					FEM			
R/T	Unstiffened	Stiffened			Unstiffened	Stiffened		
		1-Layer	2-Layers	3-Layers		1-Layer	2-Layers	3-Layers
400	1.513	1.522	1.531	1.539	1.429	1.434	1.443	1.452
500	1.210	1.219	1.228	1.237	0.937	0.955	0.974	0.994
800	0.757	0.765	0.774	0.782	0.708	0.719	0.732	0.746
1000	0.605	0.614	0.623	0.631	0.597	0.610	0.619	0.630

From the above tables (6.5 - 6.8), it can be clearly noticed that the analytical buckling stresses for stiffened cylindrical shells are independent of the length of the shell, similarly with the FE method however the effect is minimal. Moreover, the critical buckling stresses obtained numerically were matching the analytical results. In addition, it is obvious that the enhancement in the critical buckling stress is very minimal. Figures (6.15 – 6.18) show the critical buckling stress, of different L/R ratios, of the bare stainless steel tubes as well as the CFRP stiffened tubes. Also, it can be clearly seen that the enhancement in the critical buckling load is worthless.

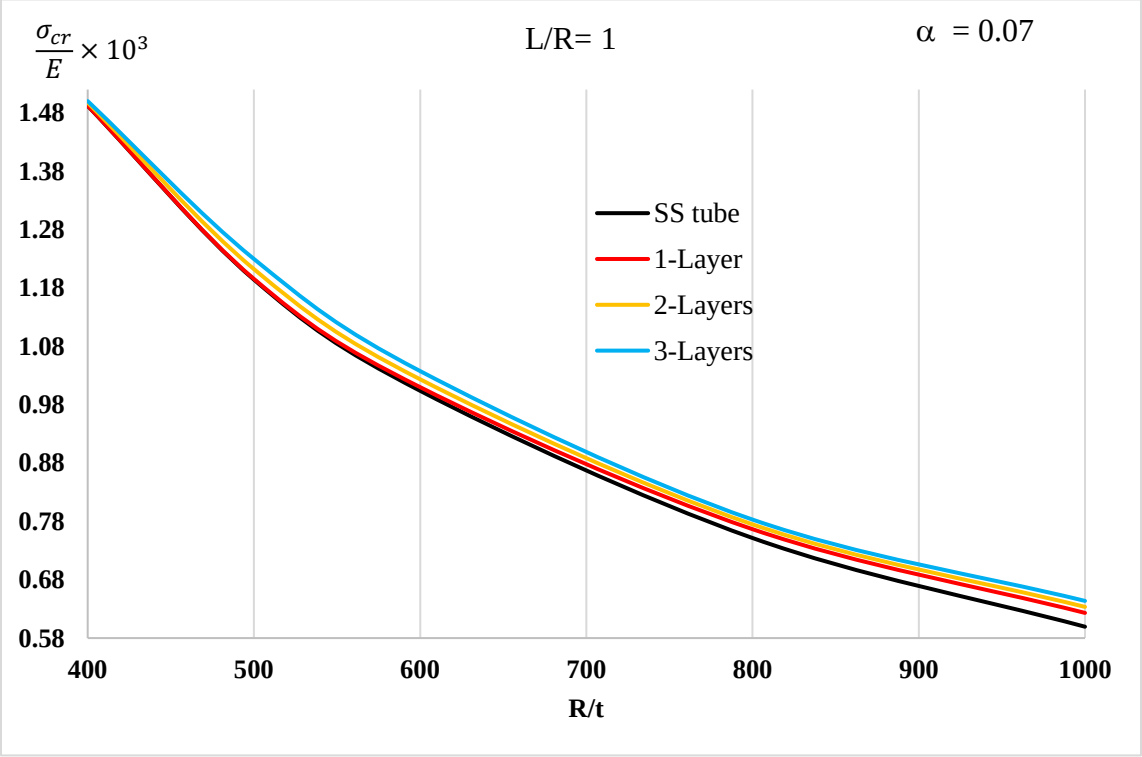

Figure 0.15: Buckling stresses of stiffened and unstiffened cylindrical shell of L/R ratio of 1

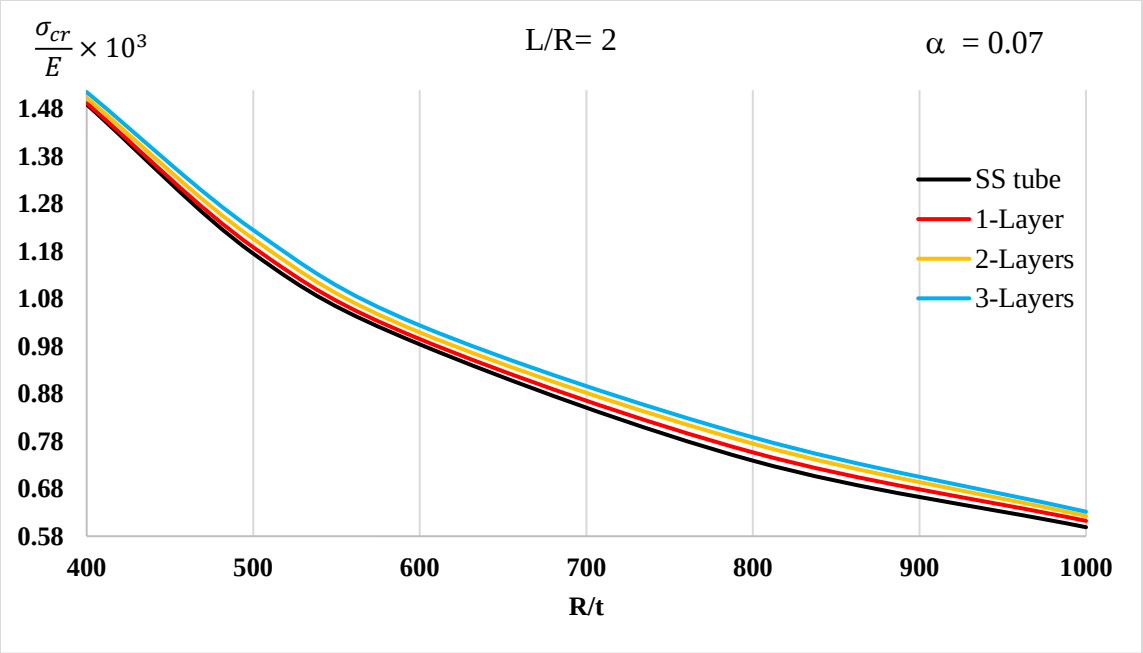

Figure 0.16: Buckling stresses of stiffened and unstiffened cylindrical shell of L/R ratio of 2

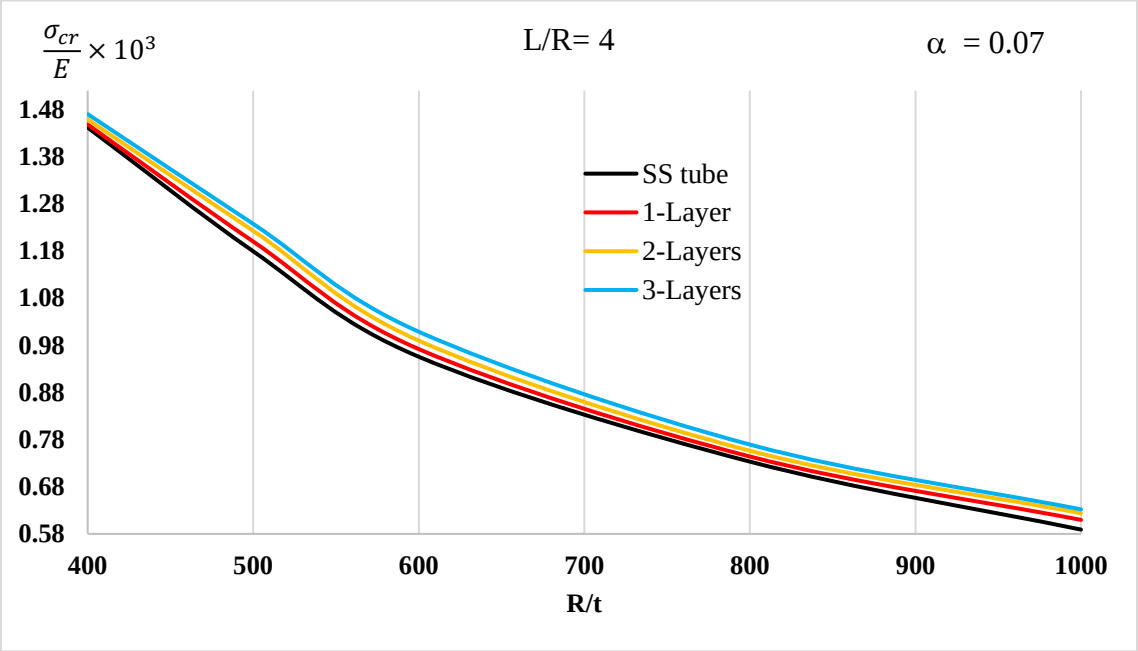

Figure 0.17: Buckling stresses of stiffened and unstiffened cylindrical shell of L/R ratio of 4

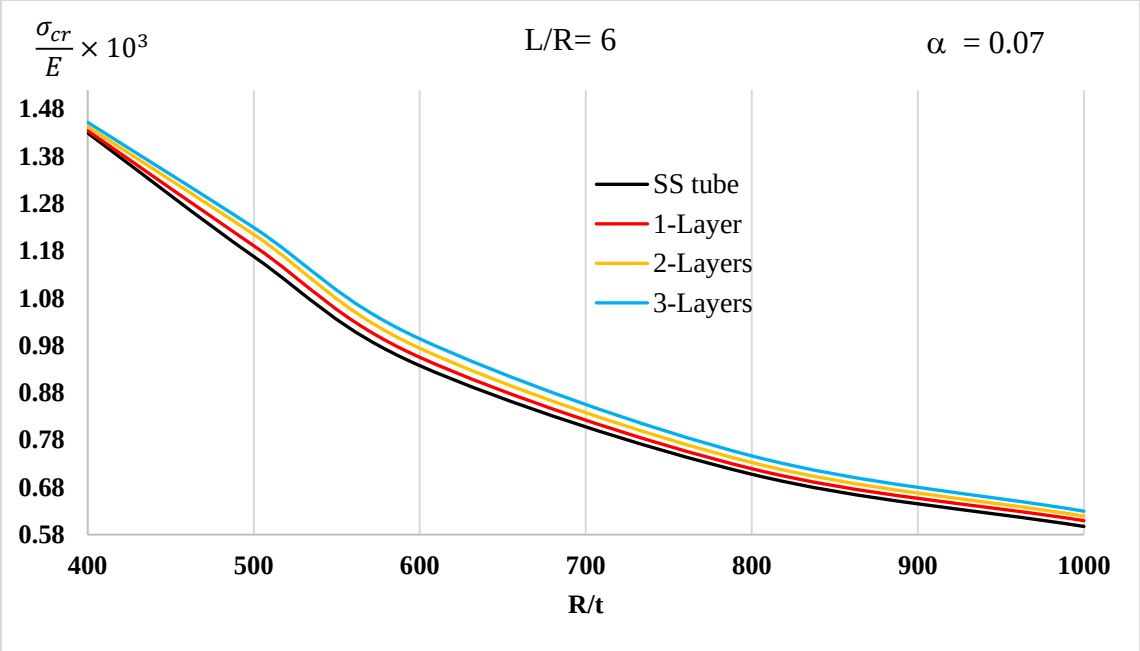

Figure 0.18: Buckling stresses of stiffened and unstiffened cylindrical shell of L/R ratio of 6

To conclude, the utilization of CFRP-stiffeners is not useful for shells that exhibit elastic buckling because the enhancement was found to be very minimal and can be ignored. The main reason is that elastic buckling occurs at early stage, therefore, the CFRP will not fully contribute to the enhancement of buckling stress. The CFRP can be fully contributed when the buckling happens in the plastic range. In this case, elastic buckling, the only contribution comes from the modules of elasticity of CFRP as well as its thickness. Since the modules of elasticity of CFRP is close to the stainless steel and the thickness is very small, the resistance against loading is minimized and a sudden buckling failure may occur. A key point to consider is that buckling modes of stiffened cylindrical shells were matching the unstiffened cylindrical shell.

6.4 Plastic Buckling

6.4.1 Finite Element Analysis

The material properties should be specified in the format of true stress and log-plastic strain in order to be analyzed in ABAQUS [42]. Therefore, the generated engineering stress-strain curves using Ramberg-Osgood model [10], [11] were converted into true stress and log-plastic strains using Equations 5.43 and 5.44 same as the procedure in Chapter 5 (worked example). The model was analyzed using Explicit/Dynamics which can be found in the STEP module in Abaqus. It can solve nonlinear transient dynamic problems by using traditional explicit integration scheme.

6.4.2 Element Type and Mesh Size

The elemental type used in this model is S4R which is a four-node doubly curved general-purpose shell element, reduced integration with finite membrane strain [42]. Each node has six degrees of freedoms (3-transilations and 3-rotations). This element type is preferred when the thickness is significantly small compared to other dimensions. It has been utilized for the numerical investigation of both unstiffened and stiffened cylindrical shells, and it has been shown to work well in modelling of thin-walled structures [40], [43]–[46].

With regards to mesh size, a uniform mesh of a size that is equal to the thickness of shell ($t \times t$) has been selected-or assigned for all elements in the model, along both circumferential and longitudinal directions. Since the failure mode is axi-symmetric in plastic buckling, only quarter of the model has been analyzed due to time concerns. Nevertheless, for unstiffened cylindrical shells a full model has been analyzed because the time was not a concern and the analysis was fast and accurate. An important point to

consider is that suitable symmetric boundary conditions should be applied for the quarter models.

6.4.3 Boundary Conditions

Two models with different boundary conditions (fixed and simply supported) have been analyzed using Abaqus. As it can be clearly seen from Figure 6.19, there is no variation in the buckling load of fixed and simply supported shells, however, the behavior after buckling has minor differences. Also, from literature, fixed supports are close to reality and experiments, hence fixed boundary conditions have been used in the plastic buckling analysis.

The nodes located at each end cross-sections were coupled at a reference point that is concentric, at the center of the shell. At one end all degrees of freedoms were restrained, similarly with the other end (loaded end) except the longitudinal translation. Regarding loading conditions, the nodes, where the load is applied, at the end section were coupled at an eccentric reference point. Moreover, the load was applied on the reference point allowing longitudinal translation at the loaded end.

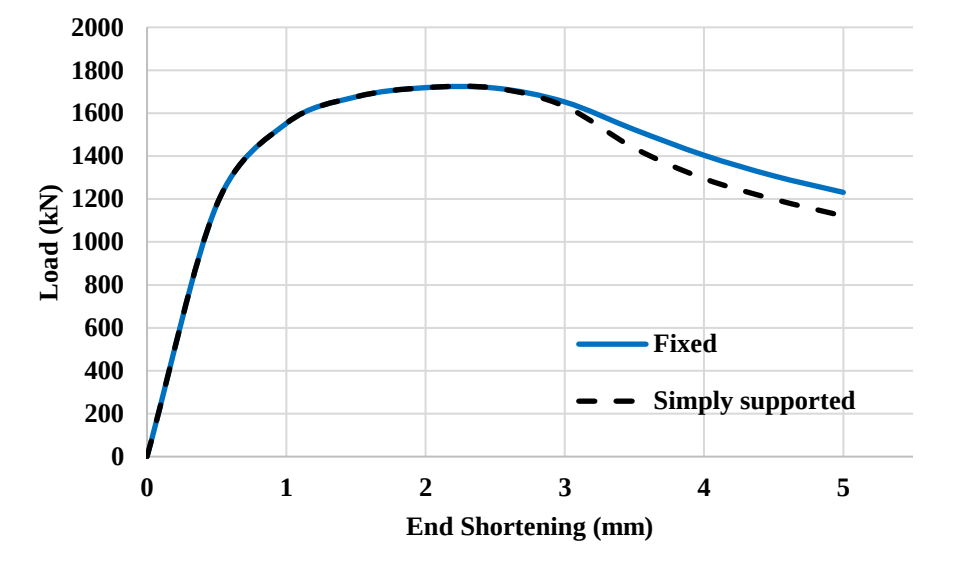

Figure 0.19: Load-End shortening curves for fixed and simply supported shells (R/t =50).

6.4.4 Results and Discussion of Unstiffened SSCS

As discussed in chapter 5 the analytical solution of unstiffened cylindrical shells is given by Eq. 5.20. The critical buckling stresses obtained numerically were close to the analytical solution. Table 6.9 shows a comparison between the analytical and numerical loads for various R/t ratios. Also, the percentage error between the obtained buckling loads is indicated in the table. The radius of the cylindrical shell and the length-to-radius ratio were selected to be 200 mm and 6 respectively. Also, the used stainless steel characteristics, in this chapter, are the same as the worked example in Chapter 5. Figure 6.20 shows the ratio of the numerical stress to the analytical stress. It can be noted that the ratio ranges approximately from 0.88 to 1.04. Moreover, the error increases as the R/t ratio increases and this little deviation was expected due to the difference in formulations used in the two solutions, total deformation theory for the Analytical solution while incremental theory is implemented for the numerical solution.

Table 0.9: The analytical and numerical buckling loads for various R/t ratios

R/t	Buckling Stress (MPa)		Error (%)
	FEM	Analytical	
25	381.26	364.04	4.73
50	343.69	344.21	0.15
75	329.39	336.78	2.20
100	316.98	333.59	4.98
125	306.03	332.05	7.84
150	293.49	331.20	11.38
175	290.84	330.71	12.06

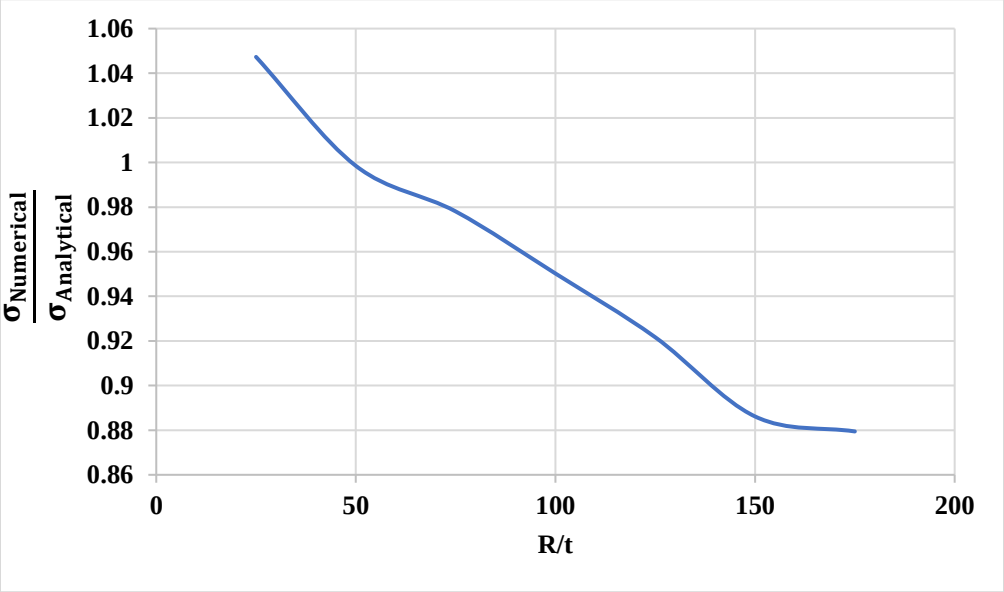

Figure 0.20: Ratio of the numerical stresses to the analytical stresses

A study was conducted to investigate the variation of L/R and its effect on the buckling stress. Table 6.10 shows the buckling loads of different shell geometries, different R/t and L/R ratios; the diameter of the shell was $110\ mm$. As it can be clearly noticed that the length-to-radius geometric ratio does not influence the plastic buckling.

Table 0.10: The buckling load for various R/t and L/R ratios

R/t	Buckling Stress (MPa)			
	FEM (L/R)			Analytical
	2	4	6	
20	377.94	377.53	377.35	353.62
30	233.55	233.37	233.06	226.86
40	167.93	167.87	167.88	166.18
50	129.36	129.62	130.68	130.85
60	106.91	107.12	104.73	107.84
70	90.34	88.11	88.36	91.72
80	77.38	77.26	77.22	79.81
90	65.48	63.37	68.39	70.66
100	57.05	56.78	59.85	63.40

From literature, the mode in plastic buckling is expected to be axi-symmetric which was validated here using FEM. For all the numerical results the buckling mode was found to be axi-symmetric, a sample of the mode obtained is shown in Figure 6.21.

Figure 0.21: Buckling mode of R/t=50 and L/R=2

6.4.5 Results and Discussion of Stiffened SSCS

The CFRP-sheets were fully wrapped in order to obtain maximum enhancement, in other words the maximum buckling load. As discussed in Chapter 5, the analytical solution of stiffened cylindrical shells was given by (Eq. 5.38).

For stiffened cylindrical shells the FEA, boundary conditions, element type and mesh density are similar to unstiffened cylindrical shells. The numerical buckling loads were compared with the obtained analytical loads for different R/t ratios as shown in Tables 6.11 and 6.12. The modulus of elasticity of the CFRP was considered as $200\ \text{GPa}$ and the thickness of each layer is $0.33\ mm$.

Table 0.11: The buckling load of un-stiffened and stiffened SSCT of R/t=80

$R/t = 80$		Buckling Stress (MPa)		Error (%)
		Analytical	Numerical	
un-stiffened		335.92	326.882	2.69
Stiffened	1-Layer	340.332	352.4342	3.56
	2-Layers	346.635	374.2388	7.96
	3-Layers	353.564	387.7266	9.66

Table 0.12: The buckling load of un-stiffened and stiffened SSCT of R/t=100

$R/t = 100$		Buckling Stress (MPa)		Error (%)
		Analytical	Numerical	
un-stiffened		333.587	307.55	7.80
Stiffened	1-Layer	336.548	343.35	2.02
	2-Layers	341.178	364.33	6.79
	3-Layers	347.129	380.06	9.49

From the tables above, the critical buckling loads obtained numerically were close from the analytical results with an error of less than 10%. Unlike elastic buckling, it is obvious

that the there is an enhancement in the buckling resistance. Figures (6.22-6.25) show the critical buckling loads of the bare stainless steel tubes as well as the CFRP stiffened tubes for different R/t ratios. The buckling loads of these figures are summarized in Table 6.13.

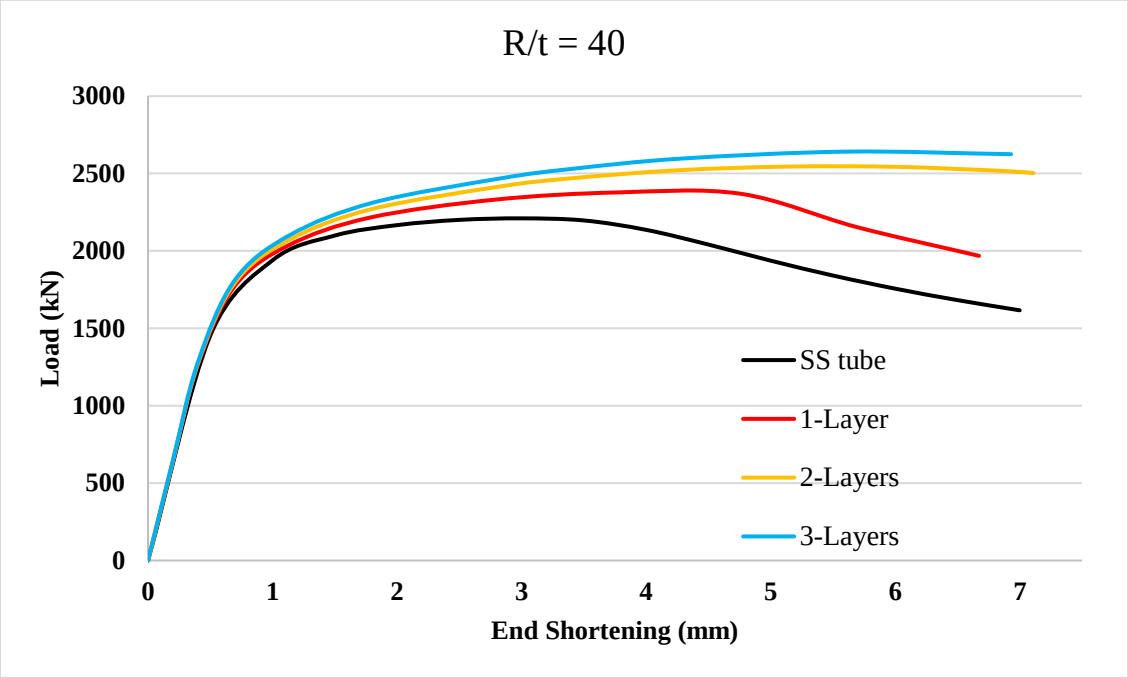

Figure 0.22: Buckling load of stiffened and unstiffened SSCS of R/t ratio of 40

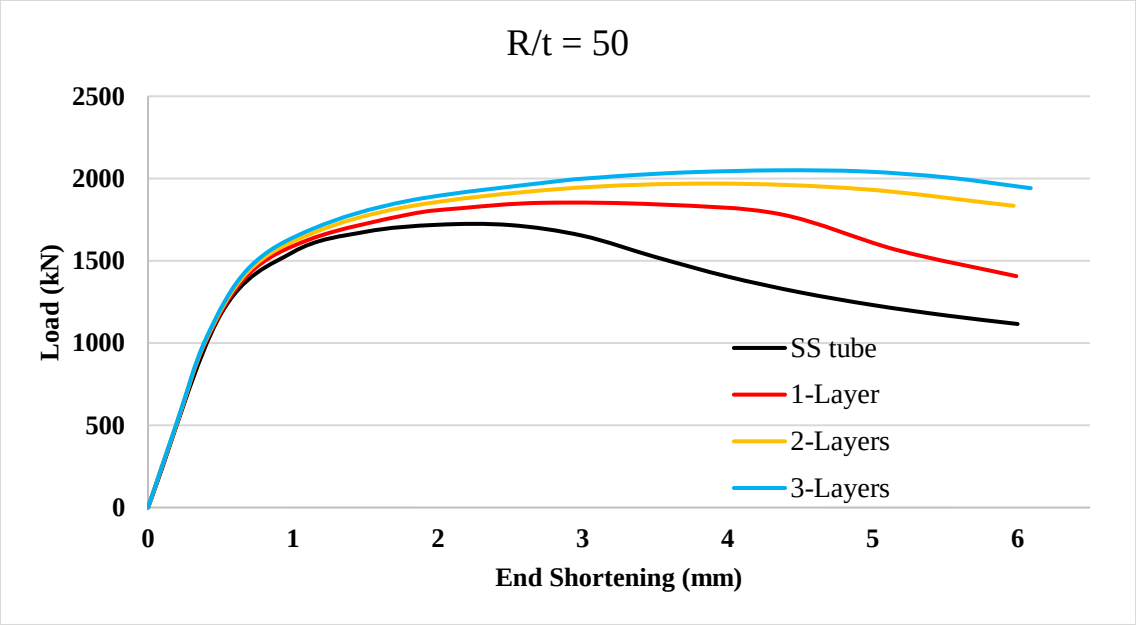

Figure 0.23: Buckling load of stiffened and unstiffened SSCS of R/t ratio of 50

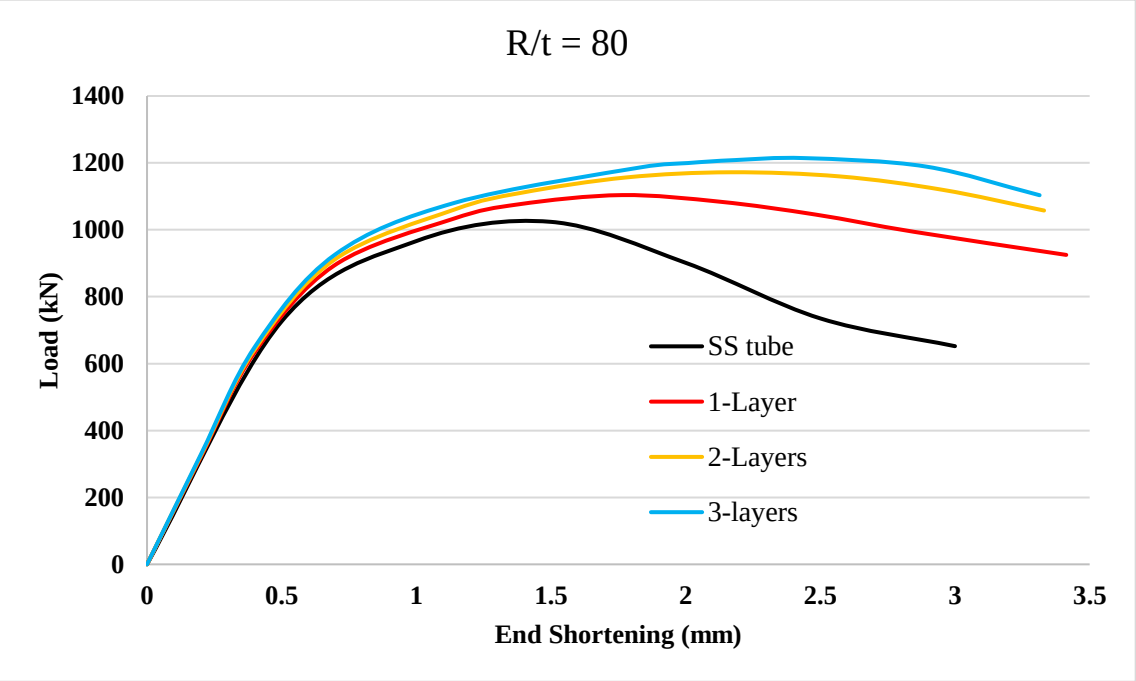

Figure 0.24: Buckling load of stiffened and unstiffened SSCS of R/t ratio of 80

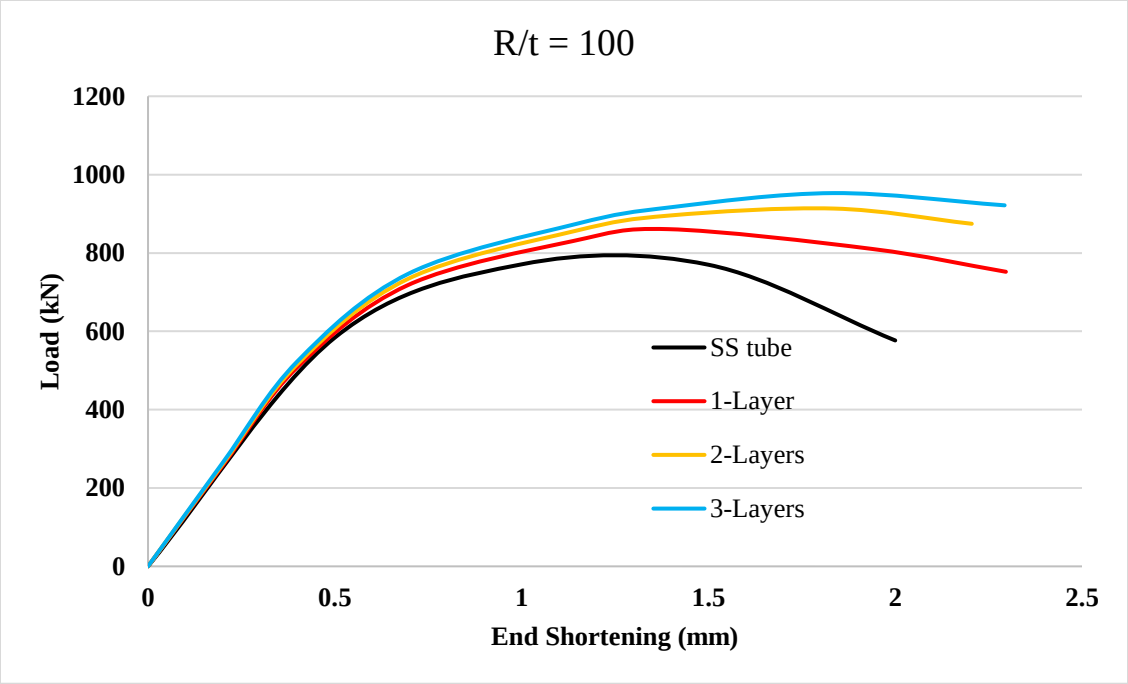

Figure 0.25: Buckling load of stiffened and unstiffened SSCS of R/t ratio of 100

Table 0.13: The buckling Stress, in MPa, for different R/t ratios

R/t		40	50	80	100
un-stiffened		354.02	343.69	326.88	307.55
Stiffened	1-Layer	380.87	370.36	352.43	343.35
	2-Layers	407.54	393.73	374.24	364.33
	3-Layers	423.06	409.87	387.73	380.06

Unlike elastic buckling, SSCS capabilities against plastic buckling is enhanced when CFRP jacketing is applied. The main reason is that the tube yields first which will enforce the CFRP stiffeners to contribute in supporting the strength of SSCS against buckling.

6.4.6 A parametric Study

The parameter α is dependent on the properties of both stainless steel tube and the CFRP-stiffeners, in which $\alpha = \frac{E_f\ t_f}{E_s\ t_s}$ as given in Chapter 3. A parametric study was conducted in order to see the behavior of α parameter with the buckling stress. Different values of alpha and n (number of CFRP layers) has been examined. Figures 6.26, 6.27 and 6.28 show different values of alpha 0.29, 0.33 and 0.4 respectively. As can be observed that as the number of layers increases, the buckling stress increases. Also, as the R/t ratio increases, the buckling stress decreases.

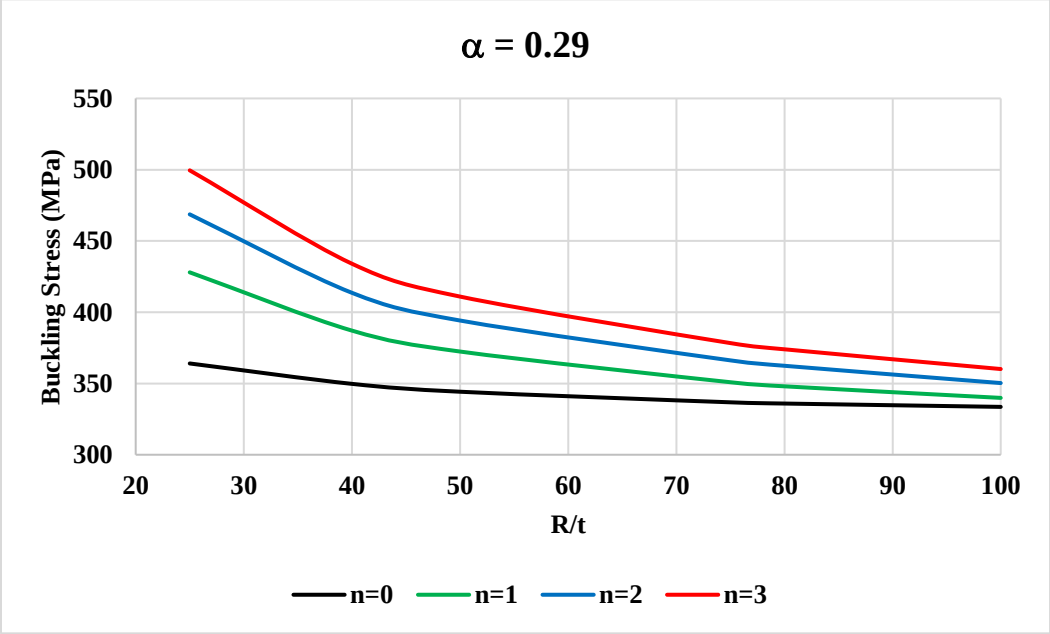

Figure 0.26: The buckling stress of un-stiffened and CFRP-stiffened SSCS with α=0.29

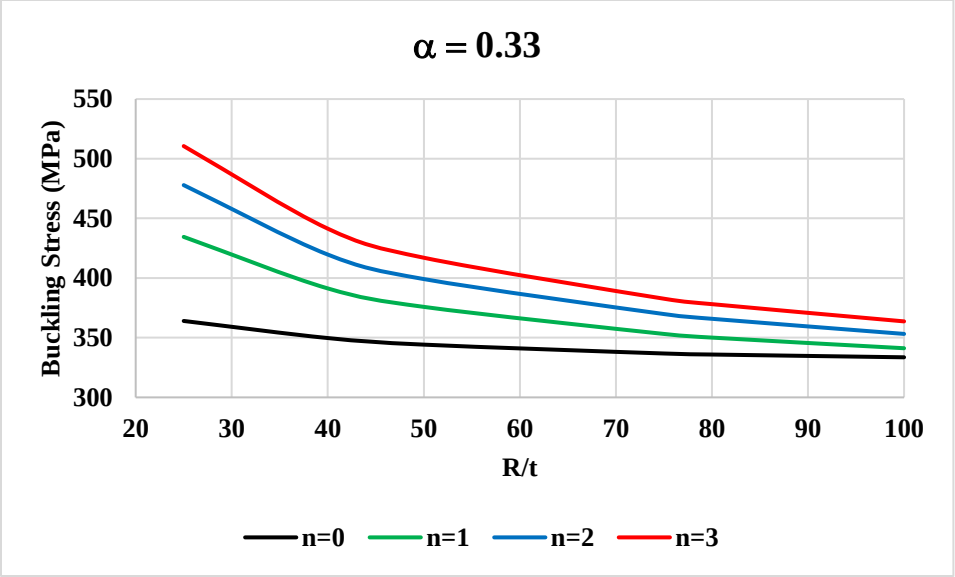

Figure 0.27: The buckling stress of un-stiffened and CFRP-stiffened SSCS with α=0.33

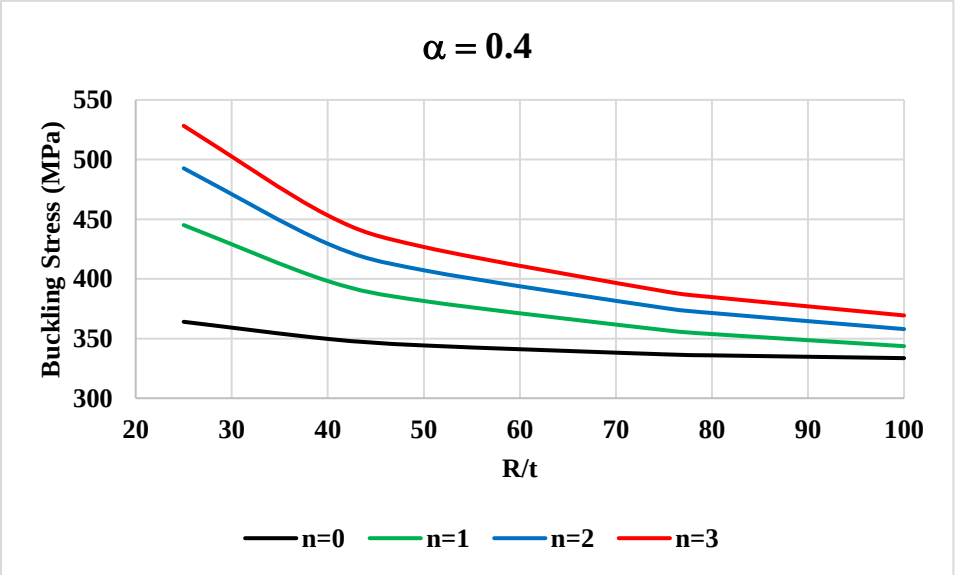

Figure 0.28: The buckling stress of un-stiffened and CFRP-stiffened SSCS with α=0.4

Table 6.14 shows the detailed values of Figure 6.28 and the enhancement of each layer in terms of buckling stresses. Furthermore, as α values increase the buckling stress increases and it can be clearly compared and noticed in Figure 6.29, the dashed lines indicate that one CFRP-layer is used while the solid lines for three CFRP-layers ($n = 3$).

Table 0.14: The buckling stress (in MPa) of un-stiffened and CFRP-stiffened SSCS using FEM for different R/t ratios.

R/t		25	50	75	100
Unstiffened (n=0)		364.04	344.21	336.78	333.59
Stiffened	1-Layer (n=1)	434.51	375.85	353.17	341.18
	2-Layers (n=2)	477.88	399.16	369.83	353.18
	3-Layers (n=3)	510.60	417.02	382.68	363.7
% Increase in Buckling Stress	1-Layer	19.36	9.19	4.87	2.28
	2-Layers	31.27	15.96	9.82	5.87
	3-Layers	40.26	21.15	13.63	9.03

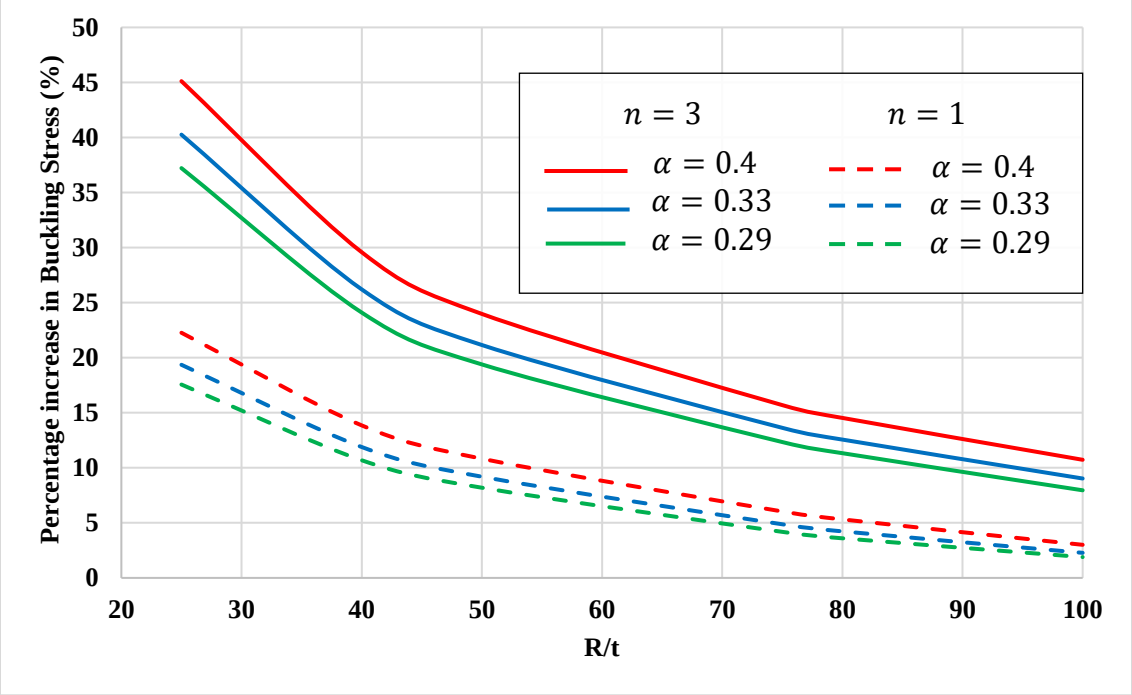

Figure 0.29: The buckling stress of un-stiffened and CFRP-stiffened SSCS with different values of α and n

CHAPTER 7

SUMMARY, CONCLUSIONS AND RECOMMENDATIONS

The key findings, main conclusions and recommendations of future work are summarized in this chapter. The main objective of this research is to study and derive analytically the buckling load of unstiffened and CFRP-stiffened SSCS based on Ritz method, in addition to verify the obtained results by numerical methods (FEM).

7.1 Summary

The considered SSCC is assumed to be perfect without any geometric imperfections. Both elastic and plastic buckling are considered. The former is analyzed based on the standard linear relations while the latter is modeled as nonlinear strain-hardening, based on theories of plasticity. The CFRP jackets used to provide an external confinement to the SSCS for the suppression of local buckling in SST columns when subjected to axial compression.

There are three possible failure types for thin circular cylindrical shells subjected to a compressive load: global (column) buckling, elastic local buckling and plastic local buckling. The elastic local buckling could be axi-symmetric buckling (ring) or non-symmetric buckling (chessboard) while plastic buckling happens to be only axi-symmetric buckling. Each type could control and produce the minimum (critical) buckling load depending on the geometric ratios. Figure 7.1 illustrates the failure types in shells and state

their limits qualitatively. The global buckling occurs when length-to-radius ratio is very high.

The critical buckling load of unstiffened and stiffened cylindrical shells has been derived by Ritz method and the list of solutions are summarized in Table 7.1. As it can be observed, the (L/R) ratio does not play a significant role in the buckling because in thin cylindrical shells the buckling most probably happens to be local.

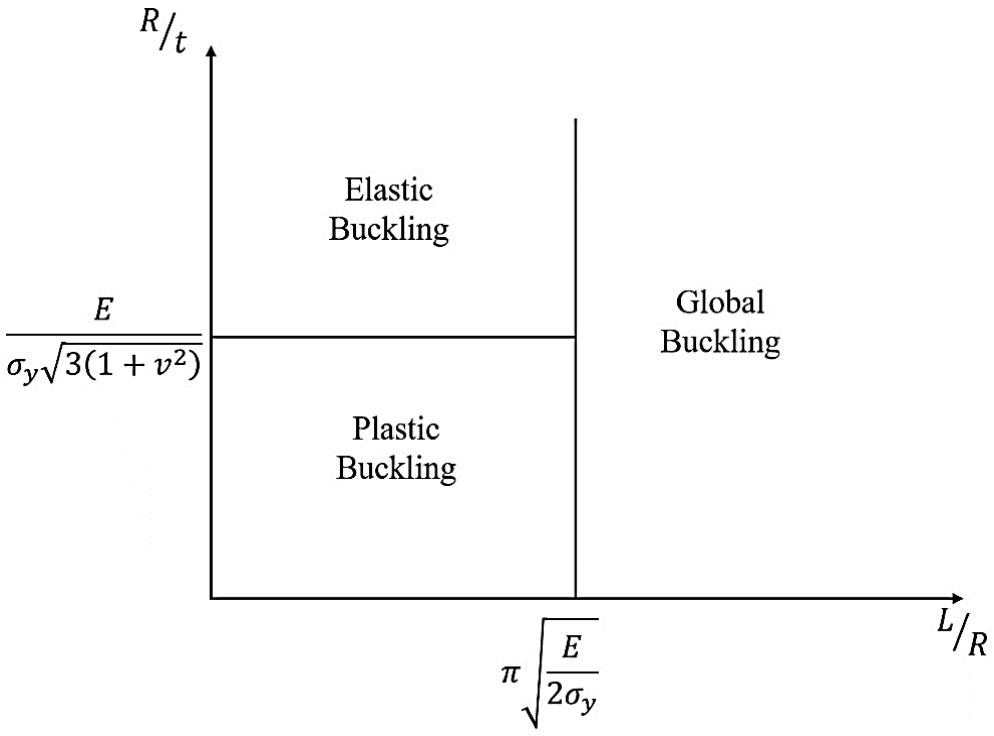

Figure 0.1: The limits and failure types in SSCS

Table 0.1: Analytical Solutions Summary

Buckling Type	Shell Condition	Buckling Load (N_{cr})
Elastic Buckling	Unstiffened	$\frac{E\,t^2}{R\sqrt{3(1-v^2)}}$
	Stiffened	$\frac{\sqrt{(1+n\,\alpha)}\,E_s\,{t_s}^2}{R\sqrt{3(1-v^2)}}$
Plastic Buckling	Unstiffened	$\left(\frac{2}{\sqrt{3}\sqrt{\lambda(5+3e-4v)-(1-2v)^2}}\right)\frac{E\,t}{R}$
	Stiffened	$\frac{2}{\sqrt{3}}\left(\frac{\sqrt{1+n\,\alpha(3/4+3/4\,e+\lambda/4)}}{\sqrt{\lambda(5+3e-4v)-(1-2v)^2}}\right)\frac{E\,t}{R}$

7.2 Conclusions

Based on the results obtained, the following conclusions can be drawn:

1- The accuracy of all derived analytical formulas was verified by comparison with those in the literature as well as by FEM. The little deviation for the case of plastic buckling was expected due to the difference in formulations used in the two solutions.

2- For axisymmetric elastic buckling, the buckling stress decreases significantly as R/t increases. On the other hand, L/R has no effect on the buckling stress. This is true for both stiffened and unstiffened SSCS.

3- For non-symmetric elastic buckling, R/t has the same effect as in the axisymmetric case. However, unlike the axisymmetric case, L/R has an appreciable effect on non-symmetric elastic buckling especially for lower values of R/t. This is due to the circumferential buckling mode which was absent in axisymmetric elastic buckling.

4- For plastic buckling, the buckling mode is axisymmetric and occurs at low R/t ratios. The buckling stress decreases significantly as the radius-to-thickness ratio increases.

5- The utilization of CFRP-stiffeners did not lead to appreciable gain in buckling capacity for practical values of α. The main reason is that elastic buckling occurs at small hoop strain and shell buckles before CFRP fibers are mobilized. For elastic buckling, the maximum gain in buckling capacity, for a practical value of α = 0.09 is approximately 12%. On the other hand, for CFRP-stiffened SSCS that exhibit plastic buckling, the buckling capacity is proportional to α and the number of CFRP layers. The gain in buckling capacity for a practical α of 0.4 is 40%. The relatively large gain compared to the elastic case is attributed to the large hoop strain which resulted in higher hoop stress in CFRP layers.

6- The proposed Ritz method offers an excellent alternative analytical solution to the buckling of unstiffened and stiffened shells and the use of Mathematica greatly reduced the effort of formulating and performing the detailed computations and achieving analytical formulas that are more suitable for design purposes.

7.3 Recommendations for Future Research

The outcome of current research can be enhanced by extending the study to account for the following:

- Consider the case of SSCS filled with concrete.
- Validate of the analytical and FEM models with experimental work.
- Study the effect of imperfection on the buckling capacity.
- Include the large strain terms which is likely to reduce the theoretical buckling stress and hence reduce the difference between the analytical and experimental values.
- Extend the shell model to include other types of loading such as pressure, shear forces, and moments.

REFERENCES

[1] J. Sun, X. Xu, C. W. Lim, and V. B. C. Tan, “An energy conservative symplectic methodology for buckling of cylindrical shells under axial compression,” *Acta Mech.*, vol. 224, no. 8, pp. 1579–1592, 2013.

[2] R. Batista and P. Gonçalves, “Non-linear Lower Bounds for Shell Buckling Design.pdf,” *Constr. Steel Res.*, 1994.

[3] B. Young and E. Ellobody, “Experimental investigation of concrete-filled cold-formed high strength stainless steel tube columns,” *J. Constr. Steel Res.*, vol. 62, no. 5, pp. 484–492, 2006.

[4] E. Ventsel and T. Krauthammer, *Thin Plates and Shells: Theory, Analysis, and Applications*. 2001.

[5] C. R. Calladine, “Understanding imperfection-sensitivity in the buckling of thin-walled shells,” *Thin-Walled Struct.*, vol. 23, no. 1–4, pp. 215–235, 1995.

[6] M. Vaghani, S. A. Vasanwala, and A. K. Desai, “Stainless Steel As A Structural Material : State Of Review,” *J. Eng. Res. Appl.*, vol. 4, no. 3, pp. 657–662, 2014.

[7] J. Haedir and X. L. Zhao, “Design of short CFRP-reinforced steel tubular columns,” *J. Constr. Steel Res.*, vol. 67, no. 3, pp. 497–509, 2011.

[8] J. G. Teng and Y. M. Hu, “Behaviour of FRP-jacketed circular steel tubes and cylindrical shells under axial compression,” *Constr. Build. Mater.*, vol. 21, no. 4, pp. 827–838, 2007.

[9] L. Gardner and M. Ashraf, “Structural design for non-linear metallic materials,” *Eng. Struct.*, vol. 28, no. 6, pp. 926–934, 2006.

[10] W. Ramberg and W. Osgood, “Description of stress-strain curves by three parameters.,” *Natl. Advis. Comm. Aeronaut.*, vol. Technical, no. Washington, DC, 1943.

[11] H. Hill, “Determination of stress-strain relations from the offset yield strength values,” *Natl. Advis. Comm. Aeronaut.*, vol. Technical, no. Washington, DC, 1944.

[12] K. Rasmussen, “Full-range Stress-strain Curves for Stainless Steel Alloys,” *J. Constr. Steel Res.*, p. 45, 2003.

[13] S. P. Timoshenko and J. M. Gere, *Theory of Elastic Stability,*. New York: McGraw-Hill, 1961.

[14] B. Thiirlimann, “Column BucklingmHistorical and Actual Notes,” *J. Constr. Steel Res.*, vol. 17, no. 1990, pp. 95–111, 1991.

[15] W. . Koiter, “Over de stabiliteit van het elastisch evenwicht.pdf,” Institutional

Repository, 1945.

[16] J. W. Hutchinson, “IMPERFECTION-SENSITIVITY IN THE PLASTIC RANGE,” *Mech. Phys. Solids*, vol. 21, pp. 191–204, 1973.

[17] J. W. Hutchinson and W. T. Koiter, “Postbuckling theory,” *Appl. Mech. Rev*, vol. 23, no. 12, pp. 1353–1366, 1970.

[18] R. Lorenz, *Achsensymmetrishce Verzerrungen in d¨unnwandigen Hohlzylindern,’ Zeitschrift des Vereines Deutscher Ingenieure*. 1908.

[19] S. Timoshenko, *Einige Stabilittsprobleme der Elastizit¨atstheorie*. ZAMP, 1910.

[20] R. V. Southwell, “On the General Theory of Elastic Stability,” *Philos. Trans. R. Soc. London*, vol. 213, 1914.

[21] W. Flügge, *Die Stabilität der Kreiszylinderschale*. Berlin, Germany, 1932.

[22] W. Flügge, *Statik und Dynamik der Schalen*. Berlin,: Springer, 1934.

[23] L. H. Donnell, “A new theory for the buckling of thin cylinders under axial compression and bending,” *Trans. ASME*, vol. 56, no. 11, pp. 795–806, 1934.

[24] P. P. Bijlaardt, “Theory and Tests on the Plastic Stability of Plates and Shells,” *J. Aeronaut. Sci.*, vol. 16, pp. 529–541, 1949.

[25] F. M. A. Silva, P. B. Goncalves, and Z. J. G. N. Del Prado, “Influence of Physical and Geometrical System Parameters Uncertainties on the Nonlinear Oscillations of Cylindrical Shells,” *J. Brazilian Soc. Mech. Sci. Eng.*, vol. 34, no. 2, pp. 622–632, 2012.

[26] C. Bisagni, “Composite cylindrical shells under static and dynamic axial loading: An experimental campaign,” *Prog. Aerosp. Sci.*, vol. 78, pp. 107–115, 2015.

[27] P. Som and A. Deb, “A generalized Ritz-based method for nonlinear buckling of thin cylindrical shells,” *Thin-Walled Struct.*, p. 14, 2014.

[28] S. E. Kim and C. S. Kim, “Buckling strength of the cylindrical shell and tank subjected to axially compressive loads,” *Thin-Walled Struct.*, vol. 40, no. 4, pp. 329–353, 2002.

[29] H. Ullah, “Buckling of thin-walled cylindrical shells under axial compression,” *Int. J. Numirical Methods Eng.*, vol. 79, no. 11, 2009.

[30] G. Jacob, K. K. Divya, and P. Prabhakaran, “Buckling Analysis of Cylindrical Shells Subjected to Axial Compression,” *Int. Res. J. Eng. Technol.*, vol. 4, no. 4, pp. 3483–3486, 2017.

[31] P. R. Jagtap, “Necessity of Strengthening of Steel Structures with FRP Composites : a Review,” vol. 5, no. 4, pp. 390–394, 2015.

[32] M. C. Sundarraja and G. G. Prabhu, “Experimental study on CFST members strengthened by CFRP composites under compression,” *J. Constr. Steel Res.*, vol. 72, pp. 75–83, 2012.

[33] M. I. Alam and S. Fawzia, “Numerical studies on CFRP strengthened steel columns under transverse impact,” *Compos. Struct.*, 2014.

[34] A. Punitha Kumar and R. Senthil, “Axial Behaviour of CFRP-Strengthened Circular Steel Hollow Sections,” *Arab. J. Sci. Eng.*, vol. 41, no. 10, pp. 3841–3850, 2016.

[35] A. Ghorbanpour Arani, A. Loghman, A. A. Mosallaie Barzoki, and R. Kolahchi, “Elastic buckling analysis of ring and stringer-stiffened cylindrical shells under general pressure and axial compression via the Ritz method,” *J. Solid Mech.*, vol. 2, no. 4, pp. 332–347, 2010.

[36] A. C. Ugural, *Stresses in Beams, Plates, and Shells*. 2010.

[37] C. M. Wang, C. Y. Wang, and J. N. Reddy, *EXACT SOLUTIONS FOR BUCKLING OF STRUCTURAL MEMBERS*. CRC PRESS, 2006.

[38] M. H. Jawad, *Theory and Design of Plate and Shell Structures*. Springer, 1994.

[39] W. F. Chen, *Plasticity for Structural Engineers*. J. Ross Publishing, 2007.

[40] L. Gardner and D. . Nethercot, “Experiments on stainless steel hollow sections-Part 1: Material and cross sectional behavior.pdf,” *J. Constr. Steel Res.*, p. 28, 2004.

[41] O. Zhao, L. Gardner, and B. Young, “Structural performance of stainless steel circular hollow sections under combined axial load and bending - Part 1: Experiments and numerical modelling,” *Thin-Walled Struct.*, vol. 101, pp. 231–239, 2016.

[42] Dassault, “ABAQUS / CAE User’s Manual,” *ABAQUS/CAE User’s Man.*, pp. 1–847, 2012.

[43] M. Ashraf, L. Gardner, and D. A. Nethercot, “Finite element modelling of structural stainless steel cross-sections,” *Thin-Walled Struct.*, vol. 44, no. 10, pp. 1048–1062, 2006.

[44] M. Theofanous and L. Gardner, “Testing and numerical modelling of lean duplex stainless steel hollow section columns,” *Eng. Struct.*, vol. 31, no. 12, pp. 3047–3058, 2009.

[45] Y. Huang and B. Young, “Experimental and numerical investigation of cold-formed lean duplex stainless steel flexural members,” *Thin-Walled Struct.*, vol. 73, pp. 216–228, 2013.

[46] I. Arrayago, F. Picci, E. Mirambell, and E. Real, “Interaction of bending and axial

load for ferritic stainless steel RHS columns," *Thin-Walled Struct.*, vol. 91, pp. 96–107, 2015.

VITAE

Name	:Osamah Hamoud Ahmad Dehwah
Nationality	:Yemeni
Date of Birth	:5/25/1993
Email	:osamah@dehwah.com
Address	:Dhahran 31261, Eastern Province, Saudi Arabia
Academic Background	:B.Sc. in Civil Engineering from King Fahd University of Petroleum and Minerals, Saudi Arabia

APPENDIX A
Constitutive Equations Constants Derivation

According to total deformation theory of plasticity, the constitutive equations are given by [28]:

$\sigma x = E\,(C_{11}\,\epsilon x + C_{12}\,\epsilon\theta)$;
$\sigma\theta = E\,(C_{12}\,\epsilon x + C_{13}\,\epsilon\theta)$;

where:

$C_{11} = \frac{\psi 1}{\psi 4}$
$C_{12} = \frac{\psi 2}{\psi 4}$
$C_{13} = \frac{\psi 3}{\psi 4}$

$\psi 1 = (1-2\beta)^2\,E + 3\,(1+e)\,E_t$;
$\psi 2 = (2-\beta)\,(1-2\beta)\,E - \left((2-\beta)\,(1-2\beta) - 4\,\nu\,\eta^2 - 3\,e1\,\beta\right)E_t$;
$\psi 3 = (2-\beta)^2\,E + 3\,(1+e)\,\beta^2\,E_t$;
$\psi 4 = \left((5-4\,\nu)\left(1+\beta^2\right) + 2\,(5\,\nu-4)\,\beta + 3\,e\,\eta^2\right)E - (1-2\,\nu)\left((1-2\,\nu)\,\eta^2 - 3\,(1+e1)\,\beta\right)E_t$;

where:
$\beta = \rho 2/\rho 1$, $\eta^2 = \beta^2 - \beta + 1$ and $E_t = \frac{E}{\lambda}$

For axial buckling, $\beta = 0$. Using the above relations and simplifying, we get the final expressions for the C_{11}, C_{12} and C_{13}. This is achieved using the Mathematica code given below:

```
Clear["Global`*"]
(*definging the parameters*)
(* E= EE and e= e1 *)
ψ1 = (1 - 2 β)^2 EE + 3 (1 + e1) Et;
ψ2 = (2 - β) (1 - 2 β) EE - ( (2 - β) (1 - 2 β) - 4 ν η^2 - 3 e1 β) Et;
ψ3 = (2 - β)^2 EE + 3 (1 + e1) β^2 Et;
ψ4 = ( (5 - 4 ν) (1 + β^2) + 2 (5 ν - 4) β + 3 e1 η^2) EE - (1 - 2 ν) ( (1 - 2 ν) η^2 - 3 (1 + e1) β) Et;


(*Solving for C11*)

C11 = Simplify[ψ1 / ψ4 /. {β → 0, η → 1, Et → EE / λ}]
```

$$\frac{3 + 3\,e1 + \lambda}{\lambda\,(5 + 3\,e1 - 4\,\nu) - (1-2\,\nu)^2}$$

```
(*Solving for C12*)

C12 = Simplify[ψ2 / ψ4 /. {β → 0, η → 1, Et → EE / λ}]
```

$$\frac{2\,(-1+\lambda+2\,\nu)}{\lambda\,(5+3\,e1-4\,\nu)-(1-2\,\nu)^2}$$

```
(*Solving for C13*)

C13 = Simplify[ψ3 / ψ4 /. {β → 0, η → 1, Et → EE / λ}]
```

$$\frac{4\,\lambda}{\lambda\,(5+3\,e1-4\,\nu)-(1-2\,\nu)^2}$$

To check: To show that the above equations may reduce to linear elastic constitutive equations, we set $\lambda = 1$ and e = 0

```
(* the constitutive equations are given by*)
σx = EE (C11 ϵx + C12 ϵΘ);
σΘ = EE (C12 ϵx + C13 ϵΘ);
Simplify[σx /. {λ → 1, e1 → 0}]
Simplify[σΘ /. {λ → 1, e1 → 0}]
(*The linear elastic constiutive equations are*)
```

$$-\frac{EE\,(\epsilon x+\epsilon\Theta\,\nu)}{-1+\nu^2}$$

$$-\frac{EE\,(\epsilon\Theta+\epsilon x\,\nu)}{-1+\nu^2}$$

As it can be seen that the constitutive equations has been reduced to linear elastic equations.

To summarize :

$$C_{11}=\frac{3+3\,e1+\lambda}{\lambda\,(5+3\,e1-4\,\nu)-(1-2\,\nu)^2}$$

$$C_{12}=\frac{2\,(-1+\lambda+2\,\nu)}{\lambda\,(5+3\,e1-4\,\nu)-(1-2\,\nu)^2}$$

$$C_{13}=\frac{4\,\lambda}{\lambda\,(5+3\,e1-4\,\nu)-(1-2\,\nu)^2}$$

APPENDIX B-1
Non-Symmetric Buckling of Thin Circular Cylindrical Shells

Governing Equations:

The general equilibrium equations governing the deformation of a thin cylindrical shell subjected to a compressive force N are given by equations:

$$A_{mn}\left(\beta^2+\frac{1-v}{2}n^2\right)+B_{mn}\frac{n(1+v)\beta}{2}+C_{mn}v\beta=0 \tag{4.28}$$

$$A_{mn}\frac{n(1+v)\beta}{2}+B_{mn}\left[(1-v)\left(\frac{1}{2}+\frac{t^2}{12R^2}\right)\beta^2+\left(1+\frac{t^2}{12R^2}\right)n^2 - \frac{N(1-v^2)}{Et}\beta^2\right]+C_{mn}n\left[1+\frac{t^2}{12R^2}(n^2+\beta^2)\right]=0 \tag{4.29}$$

$$A_{mn}v\beta+B_{mn}n\left\{1+\frac{t^2}{12R^2}[n^2+(2-v)\beta^2]\right\} + C_{mn}\left[1-\frac{N(1-v^2)}{Et}\beta^2+\frac{t^2}{12R^2}(n^2+\beta^2)^2\right]=0 \tag{4.30}$$

Non-Symmetric Buckling Load/Stress

```
Clear["Global`*"]
(*Defining the general equilibrium eqs governing
 the deformation of a thin cylindrical shell subjected
 to a compressive force N, equations 4.28-4.30.
   T is the shell thickness *)
LHS[1] = CC[1] (β^2 + (1 - ν)/2 n^2) + CC[2] (n (1 + ν) β)/2 + CC[3] ν β;
LHS[2] = CC[1] (n (1 + ν) β)/2 +
    CC[2] ((1 - ν) (1/2 + T^2/(12 R^2)) β^2 + (1 + T^2/(12 R^2)) n^2 - σcr (1 - ν^2)/EE β^2) +
    CC[3] * n (1 + T^2/(12 R^2) (n^2 + β^2));
LHS[3] = CC[1] ν β + CC[2] * n (1 + T^2/(12 R^2) (n^2 + (2 - ν) β^2)) +
    CC[3] (1 - σcr (1 - ν^2)/EE β^2 + T^2/(12 R^2) (n^2 + β^2)^2);

(* Construct the eigenvalue matrix *)
AA = Table[0, {i, 1, 3}, {j, 1, 3}];
Do[AA[[i, j]] = Coefficient[LHS[i], CC[j]], {i, 1, 3}, {j, 1, 3}]
MatrixForm[AA]

(*The matrix is*)
```

$$\begin{pmatrix} \beta^2 + \frac{1}{2} n^2 (1 - \nu) & \frac{1}{2} n \beta (1 + \nu) & \beta \nu \\ \frac{1}{2} n \beta (1 + \nu) & n^2 \left(1 + \frac{T^2}{12 R^2}\right) + \left(\frac{1}{2} + \frac{T^2}{12 R^2}\right) \beta^2 (1 - \nu) - \frac{\beta^2 \left(1-\nu^2\right) \sigma cr}{EE} & n \left(1 + \frac{T^2 (n \\ \beta \nu & n \left(1 + \frac{T^2 \left(n^2+\beta^2 (2-\nu)\right)}{12 R^2}\right) & 1 + \frac{T^2 \left(n^2+\beta^2\right)^2}{12 R^2} - \end{pmatrix}$$

```
(* Express elements of the matrix in
 terms of dimensionless geometric parameters *)
AA = Simplify[AA /. {R → RT T, β → m π / LR, ν → 3 / 10}]
(* where RT = R/T and LR=L/R *)
MatrixForm[AA]
```

$$\begin{pmatrix} \frac{7\,n^2}{20} + \frac{m^2\,\pi^2}{LR^2} & \frac{13\,m\,n\,\pi}{20\,LR} & \frac{3\,m\,\pi}{10\,LR} \\ \frac{13\,m\,n\,\pi}{20\,LR} & n^2\left(1 + \frac{1}{12\,RT^2}\right) + \frac{7\,m^2\,\pi^2\left(5\,EE\left(1+6\,RT^2\right)-78\,RT^2\,\sigma cr\right)}{600\,EE\,LR^2\,RT^2} & n\left(1 + \frac{n^2+\frac{m^2\,\pi^2}{LR^2}}{12\,RT^2}\right) \\ \frac{3\,m\,\pi}{10\,LR} & n\left(1 + \frac{n^2+\frac{17\,m^2\,\pi^2}{10\,LR^2}}{12\,RT^2}\right) & 1 + \frac{\left(n^2+\frac{m^2\,\pi^2}{LR^2}\right)^2}{12\,RT^2} - \frac{91\,m^2\,\pi^2\,\sigma cr}{100\,EE\,LR^2} \end{pmatrix}$$

```
(* Set the determinate of the matrix equal to 0 to get the eigenvalues,
critical stress (σcr) *)
sol1 = Simplify[Solve[Det[AA] == 0, σcr]]
```

$$\left\{\left\{\sigma cr \to \left(5 \left(EE\, m^2\, RT^2 \left(200\, m^6\, \pi^6 + 70\, LR^6\, n^2 \left(1 + n^2\right) \left(n^2 + 12\, RT^2\right) + 10\, LR^2\, m^4\, \pi^4 \left(14 + 47\, n^2 + 84\, RT^2\right) + LR^4\, m^2\, \pi^2 \left(340\, n^4 + 2184\, RT^2 + 3\, n^2 \left(83 + 560\, RT^2\right)\right)\right) - \sqrt{\left(EE^2\, m^4\, RT^4 \left(40\,000\, m^{12}\, \pi^{12} + 4000\, LR^2\, m^{10}\, \pi^{10} \left(-14 + 47\, n^2 - 84\, RT^2\right) + 4900\, LR^{12}\, n^4 \left(n^8 + 144\, RT^4 + n^6 \left(2 - 24\, RT^2\right) + 24\, n^2\, RT^2 \left(-1 + 12\, RT^2\right) + n^4 \left(1 + 144\, RT^2 + 144\, RT^4\right)\right) + 100\, LR^4\, m^8\, \pi^8 \left(3569\, n^4 - 24\, n^2 \left(-17 + 609\, RT^2\right) + 28 \left(7 + 396\, RT^2 + 252\, RT^4\right)\right) + 20\, LR^6\, m^6\, \pi^6 \left(17\,380\, n^6 - 3\, n^4 \left(-4419 + 41\,440\, RT^2\right) - 30\,576 \left(RT^2 + 6\, RT^4\right) + 42\, n^2 \left(83 + 8870\, RT^2 + 3360\, RT^4\right)\right) + 140\, LR^{10}\, m^2\, n^2\, \pi^2 \left(340\, n^8 + 26\,208\, RT^4 + n^6 \left(589 - 5760\, RT^2\right) + 12\, n^2\, RT^2 \left(-431 + 3864\, RT^2\right) + 3\, n^4 \left(83 + 10\,932\, RT^2 + 6720\, RT^4\right)\right) + LR^8\, m^4\, \pi^4 \left(181\,400\, n^8 + 4\,769\,856\, RT^4 - 200\, n^6 \left(-1205 + 10\,248\, RT^2\right) + 336\, n^2\, RT^2 \left(-3937 + 18\,396\, RT^2\right) + n^4 \left(81\,601 + 9\,830\,352\, RT^2 + 4\,233\,600\, RT^4\right)\right)\right)\right)\right) \Big/ \left(1092\, LR^2\, m^4\, \pi^2 \left(7\, LR^2\, n^2 + 20\, m^2\, \pi^2\right) RT^4\right)\right\}, \left\{\sigma cr \to \left(5 \left(EE\, m^2\, RT^2 \left(200\, m^6\, \pi^6 + 70\, LR^6\, n^2 \left(1 + n^2\right) \left(n^2 + 12\, RT^2\right) + 10\, LR^2\, m^4\, \pi^4 \left(14 + 47\, n^2 + 84\, RT^2\right) + LR^4\, m^2\, \pi^2 \left(340\, n^4 + 2184\, RT^2 + 3\, n^2 \left(83 + 560\, RT^2\right)\right)\right) + \sqrt{\left(EE^2\, m^4\, RT^4 \left(40\,000\, m^{12}\, \pi^{12} + 4000\, LR^2\, m^{10}\, \pi^{10} \left(-14 + 47\, n^2 - 84\, RT^2\right) + 4900\, LR^{12}\, n^4 \left(n^8 + 144\, RT^4 + n^6 \left(2 - 24\, RT^2\right) + 24\, n^2\, RT^2 \left(-1 + 12\, RT^2\right) + n^4 \left(1 + 144\, RT^2 + 144\, RT^4\right)\right) + 100\, LR^4\, m^8\, \pi^8 \left(3569\, n^4 - 24\, n^2 \left(-17 + 609\, RT^2\right) + 28 \left(7 + 396\, RT^2 + 252\, RT^4\right)\right) + 20\, LR^6\, m^6\, \pi^6 \left(17\,380\, n^6 - 3\, n^4 \left(-4419 + 41\,440\, RT^2\right) - 30\,576 \left(RT^2 + 6\, RT^4\right) + 42\, n^2 \left(83 + 8870\, RT^2 + 3360\, RT^4\right)\right) + 140\, LR^{10}\, m^2\, n^2\, \pi^2 \left(340\, n^8 + 26\,208\, RT^4 + n^6 \left(589 - 5760\, RT^2\right) + 12\, n^2\, RT^2 \left(-431 + 3864\, RT^2\right) + 3\, n^4 \left(83 + 10\,932\, RT^2 + 6720\, RT^4\right)\right) + LR^8\, m^4\, \pi^4 \left(181\,400\, n^8 + 4\,769\,856\, RT^4 - 200\, n^6 \left(-1205 + 10\,248\, RT^2\right) + 336\, n^2\, RT^2 \left(-3937 + 18\,396\, RT^2\right) + n^4 \left(81\,601 + 9\,830\,352\, RT^2 + 4\,233\,600\, RT^4\right)\right)\right)\right)\right) \Big/ \left(1092\, LR^2\, m^4\, \pi^2 \left(7\, LR^2\, n^2 + 20\, m^2\, \pi^2\right) RT^4\right)\right\}\right\}$$

```
(*As can be seen there are two
 solutions for the critical stress therefore,
Let us compare the obtained solutions with the results of
  Wang (Table 5.1)[15]. Note that the results of Wang are
  in terms of Ncr R/(ET^2) Sqrt[3 (1-ν^2)] =σcr RT/E Sqrt[3 (1-ν^2)] *)
α1 = σcr RT Sqrt[3 (1 - ν^2)] /. sol1[[1]] /. {EE → 1, ν → 3 / 10};
α2 = σcr RT Sqrt[3 (1 - ν^2)] /. sol1[[2]] /. {EE → 1, ν → 3 / 10};
{α1, α2} /. {m → 1, n → 7, LR → 1, RT → 100.}
{0.962416, 843.239}
```

Therefore, the first solution is the correct one.

Verification of the obtained formula

```
(*Let us generate Table 5.1 in Wang [15]*)
(*entering the needed parameters*)
mdat = {1, 1, 3, 1, 1, 2};
ndat = {7, 3, 4, 11, 5, 5};
LRdat = {1., 5., 10., 1., 5., 10.};
RTdat = {100, 100, 100, 500, 500, 500};
```

```
(*Generating the table*)
Results = Table[{1/RTdat[[i]], LRdat[[i]], α1 /.
    {m → mdat[[i]], n → ndat[[i]], LR → LRdat[[i]], RT → RTdat[[i]]},
   " (m=", mdat[[i]], ",n=", ndat[[i]], ")"}, {i, 1, 6}];
Print[TableForm[Results, TableHeadings ->
  {None, {"T/R", "L/R", "σcr R/T √(3 (1 - ν^2)) / E"}}]]
(*The generated table is*)
```

T/R	L/R	$\frac{\sigma cr \frac{R}{T}\sqrt{3\left(1-\nu^2\right)}}{E}$					
1/100	1.	0.962416	(m=	1	,n=	7	)
1/100	5.	0.904858	(m=	1	,n=	3	)
1/100	10.	0.886141	(m=	3	,n=	4	)
1/500	1.	0.984486	(m=	1	,n=	11	)
1/500	5.	0.92424	(m=	1	,n=	5	)
1/500	10.	0.92424	(m=	2	,n=	5	)

```
(*Table 5.1 in Wang [15]*)
```

Table 5.1: Critical buckling factors $N_c R\sqrt{3(1-\nu^2)}/Eh^2$ for simply supported cylindrical shells under axial compression ($\nu = 0.3$)

h/R	L/R	$N_c R\sqrt{3(1-\nu^2)}/Eh^2$
1/100	1	0.962416 $(m=1, n=7)$
	5	0.904858 $(m=1, n=3)$
	10	0.886141 $(m=3, n=4)$
1/500	1	0.984486 $(m=1, n=11)$
	5	0.924240 $(m=1, n=5)$
	10	0.924240 $(m=2, n=5)$

As can be clearly seen that the solution exactly matching, in terms of eigenvalues and eigenmodes, the exact solution by Wang.

To conclude: The non - symmetric buckling stress (σ_{cr})formula is given by the following equation :

$$\sigma_{cr} = \Big(5\Big(E\,m^2\,(R/t)^2\Big(200\,m^6\,\pi^6 + 70\,(L/R)^6\,n^2\Big(1+n^2\Big)\Big(n^2+12\,(R/t)^2\Big) + 10\,(L/R)^2\,m^4\,\pi^4\Big(14+47\,n^2+84\,(R/t)^2\Big) + (L/R)^4\,m^2\,\pi^2\Big(340\,n^4+2184\,(R/t)^2+3\,n^2\Big(83+560\,(R/t)^2\Big)\Big)\Big) - \sqrt{\Big(E^2\,m^4\,(R/t)^4\Big(40\,000\,m^{12}\,\pi^{12}+4000\,(L/R)^2\,m^{10}\,\pi^{10}\Big(-14+47\,n^2-84\,(R/t)^2\Big) + 4900\,(L/R)^{12}\,n^4\Big(n^8+144\,(R/t)^4+n^6\Big(2-24\,(R/t)^2\Big)+24\,n^2\,(R/t)^2\Big(-1+12\,(R/t)^2\Big)+n^4\Big(1+144\,(R/t)^2+144\,(R/t)^4\Big)\Big) + 100\,(L/R)^4\,m^8\,\pi^8\Big(3569\,n^4-24\,n^2\Big(-17+609\,(R/t)^2\Big)+28\Big(7+396\,(R/t)^2+252\,(R/t)^4\Big)\Big) + 20\,(L/R)^6\,m^6\,\pi^6\Big(17\,380\,n^6-3\,n^4\Big(-4419+41\,440\,(R/t)^2\Big)-30\,576\,\Big((R/t)^2+6\,(R/t)^4\Big)+42\,n^2\Big(83+8870\,(R/t)^2+3360\,(R/t)^4\Big)\Big) + 140\,(L/R)^{10}\,m^2\,n^2\,\pi^2\Big(340\,n^8+26\,208\,(R/t)^4+n^6\Big(589-5760\,(R/t)^2\Big)+12\,n^2\,(R/t)^2\Big(-431+3864\,(R/t)^2\Big)+3\,n^4\Big(83+10\,932\,(R/t)^2+6720\,(R/t)^4\Big)\Big) + (L/R)^8\,m^4\,\pi^4\Big(181\,400\,n^8+4\,769\,856\,(R/t)^4-200\,n^6\Big(-1205+10\,248\,(R/t)^2\Big)+336\,n^2\,(R/t)^2\Big(-3937+18\,396\,(R/t)^2\Big)+n^4\Big(81\,601+9\,830\,352\,(R/t)^2+4\,233\,600\,(R/t)^4\Big)\Big)\Big)\Big)\Big)\Big/\Big(1092\,(L/R)^2\,m^4\,\pi^2\Big(7\,(L/R)^2\,n^2+20\,m^2\,\pi^2\Big)\,(R/t)^4\Big);$$

APPENDIX B-2
Simplified Buckling Formulas for Non-Symmetric Elastic Buckling

```
(*Define the non-symmetric buckling stress formula*)
σcr =
  (5 (EE m^2 RT^2 (200 m^6 π^6 + 70 LR^6 n^2 (1 + n^2) (n^2 + 12 RT^2) + 10 LR^2 m^4 π^4 (14 + 47 n^2 + 84 RT^2) +
          LR^4 m^2 π^2 (340 n^4 + 2184 RT^2 + 3 n^2 (83 + 560 RT^2)))) -
      √(EE^2 m^4 RT^4 (40 000 m^12 π^12 + 4000 LR^2 m^10 π^10 (-14 + 47 n^2 - 84 RT^2) +
          4900 LR^12 n^4 (n^8 + 144 RT^4 + n^6 (2 - 24 RT^2) + 24 n^2 RT^2 (-1 + 12 RT^2) + n^4
              (1 + 144 RT^2 + 144 RT^4)) + 100 LR^4 m^8 π^8 (3569 n^4 - 24 n^2 (-17 + 609 RT^2) + 28
              (7 + 396 RT^2 + 252 RT^4)) + 20 LR^6 m^6 π^6 (17 380 n^6 - 3 n^4 (-4419 + 41 440 RT^2) -
            30 576 (RT^2 + 6 RT^4) + 42 n^2 (83 + 8870 RT^2 + 3360 RT^4)) +
          140 LR^10 m^2 n^2 π^2 (340 n^8 + 26 208 RT^4 + n^6 (589 - 5760 RT^2) + 12 n^2
              RT^2 (-431 + 3864 RT^2) + 3 n^4 (83 + 10 932 RT^2 + 6720 RT^4)) +
          LR^8 m^4 π^4 (181 400 n^8 + 4 769 856 RT^4 - 200 n^6 (-1205 + 10 248 RT^2) + 336
              n^2 RT^2 (-3937 + 18 396 RT^2) + n^4 (81 601 + 9 830 352 RT^2 +
                4 233 600 RT^4))))))) / (1092 LR^2 m^4 π^2 (7 LR^2 n^2 + 20 m^2 π^2) RT^4);

(*Define the stainless steel properties
  EE = E*)
σcr = σcr /. {EE → 200 000, ν → 3 / 10};
σy = 330;
```

Now Simplification of the lengthy formula for non -symmetric buckling

```
(*The first model: for 1 < L/R < 5*)
```

```
(* a 3-D plot that shows the variation of σcr with L/R and R/T *)
(* "Minimize" function is used to obtain the lowest
 buckling load(critical) for different L/r and R/t ratios*)

Do[sol = Minimize[{(σcr /. {LR → 1. i, RT → 300 + 25. j}),
      m > 0, n > 0, m ∈ Integers, n ∈ Integers}, {m, n}];
  αα[i, j] = sol[[1]] / 200000. * 10^3, {i, 1, 5, 0.5}, {j, 1, 12}];
σcrData = Flatten[Table[{i, 300 + 25. j, αα[i, j]}, {i, 1, 5, 0.5}, {j, 1, 12}], 1];
ListPlot3D[σcrData]
```

NMinimize: Failed to converge to the requested accuracy or precision within 100 iterations.

NMinimize: Failed to converge to the requested accuracy or precision within 100 iterations.

NMinimize: Failed to converge to the requested accuracy or precision within 100 iterations.

General: Further output of NMinimize::cvmit will be suppressed during this calculation.

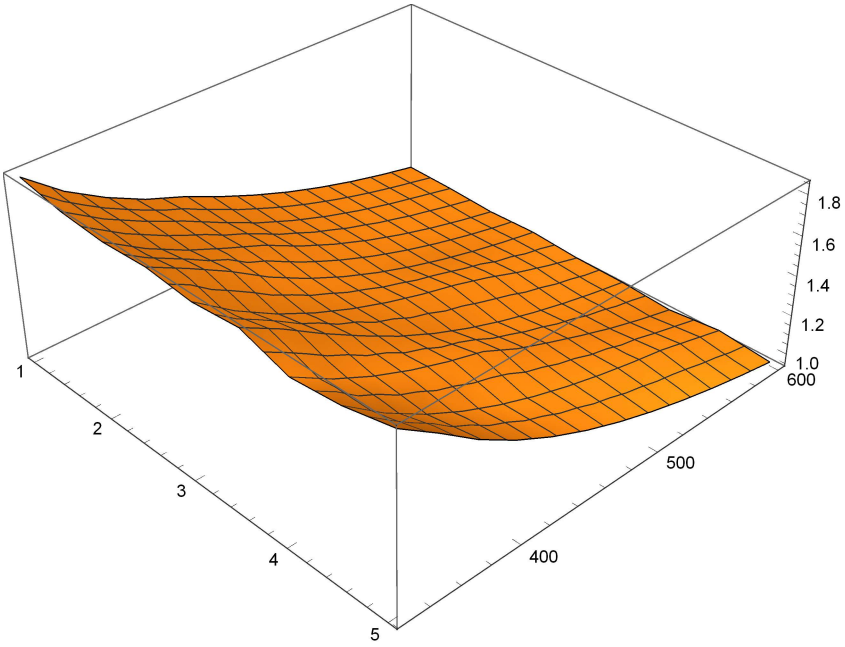

```
(* fitting the data with a compact model *)
(* The compact model is defined as: *)
σcrModel = c1/RT LR^c2 ;

(* Now fitting the data with the compact model *)
(*"FindFit" fuction is used to fit the data*)
fit = FindFit[σcrData, σcrModel, {c1, c2}, {LR, RT}];
σcrModel1 = σcrModel /. fit;
Print[Show[{Plot3D[Evaluate[σcrModel1], {LR, 1, 5}, {RT, 325, 600}],
   Graphics3D[{Red, PointSize[.025], Map[Point, σcrData]}]},
  PlotRange → All, AxesLabel → {LR, RT, "σcr/E x10^3"}]];
Print["σcr= ", σcrModel1]
(*The fitted buckling stresses with the compact model is shown in the Figure below,
dotted points indicate the fitted data*)
```

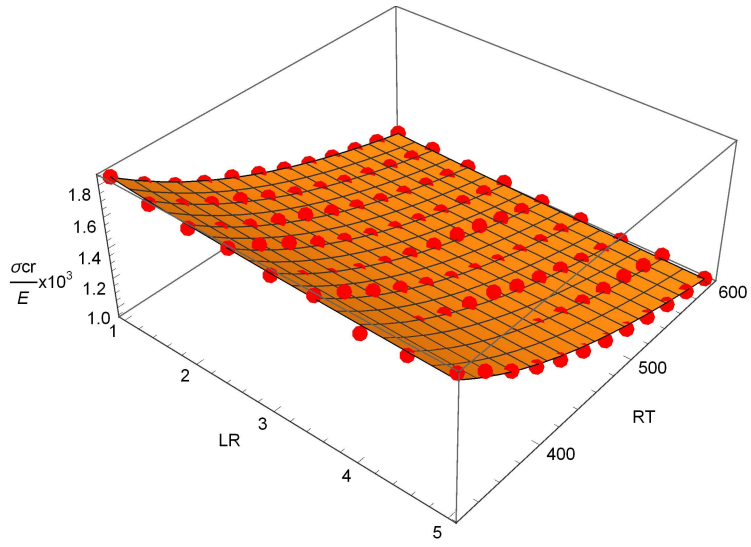


```
(*The model is*)
```

$$\sigma cr = \frac{600.417}{LR^{0.0296907}\,RT}$$

```
(*Comparison of the suggested model and the theoritical non-symmetrical formula*)
σrResults =
  Flatten[Table[{i, 350 + 25 j, αα[i, j], σcrModel1 /. {LR → i, RT → 300 + 25 j},
      (αα[i, j] - σcrModel1 /. {LR → i, RT → 300 + 25 j}) / αα[i, j] * 100},
    {i, 1, 5, 0.5}, {j, 1, 12}], 1];
(*Generating the comparison Table*)
Print[TableForm[σrResults, TableHeadings ->
   {None, {"L/R", "R/T", "(σcr - Analytical)/E x10^3", "(σcr - Model)/E x10^3", "%Error"}},
  {LR, 1, 5}, {RT, 325., 600., 25}]]
```

L/R	R/T	$\frac{\sigma cr-Analytical}{E}x10^3$	$\frac{\sigma cr-Model}{E}x10^3$	%Error
1.	375	1.84868	1.84744	0.0672123
1.	400	1.69702	1.71548	-1.08766
1.	425	1.58259	1.60111	-1.17
1.	450	1.48895	1.50104	-0.812285
1.	475	1.41825	1.41274	0.387892
1.	500	1.33436	1.33426	0.00782485
1.	525	1.25869	1.26403	-0.424936
1.	550	1.19168	1.20083	-0.76845
1.	575	1.13401	1.14365	-0.850295
1.	600	1.08402	1.09167	-0.704988
1.	625	1.04042	1.0442	-0.363857
1.	650	1.00215	1.00069	0.144905
1.5	375	1.80547	1.82533	-1.09991
1.5	400	1.68392	1.69495	-0.65481
1.5	425	1.58586	1.58195	0.246606
1.5	450	1.50067	1.48308	1.17249
1.5	475	1.40632	1.39584	0.745571
1.5	500	1.31859	1.31829	0.0223717
1.5	525	1.24434	1.24891	-0.367494
1.5	550	1.18094	1.18646	-0.46762
1.5	575	1.12639	1.12997	-0.317833
1.5	600	1.0791	1.0786	0.0458757
1.5	625	1.03784	1.03171	0.591282
1.5	650	0.996949	0.98872	0.825453
2.	375	1.78808	1.8098	-1.21486
2.	400	1.66746	1.68053	-0.784146
2.	425	1.57014	1.5685	0.104863
2.	450	1.4905	1.47047	1.34407
2.	475	1.41601	1.38397	2.26318

2.	500	1.32244	1.30708	1.16119
2.	525	1.24324	1.23829	0.398522
2.	550	1.17563	1.17637	−0.063508
2.	575	1.11744	1.12035	−0.261046
2.	600	1.067	1.06943	−0.227463
2.	625	1.023	1.02293	0.00675122
2.	650	0.984386	0.98031	0.413972
2.5	375	1.80075	1.79785	0.161065
2.5	400	1.70248	1.66944	1.9412
2.5	425	1.59703	1.55814	2.43495
2.5	450	1.47687	1.46076	1.09082
2.5	475	1.37728	1.37483	0.177927
2.5	500	1.29383	1.29845	−0.357415
2.5	525	1.2232	1.23011	−0.565097
2.5	550	1.1629	1.1686	−0.49078
2.5	575	1.111	1.11296	−0.175738
2.5	600	1.06603	1.06237	0.343109
2.5	625	1.02678	1.01618	1.03303
2.5	650	0.992346	0.973837	1.8652
3.	375	1.77585	1.78815	−0.692367
3.	400	1.63798	1.66042	−1.37007
3.	425	1.52675	1.54973	−1.50475
3.	450	1.43572	1.45287	−1.19433
3.	475	1.36028	1.36741	−0.524078
3.	500	1.29705	1.29144	0.432886
3.	525	1.24355	1.22347	1.61468
3.	550	1.19787	1.1623	2.96947
3.	575	1.14325	1.10695	3.17507
3.	600	1.07971	1.05663	2.13766
3.	625	1.02428	1.01069	1.32702
3.	650	0.975639	0.96858	0.723533
3.5	375	1.79788	1.77998	0.995599
3.5	400	1.69347	1.65284	2.39943
3.5	425	1.5734	1.54265	1.95445
3.5	450	1.46366	1.44624	1.19027
3.5	475	1.36258	1.36116	0.104192
3.5	500	1.27788	1.28554	−0.599549
3.5	525	1.2062	1.21788	−0.968678
3.5	550	1.145	1.15699	−1.04731
3.5	575	1.09233	1.10189	−0.875699
3.5	600	1.04668	1.05181	−0.490163
3.5	625	1.00685	1.00608	0.0768097
3.5	650	0.971897	0.964157	0.796394
4.	375	1.72095	1.77294	−3.0211
4.	400	1.60833	1.6463	−2.36113
4.	425	1.51747	1.53655	−1.25728

4.	450	1.44311	1.44051	0.179832
4.	475	1.38148	1.35578	1.86056
4.	500	1.32984	1.28046	3.71319
4.	525	1.24324	1.21306	2.42737
4.	550	1.17563	1.15241	1.97475
4.	575	1.11175	1.09753	1.27871
4.	600	1.05274	1.04765	0.483638
4.	625	1.00125	1.0021	-0.0841505
4.	650	0.95607	0.960342	-0.446827
4.5	375	1.74533	1.76675	-1.22731
4.5	400	1.60424	1.64055	-2.26351
4.5	425	1.49042	1.53118	-2.73512
4.5	450	1.39726	1.43548	-2.73546
4.5	475	1.32006	1.35104	-2.34735
4.5	500	1.25536	1.27599	-1.64313
4.5	525	1.2006	1.20883	-0.685033
4.5	550	1.15386	1.14839	0.47392
4.5	575	1.11363	1.0937	1.78901
4.5	600	1.07875	1.04399	3.22282
4.5	625	1.03087	0.998598	3.13037
4.5	650	0.982756	0.956989	2.62183
5.	375	1.80075	1.76123	2.19475
5.	400	1.67072	1.63543	2.11232
5.	425	1.53122	1.5264	0.315049
5.	450	1.41706	1.431	-0.983919
5.	475	1.32244	1.34682	-1.84394
5.	500	1.24315	1.272	-2.32095
5.	525	1.17604	1.20505	-2.46673
5.	550	1.11875	1.1448	-2.32847
5.	575	1.06945	1.09029	-1.94867
5.	600	1.02671	1.04073	-1.36521
5.	625	0.989428	0.995479	-0.611563
5.	650	0.956707	0.954	0.282916

As it can be clearly seen that the simplified design model is very close from the analytical solution

```
(*The Second model: for 5 < L/R < 10*)
(* a 3-D plot that shows the variation of σcr with L/R and R/T *)
(* "Minimize" function is used to obtain the lowest
 buckling load(critical) for different L/r and R/t ratios*)
Do[sol = Minimize[{(σcr /. {LR → 1. i, RT → 325 + 25. j}),
      m > 0, n > 0, m ∈ Integers, n ∈ Integers}, {m, n}];
  αα[i, j] = sol[[1]] / 200000. * 10^3, {i, 6, 10, 0.5}, {j, 1, 11}];
σcrData = Flatten[Table[{i, 325 + 25. j, αα[i, j]}, {i, 6, 10, 0.5}, {j, 1, 11}], 1];
ListPlot3D[σcrData]
```

NMinimize: Failed to converge to the requested accuracy or precision within 100 iterations.

NMinimize: Failed to converge to the requested accuracy or precision within 100 iterations.

NMinimize: Failed to converge to the requested accuracy or precision within 100 iterations.

General: Further output of NMinimize::cvmit will be suppressed during this calculation.

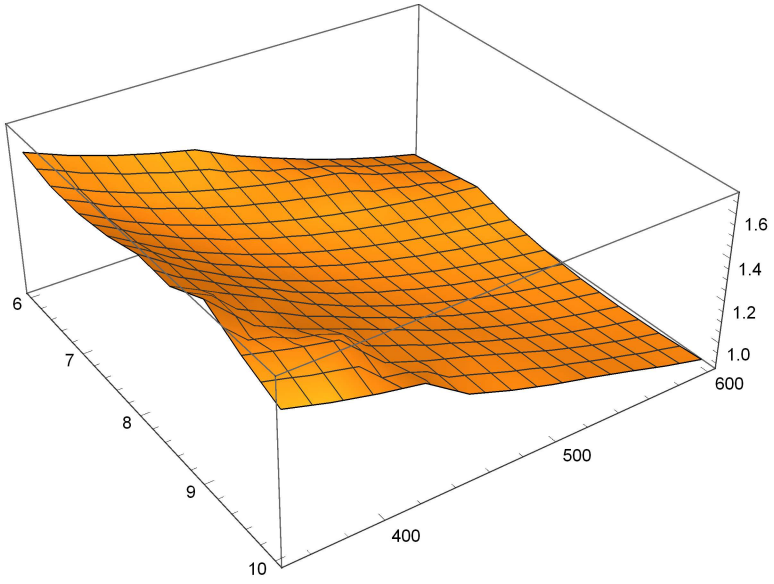

```
(* fitting the data with a compact model *)
(* The compact model is defined as: *)
σcrModel = c1 RT^c2 LR^c3 ;

(* Now fitting the data with the compact model *)
(*"FindFit" fuction is used to fit the data*)
fit = FindFit[σcrData, σcrModel, {c1, c2, c3}, {LR, RT}];
σcrModel1 = σcrModel /. fit;
Print[Show[{Plot3D[Evaluate[σcrModel1], {LR, 6, 10}, {RT, 350, 600}],
    Graphics3D[{Red, PointSize[.025], Map[Point, σcrData]}]},
  PlotRange → All, AxesLabel → {LR, RT, "σcr/E x10^3"}]];
Print["σcr= ", σcrModel1]
(*The fitted buckling stresses with the compact model is shown in the Figure below,
dotted points indicate the fitted data*)
```

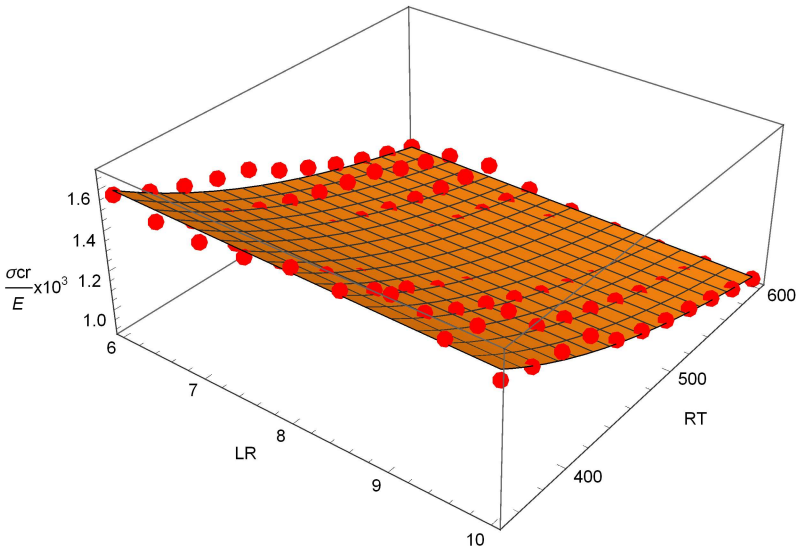


```
(*The model is*)
```

$$\sigma cr = \frac{534.795}{LR^{0.0333005}\, RT^{0.982672}}$$

```
(*Comparison of the suggested model and the theoritical non-symmetrical formula*)
```

```
σrResults =
  Flatten[Table[{i, 325 + 25 j, αα[i, j], σcrModel1 /. {LR → i, RT → 325 + 25 j},
      (αα[i, j] - σcrModel1 /. {LR → i, RT → 325 + 25 j}) / αα[i, j] * 100},
    {i, 6, 10, 0.5}, {j, 1, 11}], 1];
(*Generating the comparison Table*)
Print[TableForm[σrResults, TableHeadings ->
   {None, {"L/R", "R/T", "(σcr - Analytical)/E x10^3", "(σcr - Model)/E x10^3", "%Error"}},
  {LR, 6, 10}, {RT, 350., 600., 25}]]
```

L/R	R/T	(σcr−Analytical)/E x10^3	(σcr−Model)/E x10^3	%Error
6.	350	1.57128	1.59327	−1.40004
6.	375	1.49426	1.48884	0.362844
6.	400	1.43122	1.39735	2.36705
6.	425	1.37898	1.31653	4.52875
6.	450	1.3352	1.24462	6.78401
6.	475	1.24355	1.18022	5.09248
6.	500	1.16896	1.12221	3.99989
6.	525	1.09864	1.06967	2.63691
6.	550	1.03769	1.02187	1.52419
6.	575	0.984515	0.978198	0.641602
6.	600	0.937847	0.938132	−0.0303941
6.5	350	1.53166	1.58903	−3.7457
6.5	375	1.44173	1.48487	−2.99262
6.5	400	1.36812	1.39363	−1.86417
6.5	425	1.30712	1.31303	−0.451934
6.5	450	1.256	1.24131	1.16951
6.5	475	1.21273	1.17708	2.94008
6.5	500	1.1758	1.11922	4.81182
6.5	525	1.14401	1.06683	6.74683
6.5	550	1.07275	1.01915	4.99611
6.5	575	1.02176	0.975594	4.51785
6.5	600	0.967162	0.935634	3.25979
7.	350	1.52793	1.58512	−3.74256
7.	375	1.42405	1.48121	−4.01429
7.	400	1.33902	1.39019	−3.8212
7.	425	1.26856	1.30979	−3.25025
7.	450	1.20951	1.23825	−2.37631
7.	475	1.15953	1.17418	−1.26299
7.	500	1.11687	1.11646	0.0362422
7.	525	1.08015	1.0642	1.47681

7.	550	1.04832	1.01664	3.02187
7.	575	1.02056	0.97319	4.64116
7.	600	0.996187	0.933328	6.30997
7.5	350	1.5532	1.58148	−1.82052
7.5	375	1.43433	1.47781	−3.03149
7.5	400	1.33704	1.387	−3.73631
7.5	425	1.25641	1.30678	−4.009
7.5	450	1.18885	1.23541	−3.91657
7.5	475	1.13166	1.17148	−3.51878
7.5	500	1.08284	1.1139	−2.86822
7.5	525	1.04083	1.06175	−2.01069
7.5	550	1.00441	1.01431	−0.985706
7.5	575	0.972638	0.970956	0.172857
7.5	600	0.944755	0.931186	1.43618
8.	350	1.60257	1.57808	1.52815
8.	375	1.46768	1.47464	−0.474036
8.	400	1.35728	1.38402	−1.96993
8.	425	1.26579	1.30398	−3.01702
8.	450	1.18912	1.23276	−3.66999
8.	475	1.12423	1.16897	−3.97985
8.	500	1.06882	1.11151	−3.99346
8.	525	1.02115	1.05947	−3.75329
8.	550	0.979823	1.01213	−3.29742
8.	575	0.94377	0.968872	−2.65972
8.	600	0.91213	0.929187	−1.87008
8.5	350	1.59609	1.5749	1.32766
8.5	375	1.49409	1.47167	1.50086
8.5	400	1.39619	1.38123	1.07144
8.5	425	1.29313	1.30135	−0.635733
8.5	450	1.20676	1.23027	−1.94813
8.5	475	1.13367	1.16661	−2.90593
8.5	500	1.07126	1.10927	−3.54761
8.5	525	1.01756	1.05734	−3.90937
8.5	550	0.971008	1.01009	−4.02491
8.5	575	0.930398	0.966918	−3.92523
8.5	600	0.894757	0.927313	−3.63856
9.	350	1.68013	1.57191	6.44109
9.	375	1.49042	1.46887	1.44591
9.	400	1.39726	1.3786	1.33532
9.	425	1.32006	1.29887	1.60473
9.	450	1.23915	1.22793	0.905561
9.	475	1.15736	1.16439	−0.607863
9.	500	1.08752	1.10716	−1.80534
9.	525	1.02743	1.05533	−2.71564
9.	550	0.975335	1.00817	−3.36647
9.	575	0.929891	0.965079	−3.78418

9.	600	0.890007	0.92555	−3.99354
9.5	350	1.58882	1.56908	1.24265
9.5	375	1.53681	1.46623	4.59297
9.5	400	1.49424	1.37612	7.9049
9.5	425	1.31448	1.29654	1.3649
9.5	450	1.24268	1.22572	1.36439
9.5	475	1.18191	1.1623	1.6593
9.5	500	1.11563	1.10516	0.93815
9.5	525	1.04878	1.05343	−0.443666
9.5	550	0.990827	1.00636	−1.56728
9.5	575	0.940272	0.963343	−2.4537
9.5	600	0.895903	0.923885	−3.12331
10.	350	1.51836	1.5664	−3.16394
10.	375	1.46087	1.46372	−0.19545
10.	400	1.41381	1.37378	2.83192
10.	425	1.37482	1.29432	5.85477
10.	450	1.24315	1.22363	1.57008
10.	475	1.17604	1.16031	1.33745
10.	500	1.11875	1.10328	1.38296
10.	525	1.06945	1.05163	1.66588
10.	550	1.01597	1.00464	1.11579
10.	575	0.960032	0.961699	−0.173607
10.	600	0.910936	0.922308	−1.24839

As it can be seen that the simplified design model is very close from the analytical solution

APPENDIX C
Worked Example

Full-range Ramberg - Osgood Model

```
Clear["Global`*"]
(* Computation of plastic buckling stress *)
(* Entering the parameters and dimentions *)

(* RT=R/t*)
RT = 110 / 2 / 1.1;
(* A= Area*)
A = π (110 - 1.1/2) (1.1);
(* E0= E which is the Modulus of Elasticity*)
E0 = 200000;
(* σ2= σ0.2 is the 0.2% proof stress*)
σ2 = 330;
(* σ1= σ1 is the 1% proof stress*)
σ1 = 370;
(*Poisson's ratio*)
ν = 0.3;
(* n1= n is the strain hardening exponent
   n2= n'0.2,1.0 is the strain hardening
   coefficient that passes through both stresses σ0.2 and σ1.0*)
n1 = 9.5;
n2 = 1.95;
(* E2 = E 0.2 is the stiffness at 0.2% proof stress*)
E2 = E0 σ2 / (σ2 + 0.002 (n1) (E0)) ;

(*Buckling Stress Calculations*)
(*Ramberg-Osgood Full Model*)
ϵ = If[σ < σ2, σ/E0 + 0.002 (σ/σ2)^n1, (σ - σ2)/E0 + (0.008 - (σ1 - σ2)/E2) ((σ - σ2)/(σ1 - σ2))^n2 + σ2/E0 + 0.002];

(*Solution*)
Es = σ/ϵ;
Et = 1/D[ϵ, σ];
e1 = E0/Es - 1;
λ = E0 / Et;
```

$$\mathbf{eq} = \sigma == \frac{2}{\sqrt{3}} \frac{\frac{E0}{RT}}{\sqrt{\lambda\,(5 + 3\,e1 - 4\,\nu) - (1 - 2\,\nu)^2}};$$

```
"Buckling stress is"
sol = FindRoot[eq, {σ, σ2}]
σ1 = σ /. sol[[1]];
"Buckling Load is (kN)"
A * σ1 / 1000
```

Buckling stress is

$\{\sigma \to 344.212\}$

Buckling Load is (kN)

130.192